MÖSSBAUER EFFECT STUDY ON THE MAGNETIC PROPERTY AND PHASE DECOMPOSITION OF IRON-CHROMIUM ALLOYS

HISASHI KUWANO

Synopsis

Mössbauer spectra are measured on the random solid solutions over the nearly whole concentration range of the Fe-Cr alloy system and the temperature range of 0.03-300K, and are analyzed by a computer taking consideration of the environment effect of the first and second near neighbour Cr atoms around an Fe atom. Isolated Fe atoms in the Cr-rich solid solution have a low internal field of about -2.4MA/m(30kOe) even at temperatures lower than 14K, which is independent of the concentration in the range of higher than 86.7 at%Cr. The low interanl field and its temperature dependence are interpreted in terms of the Kondo effect.

The internal field and isomer shift are measured at room temperature for alloys annealed at temperatures, 700-1100K, to clarify the miscibility gap of the Fe-Cr phase diagram. The Mössbauer spectroscopy is so sensitive that it discloses the existence of the 'metastable' miscibility gap which has not been detected by previous studies using conventional methods. The miscibility gap discovered is confirmed to be thermodynamically describable by the regular solution approximation.

The kinetics of the early stage phase decomposition of solid solution which is accompanied by the aging at temperatures within the miscibility gap is systematically studied by computing the internal field probability and 'difference' spectrum with a combination of the transmission electron microscopy. In addition to an evidence for the gradual transition from the nucleation-growth to the spinodal decomposition in the concentration range of 30-40 at%Cr, the conspicuous superiority of the former is confirmed for alloys with the Cr content of less than 38 at%Cr.

Contents

Chapter 1. Introduction

The addition of chromium atoms into iron matrix improves its mechanical and chemical properties such as strength, resistance to corrosion, to oxidation and to creep and so on. Therefore most of industrial steels contain Cr atoms more or less. Among others, ferritic stainless steels which contain Cr atoms up to 30% of the total mass are representative examples of the commercial use of Fe-Cr binary alloys. In recent years, high chromium stainless steels have been receiving considerable attention because of the excellent resistance to stress-corrosion cracking which is widely known as "Achiless' tendon" of austenitic stainless steels. High chromium ferritic stainless steels, however, have also a fatal shortcoming called "475°C embrittlement"[1,2]: they become unsuitable for many industrial application because of the severe brittleness when heated at temperatures around 750K. There is no available way to suppress the embrittlement at present. A numerous number of studies has been carried out so far by means of hardness[3,4] and strength tests[5,6], electrical resistivity[3,7] and magnetization measurements[8,9,10], X-ray diffraction[3,11,12], electron microscope observation[4,13,14] and so on. These studies presented a conclusion that the embrittlement is phenomenologically ascribed to the phase decomposition of solid solutions stable at high temperatures into two bcc phases with different Cr content, that is, the Fe-rich phase and the Cr-rich phase, within the miscibility gap which exists below 830K in Fe-Cr binary alloy system (*cf.*p.41). But, these traditional experimental techniques were not effective to clarify the detailed mechanism of the phase decomposition because of a small difference in the lattice parameter between Fe and Cr metals and of closeness of the atomic scattering factor of

the constituent atoms.

Besides such practical importance in industrial materials, Fe-Cr alloys may be one of the most favorable objects for a study of the spinodal decomposition on which there is an ardent controversy in physical metallurgy and statistical physics, because of the following reasons:

(1) Miscibility gap spreads over the wide concentration range, having a rough symmetry about x=0.5.

(2) Strain effect is expected to be small because of a rather small difference in lattice parameter between Cr and Fe metal.

(3) Both of the precipitate phase and the matrix have a bcc structure, which will result in a simple precipitaion process.

Classical, linearized spinodal theory due to Cahn and Hilliard[16-18] defines a clear spinodal line between the nucleation and growth(N-G) and the spinodal decomposition(S) as a locus at which the second derivatives of the Gibbs free energy with respect to the solute concentration become zero. However, Langer[19,20] emphasized in his non-linearized spinodal theory based on the statistical mechanics that the free energy used in the classical theory should be defined more carefully: conventional Gibbs free energy, G , which has two inflection points below a critical temperature for the phase separation can not be a 'true' free energy for temperatures and concentrations within the miscibility gap. He stressed that the true free energy must be a convex function of composition x, thus the spinodal line defined by $\partial^2 G/\partial x^2=0$ has no physical significance. The change from the N-G to the S mechanism is expected to take place continuously as a function of x.[19] Computer simulations based on the kinetic

Ising model[21-24] have confirmed that a time evolution of the structure function $S(k,t)$—the Fourier transform of the concentration correlation function—exhibits a qualitative agreement with the Langer's theory: $S(k,t)$ vs. k curves show a gradual change with increasing its broadness and decreasing its altitude when the solute concentration is varied across the spinodal line. The Computer simulation based on the cluster kinetics due to Mirold and Binder[25] has also confirmed that the spinodal line has no physical significance. But, their result was in opposition to the Langer's theory in the point that the decomposition kinetics within the classical spinodal line is qualitatively consistent with the nucleation.

Besides these theoretical approaches to the phase decomposition, it is now strongly needed to accumulate systematic and considerable data about the subject by means of recent advanced experimental techniques. Mössbauer spectroscopy and neutron scattering measurements are the most effective means for the purpose of study from the microscopic view point on the decomposition. According to the neutron scattering study due to Katano and Iizumi[26,27], a time evolution of the scattering intensity is qualitatively consistent with the result of computer simulation due to Binder and Stauffer[28] and Sur *et al.*[24] in the case of the 32at%Cr and 40at%Cr sample aged at 723K and 773K, respectively. Concentration dependence of the scattering intensity curve is rather agreeable with the predictions of the Langer's theory. They concluded that the decomposition kinetics of Fe-Cr alloys is well described by the recent spinodal theory and computer simulations on the whole. However, neutron scattering intensity

measurement observes the concentration profile in the Fourier space, so that it overlooks information about the precipitation of the second phase which is usually accompanied by the early stages of the N-G mechanism and by the later stages of the S decomposition. Mössbauer spectroscopy is more suitable than neutron scattering measurements to detect such a small concentration changes accompanied by the precipitation of the second phase, because the internal field and the isomer shift at ^{57}Fe nuclei feel sensitively the atomic configuration changes in its neighbouring sites. If there is an essential difference between the N-G and the S mechanism, it will be recognized in the initial stages of the decomposition. It is main features of this study to carry out a systematic, accurate Mössbauer spectroscopy measurements on the magnetic properties and the initial stages of the phase separation of Fe-Cr alloys with the aid of numerical analysis and simulation of Mössbauer spectra with a computer.

Main contents of this paper consists of four parts. In §1, fundamental magnetic properties of iron-chromium solid solution and parameters available for computer analysis of Mössbauer spectra are obtained. In §2, the magnetic phase diagram and the magnetic behavior of Fe atoms in the Cr-rich solid solution are studied. In §3, the miscibility gap of the solid solution is determined experimentally and calculated on the basis of thermodynamics. In §4, kinetics of the phase decomposition and the difference between the nucleation and growth process and the spinodal decomposition are discussed.

References

1) R.W.Fountain and J.L.Lamont: *Ductile Chromium*(American Society for Metals,Cleveland,Ohio, 1957) P.255.
2) J.J.Demo: *Handbook of Stainless Steels*(Ed. by D.Peckner and I.M.Bernstein,McGraw-Hill Book Company, 1977) P.5-1.
3) R.O.Williams and H.W.Paxton: J.Iron Steel Inst. 185(1957) 358.
4) M.J.Marcinkowski, R.M.Fisher and A.Szimae: Trans. Met. Soc. AIME, 230(1964) 676.
5) R.Lagneborg: Acta Met. 15(1967) 1737.
6) P.J.Grobner: Met.Trans. 4(1973) 251.
7) R.O.Williams: Trans. Met. Soc. AIME,212(1958),497.
8) K.Bungradt and W.Spyra: Archiv Eisenhüttenwes. 12(1956) 777.
9) Y.Imai,M.Izumiyama and T.Masumoto: J.Japan Inst.Metals 30 (1966) 284.
10) W.Köster and A.von Kienlin: Archiv Eisenhüttenwes. 27(1956) 793.
11) A.J.Lena and M.F.Hawkes: Trans.AIME. 200(1954) 607 .
12) T.Miyazaki, M.Nakagaki and E.Yajima: J.Japan Inst.Metals 38 (1974) 70.
13) R.Lagneborg: Trans.ASM 60(1967) 67.
14) M.J.Blackburn and J.Nutting: J.Iron Steel Inst. 202(1964) 610.
15) R.M.Fisher, E.J.Dulis and K.G.Carroll: Trans.AIME,(J.Metals) 197(1953) 690.
16) J.W.Cahn: Trans.Met.Soc.AIME 242(1968) 166.
17) J.W.Cahn: J.Chemi.Phys.42(1965) 93.
18) J.E.Hilliard: *Phase Transformations*(American Society for Metals, 1968) P.497.
19) J.S.Langer: Physica 73(1974) 61.
20) J.S.Langer: Acta Met. 21(1973) 1649.
21) A.B.Bortz, M.H.Kalos, J.L.Lebowitz and M.A.Zendejas: Phys.Rev. B 10(1974) 535.
22) J.Marro, A.B.Bortz, M.H.Kalos and J.Lebowitz: Phys.Rev.B 12 (1975) 2000.
23) M.Rao, M.H.Kalos, J.L.Lebowitz and J.Marro: Phys.Rev.B 13 (1976) 4328.

24) A.Sur,J.L.Lebowitz,J.Marro and M.H.Kalos: Phys.Rev.B 15(1977) 3014.
25) P.Mirold and K.Binder: Acta Met. 25(1977) 1435.
26) S.Katano and M.Iizumi: Physica 120B(1983) 392.
27) S.Katano and M.Iizumi: J.Phys.Soc.Japan 51(1982) 347.
28) K.Binder and D.Stauffer: Phys.Rev.Lett. 33(1974) 1006.

Chapter 2. Magnetic Properties of Iron-Chromium Solid Solutions

§1. Concentration dependence of the internal field and the isomer shift

1.1 Introduction

Physical properties of 3d-transition metals, such as magnetism, atomic volume, bulk modulus and so on, are closely related to the 3d-band structure. When Cr atoms are added to pure iron, the electron transfer takes place to screen the nuclear charge difference, so that physical properties vary with Cr content, x. A theoretical treatment[1] based on the coherent potential approximation predicts that the number of 3d-electrons and the magnetic moment of Fe atoms first increase, and then decrease with increasing x , showing a good agreement to the neutron diffraction data.[2] The Mössbauer spectroscopy is also effective to interpret the magnetic and the electronic properties of alloys:the internal field and the isomer shift measure the magnetic moment of Fe atoms and the total s-electron density at the nucleus, respectively. The effect of Cr on the internal field at Fe nuclei was examined by Wertheim,[3] Vincze,[4] Sauer[5] and Schwartz.[6] It was confirmed that single Cr atom in the first and the second nearest neighbour shell causes about 6% decrease in the internal field. A linear relationship between the mean internal field and the Cr content has been obtained by Johnson *et al.*[7] in the concentration range of $0 \leq x \leq 0.64$ at 4.2K and 300K, and by Yamamoto[8] in the concentration range $0.21 \leq x \leq 0.48$ at 300K.

The effect of Cr impurity on the ^{57}Fe isomer shift was studied by Sauer *et al.*[5] in the concentration range 0.1 to 5%Cr: The isomer shift first increases with increasing Cr content,

then tends to decrease when the Cr content exceeds 3%. They explained qualitatively the anomalous isomer shift change in terms of the change in the number of 3d- and 4s-like electrons. Walker *et al.*[9] measured the isomer shift of Fe atom dilutely dissolved in Cr as well as Ni and Co, and interpreted quantitatively in terms of the change in the 4s-like electrons.

These experiments were, however, mostly limited in the narrow concentration ranges, or sometimes were made under different experimental conditions. As will be mentioned in chapter 3, since the practical and industrial problems such as the phase decomposition in the Fe-Cr system spread over a wide concentration range, it is first needed to accumulate fundamental and systematic Mössbauer data in the same wide range of concentration. Present section treats concentration dependences of the internal field and isomer shift in the whole concentration range of the Fe-Cr system, and a computer analysis of Mössbauer spectra considering the effect of the local environment around Fe atoms.

1.2 Experimental procedure

a. Sample preparation and Mössbauer effect measurement

Cr contents of specimens used in the present study are compiled in Table 1.1. Specimens with x=0.21, 0.287, 0.363 and 0.556 were prepared from electrolytic iron with 99.95% purity and electrolytic chromium with 99.97% purity by using an electrical induction furnace in vacuo. Others were melted in an electrical arc furnace in an argon atmosphere by using electrolytic iron with 99.999% purity and electrolytic chromium with 99.97% purity as raw materials. Specimens with the Cr content $x \leq 0.7$ were first

Table 1.1 Chromium content x of specimens used.

No.	x	*	No.	x	*	No.	x	*	No.	x	*
1	0.028	c	11	0.363	c	21	0.668	a	31	0.867	a
2	0.050	c	12	0.377	c	22	0.695	a	32	0.894	a
3	0.078	c	13	0.405	c	23	0.705	a	33	0.905	a
4	0.102	c	14	0.416	c	24	0.711	a	34	0.910	a
5	0.133	c	15	0.503	c	25	0.767	a	35	0.932	a
6	0.153	c	16	0.556	c	26	0.803	a	36	0.941	a
7	0.179	c	17	0.571	c	27	0.813	a	37	0.966	a
8	0.210	c	18	0.590	c	28	0.827	a	38	0.967	a
9	0.287	c	19	0.626	c	29	0.845	a	39	0.990	a
10	0.315	c	20	0.639	a	30	0.864	a	40	0.994	a

*a; by atomic absorption spectroscopy, c;by chemical analysis

hot-rolled at temperatures around 1400K, then rolled at room temperature down to 0.02mm in thickness. Others, being brittle, were ground into powders with metallic files following to the compositional homogenization-annealing at 1500K for 173ks(48h). Fine powders passed through a 400 mesh sieve were used as Mössbauer absorbers. These foils and powders, the latter being sealed into a silica tube, were finally heated in vacuo to a temperature range of 1000 to 1300K where only α-phase exists in equilibrium, and then quenched into iced water. The tube was crushed at the moment immersed into the water. As a Mössbauer source, 1.11 GBq (30mCi) ^{57}Co plated onto a Rh foil was used. The source velocity was changed in a saw-tooth wave with a constant acceleration mode ranging from -10 to 10 mm/s in the case of the whole spectrum measurement, and -2 to 2 mm/s in the case of the partial spectrum measurement. Before and after the measurement on each alloy specimen, pure iron containing more than 90% of ^{57}Fe was measured to check the velocity reliability, which proved that a fluctuation of velocity axis was within ±one channel.

b. Computer calculation of the Mössbauer spectrum

In the computer calculations of Mössbauer spectra to see the local environment effect, the effect of Cr atoms in the first two coordination shells on a central Fe atom is considered. The measured spectrum is regarded as the superposition of 63 spectra with the internal field,[3)]

$$H(m,n)=H_0-am-bn, \tag{1.1}$$

and the isomer shift,

$$IS(m,n)=d(H(m,n)-H_p), \tag{1.2}$$

for an Fe atom with m nearest neighbour (nn) and n next nearest neighbour (nnn) Cr atoms. Here H_p is the internal field of pure iron at room temperature: -26.5MA/m(333kOe). Other parameters, $H_0, a, b,$ and d are determined to give the best fit of the calculated spectra to the experimental data by computing the values of the mean square deviation, $\Sigma\rho^2$. Relative amplitudes of the component spectra are assumed to be given by the binomial distribution,

$$P(m,n)={}_8C_m\ {}_6C_n x^{m+n}(1-x)^{14-m-n}. \tag{1.3}$$

1.3 Results and discussion

1.3.1 General aspects of the Mössbauer spectrum

Experimental Mössbauer spectra for various alloys are shown by dots in Figs.1.1(a) through (f) after the background expressed by a quadratic equation is subtracted from raw data. Solid lines stand for spectra synthesized by a computer to examine the environmental effect. These are the examples among eleven specimens studied ranging from x=0.05 to x=0.65. Even if x is varied in such a wide range, good fit of the calculation to the

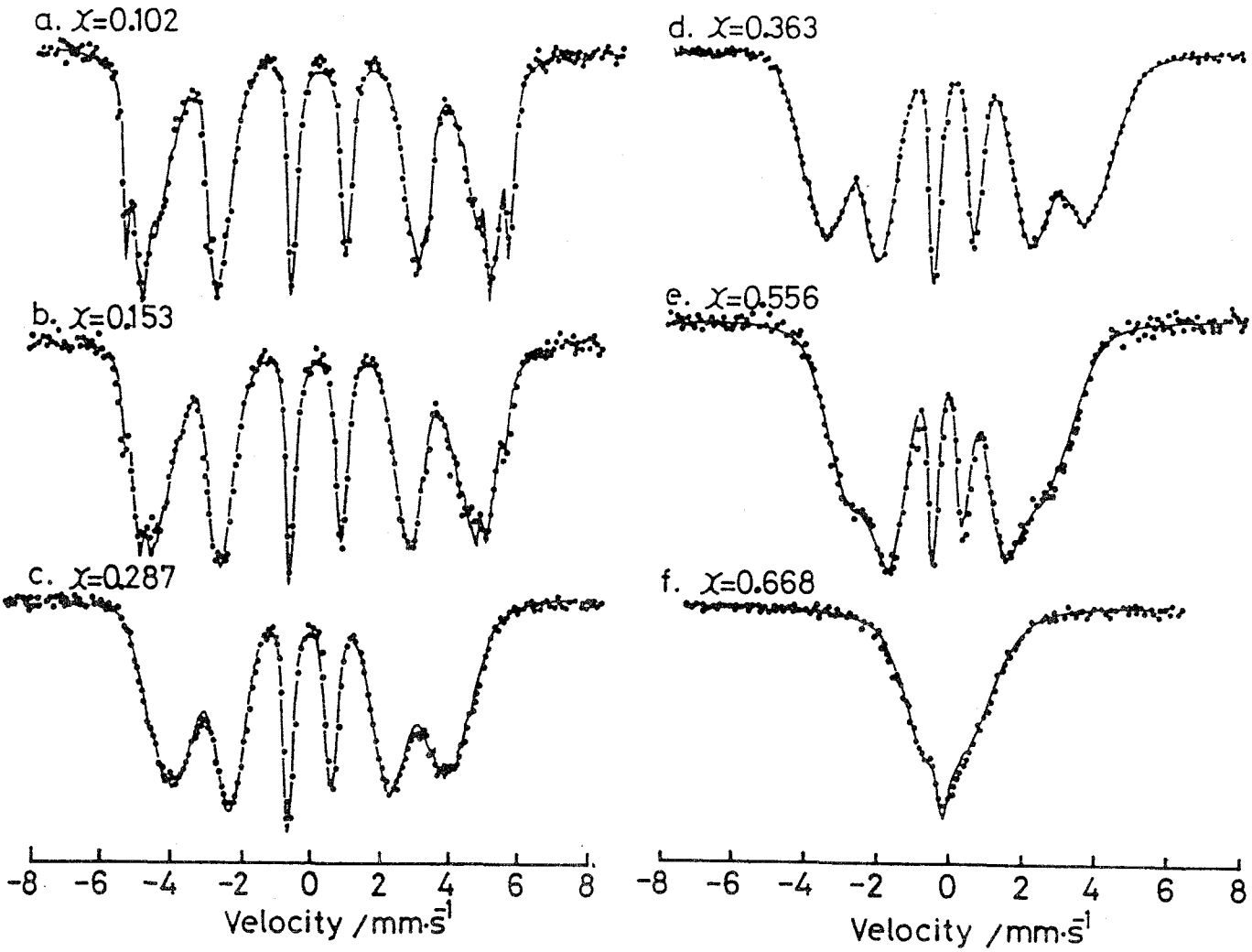

Fig.1.1 Experimental Mössbauer spectra(dot) obtained at room temperature and spectra synthesized(solid line) by a computer to see the local environment effect for various $Fe_{1-x}Cr_x$ alloys.

experimental data is obtained with a careful selection of parameters in eq.(1.1). The half width, Γ, of a Lorentzian curve and the isomer shift coefficient, d, in eq.(1.2) are iteration parameters in addition to H_0, a, and b. But, they scarcely depend upon x within the limit tried: Γ=0.27mm/s, d=9.7x10^{-3}mm s^{-1}/MAm^{-1}(7.7x10^{-4} mm s^{-1}/kOe). For the alloys with $x \leq 0.153$, rather poor fits are observed for the outermost peaks than the inner peaks. For the higher Cr content alloys with $x \geq 0.287$, the fit between the calculation and the experimental points is satisfactory. Nys and Gielen[10] reached

to a conclusion that the computation method holds for dilute Cr contents, because their calculated spectrum for the Fe-30%Cr alloy agreed little with the experimental data. This was a natural result because they used parameters for dilute Cr alloys and ignored its concentration dependence. Parameters , H_0 , a, and b, which give the best fit to the experimental spectrum within the limit calculated are shown in Fig.1.2 as a function of x. In the concentration range $0.05 \leq x \leq 0.57$, H_0 is substantially independent of x: $H_0 = -26.7 \pm 0.1$MA/m(335 ± 1kOe). In the concentration range $0.57 \leq x \leq 0.64$, H_0 is given by an empirical equation,

$$H_0 / \mathrm{MA\,m^{-1}} = -73.7x + 67.5 . \qquad (1.4)$$

Values of a, b are also independent of x in the concentration range $x \geq 0.2$: $a = 2.06 \pm 0.02$MA/m(25.9 ± 0.3kOe), $b = 1.47 \pm 0.01$ MA/m (18.5 ± 0.2kOe). Percent decrease of the internal field relative to the value of pure iron is about 7.8% and 5.5% per single Cr atom in the nn and nnn shell, respectively. It should be noted that, as far as the effect on the magnitude of the internal

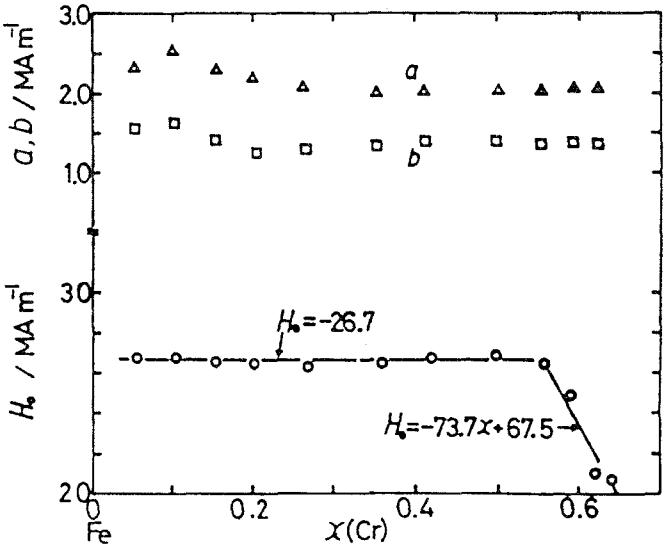

Fig.1.2 Parameters, a, b, and H_0, in eq.(1.1) as a function of Cr content for the room-temperature Mössbauer spectrum of the Fe-Cr alloy.

field is concerned, single Cr atom in the nn shell is equivalent to 1.4 Cr atoms in the nnn shell. Schwartz and Chandra[6] obtained 8.1% and 6.8% of the percent decrease of the internal field per single Cr atom in the nn and the nnn shell, respectively, for alloys with x =0.24 to x =0.60. These values are slightly larger than those obtained here. Since their resultant synthesized spectra showed poorer fit to the experimental ones than those calculated here, present results are more favorable. As seen in Fig.1.1(f), the paramagnetic component in the spectrum increases rapidly when x exceeds 0.6, because the Curie temperature approaches to the room temperature[11]. These rapid changes in the spectrum are ascribed to the sharp decrease in H_0, according to Fig.1.2. It should be emphasized that, since parameters in eqs.(1.1) and (1.2) are substantially constant in the concentration range $0.2 \leq x \leq 0.57$, Mössbauer spectra are uniquely calculable, if the Cr contents are known and the random distribution of constituents atoms is assumed to be given by eq.(1.3). This is one of the greatest advantage of the computational method in practical use to synthesize the Mössbauer spectra of the decomposed alloys, as mentioned in §4.

1.3.2 Concentration dependence of the internal field

The mean internal field $\bar{H}$ at ^{57}Fe in various alloys is evaluated from the interval between the second and the fifth absorption peaks of the ferromagnetic Mössbauer spectrum. Full circles in Fig.1.3 show the values of $\bar{H}$ thus obtained at room temperature. An empirical relation,

$$\bar{H}/\mathrm{MA\,m^{-1}} = 21.3x - 26.5, \qquad (1.5)$$

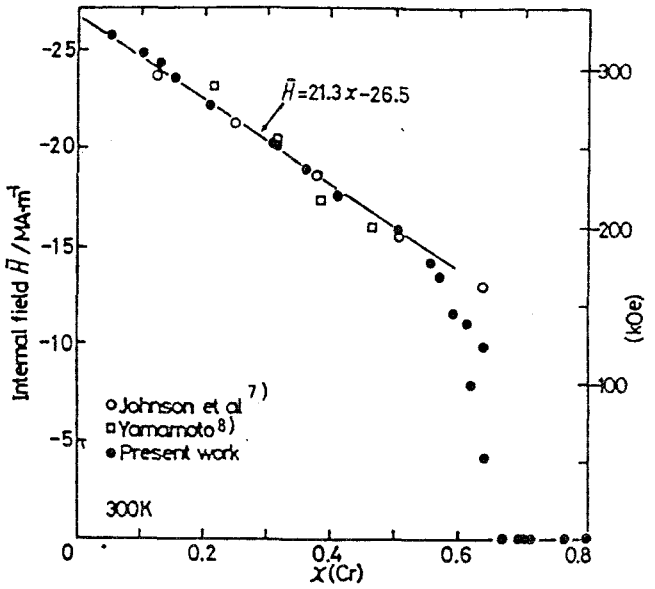

Fig.1.3 Concentration dependence of $\bar{H}$ measured at room temperature for $Fe_{1-x}Cr_x$ alloys

is obtained by the least square fit to the experimental points in the concentration range from x=0 to x=0.56, as drawn by the solid line in the figure. Values of $\bar{H}$ deviate sharply from eq.(1.5) when x exceeds 0.60, because the Curie temperature of the Fe-Cr alloy locates near the room temperature around x=0.7. The alloys are paramagnetic at room temperature for $x \geq 0.67$. Values published by Johnson *et al.*[7] (open circles) agree very well with the present results except for the point at x=0.63. Those obtained by Yamamoto[8] (cubics) show a slight departure from eq.(1.5). The accuracy for measuring $\bar{H}$ is estimated about ±0.16MA/m(2kOe) for the present measurement. One can, therefore, evaluate the unknown Cr content with an accuracy of ±0.01, if $\bar{H}$ is known, on the assumption of the random distribution of the constituent atoms.

Figure 1.4 shows the mean internal filed, $\bar{H}$, obtained at 4.2K as a function of x. Present results marked by open circles are in accord with those obtained by Johnson *et al.*[7] (full circles) and by Herbert *et al.*[12] (triangles). An empirical equation,

$$\bar{H}/\mathrm{MA\,m^{-1}} = 18.7x - 26.8, \qquad (1.6)$$

is obtained by the least square method in the concentration range $0 \leq x \leq 0.85$. In general, $\bar{H}$ is related to the atomic magnetic moment by an empirical expression,

$$\bar{H} = \alpha \mu_{Fe} + \beta \bar{\mu}, \qquad (1.7)$$

where $\bar{\mu}$ is the average atomic magnetic moment which is given by

$$\bar{\mu} = (1-x)\mu_{Fe} + \mu_{Cr} + \mu_0 . \qquad (1.8)$$

Here μ_{Fe}, μ_{Cr}, and μ_0 are the magnetic moment of Fe atoms, that of Cr atoms and that associated with conduction electrons, respectively. According to Lander and Heaton,[13] μ_0 is assumed as

$$\mu_0 = -0.1\,\bar{\mu} . \qquad (1.9)$$

The coefficients, α and β, are evaluated by substituting the experimental value of $\bar{\mu}$ obtained by the magnetization measurement[14] and those of μ_{Fe} and μ_{Cr} by the neutron diffraction experiment[15] into eqs.(1.7) to (1.9): $\alpha = -5.7\,\mathrm{MA\,m^{-1}}/\mu_B$, $\beta = -6.3\,\mathrm{MA\,m^{-1}}/\mu_B$. The dashed line in Fig.1.4 is the calculated result of eq.(1.7) by using these values. According to the susceptibility measurement[6] on Cr-Fe alloys of the concentrations x=0.95 to 0.98, iron atoms have the localized magnetic moment of $1.4\,\mu_B$, then eq.(1.7) suggests that $\bar{H}$ of more

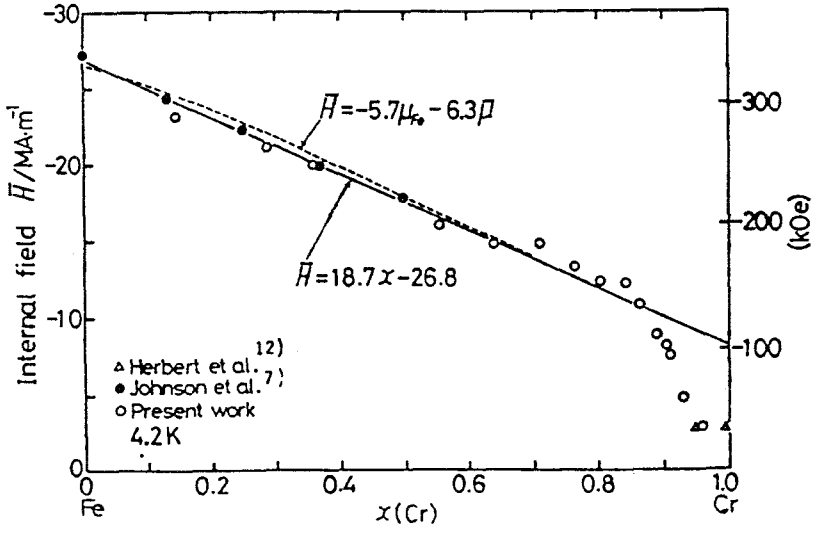

Fig.1.4 Concentration dependence of $\bar{H}$ measured at 4.2K for $Fe_{1-x}Cr_x$ alloys.

than -8MA/m(100kOe) should be measured at 4.2K. The extrapolation of eq.(1.6) to x=1.0 yields the similar result as eq.(1.7). However, the experimentally obtained value is at most -2.8MA/m (35kOe)[12] for $x \geq 0.95$. Therefore, it is concluded that most Fe atoms are not ferromagnetic in the dilute Cr-Fe alloys at low temperatures. Details will be discussed in §2.

1.3.3 Concentration dependence of the isomer shift

Figure 1.5(a) shows the innermost two peaks of the ferromagnetic Mössbauer spectra measured at room temperature for the alloys with $x \geq 0.05$. The average isomer shift, IS , of ^{57}Fe in these alloys is determined at the center of gravity of these two peaks, the center of which being measured at the intermediate point of the full width of the half maximum(FWHM). Fig.1.5(b) shows single peaks measured at room temperature for paramagnetic alloys with $x \geq 0.695$. The values of IS of these alloys are determined at the intermediate point of the FWHM of these single peaks. Measurements were carried out twice on a single specimen. The deviation of the measured values from the average was within ±0.002mm/s. As seen in Fig.1.6, IS decreases linearly with decreasing x in the concentration range from x=0.15 to 1.0, being expressed by an empirical equation,

$$IS = -0.145x \, . \qquad (1.10)$$

It should be noted that the relation is available for the determination of the unknown Cr content of Fe-Cr alloys, in particular, in the concentration range $x \geq 0.7$ where eq.(1.5) is unavailable. The concentration dependence is interpreted in terms of the contribution of (a) 4s-like electrons and (b) 3d-like electrons.

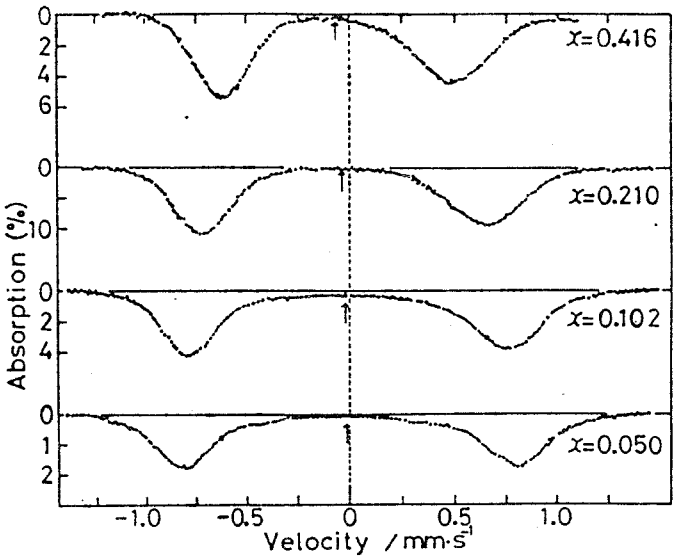

Fig.1.5a Innermost two peaks of Mössbauer spectra of ferromagnetic $Fe_{1-x}Cr_x$ alloys at room temperature. Arrows indicate the center of gravity of two peaks.

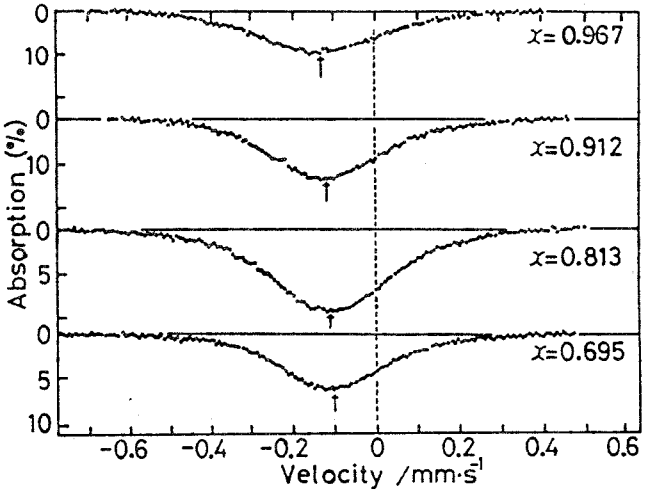

Fig.1.5b Mössbauer spectra of paramagnetic $Fe_{1-x}Cr_x$ alloys at room temperature. Arrows indicate the center of peaks determined at the intermediate point of the FWHM.

a. Contribution of 4s-like electrons

The isomer shift, IS, is directly related with the total electron density, $\rho(0)$, at Fe nuclear site with an expression,[17]

$$IS = -\gamma \rho(0), \tag{1.11}$$

where γ is a calibration factor(=0.386 a.u.mm/s). Assuming that

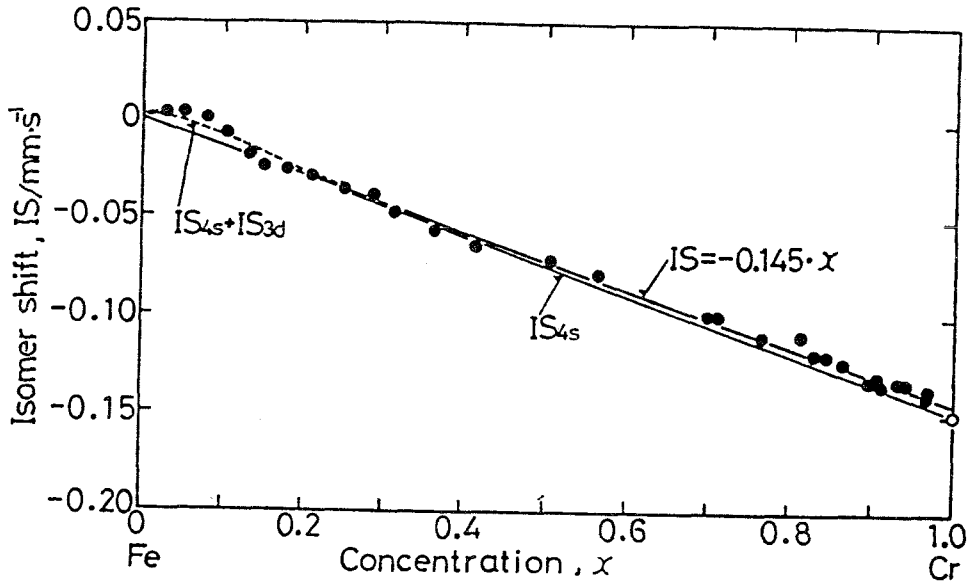

Fig.1.6 Concentration dependence of the internal field, IS, of ^{57}Fe measured at room tempearture for $Fe_{1-x}Cr_x$ alloys.

the addition of Cr atoms to Fe metal has little effect on the density of inner core s-electrons at Fe nuclei, the change in $\rho(0)$ is mainly attributable to the change in 4s-like electron density. According to Walker *et al*.[9], the isomer shift associated with the change in the number of 4s-like electrons Δn_{4s} is given by

$$IS_{4s} = -1.5\,\Delta n_{4s} \qquad (1.12)$$

for the $3d^7 4s^1$ configuration. Comparison of eq.(1.12) with eq.(1.10) leads to a conclusion that concentration dependence of Δn_{4s} should be given by

$$\Delta n_{4s} \simeq 0.1\,x\,. \qquad (1.13)$$

Thus the isomer shift change due to the addition of Cr atoms to Fe matrix is mainly interpreted in terms of the increase of 0.1 4s-like electrons per Cr atom.

b. Contribution of 3d-like electrons

The experimental data for IS deviate positively from the extrapolation of eq.(1.10) to $x=0$ in the vicinity of $x=0.1$, where the magnetic moment of Fe atoms has a maximum as a function of x.[15]

These experimental features may be closely related with the 3d-band structure as suggested in the CPA calculation.[1] Because 3d-electrons screen the nuclear charge against outside 4s-electrons, they may indirectly contribute to the isomer shift; the increase in 3d-electrons results in the decrease in 4s= electron density at nucleus, which means the increase in the isomer shift. The CPA calculation points out that the addition of Cr atoms to Fe metal increases 3d-electrons in the concentration range $x \leq 0.2$. According to Walker *et al.*[9], the contribution of 3d-electrons to the isomer shift is given by

$$IS_{3d} \approx 0.2\ \Delta n_{3d} \qquad (1.14)$$

for the $3d^7$ configuration. A dotted line in Fig.1.6 stands for the sum of terms of IS_{4s} and IS_{3d} in which the values of Δn_{3d} are quated from the CPA calculation.[1] It is evident that the positive deviation of the isomer shift from eq.(1.10) is attributable to the contribution of the 3d-electrons.

1.4 Conclusion

1. The local environmental effect approximation accounts for very well the concentration dependence of the Mössbauer spectrum of Fe-Cr solid solutions quenched from 1000K to 1300K. An empirical equation for the internal field, $H(m,n)=H_0-am-bn$, for an Fe atom with m and n Cr atoms in the first and the second nearest shell holds for the whole concentration range studied from x=0.05 to x=0.65. Parameters obtained at room temperature are shown in Fig.1.2.

2. The mean internal field, $\bar{H}$, changes linearly with increasing

Cr content, being expressed by an empirical relation, $\bar{H}/\mathrm{MAm}^{-1}=21.3x-26.5$, in the concentration range from $x=0$ to $x=0.56$ at room temperature, and $\bar{H}/\mathrm{MAm}^{-1}=18.7x-26.8$ in the concentration range from $x=0$ to $x=0.85$ at 4.2K.

3. The mean internal field, $\bar{H}$, at 4.2K measures the change in the localized magnetic moment of Fe atom μ_{Fe} and the average magnetic moment $\bar{\mu}$ as a function of Cr content, being expressed by an empirical equation, $\bar{H}/\mathrm{MAm}^{-1}=-5.7\mu_{Fe}-6.3\bar{\mu}$.

4. The isomer shift, IS, obtained at room temperature decreases linearly with increasing x, being expressed by an empirical equation, $IS/\mathrm{mms}^{-1}=-0.145x$. The isomer shift change is mainly attributable to the change in the 4s-like electrons at Fe atom sites. Deviation of the experimental isomer shift from the above relationship is interpreted in terms of the contribution of 3d-like electrons.

References

1) H.Hasegawa and J.Kanamori: J.Phys.Soc.Japan 33(1972) 1607.
2) C.G.Shull and M.K.Wilkinson: Phys.Rev. 97(1955) 304.
   G.H.Lander and L.Heaton: J.Phys.Chem.Solids 32(1971) 427.
3) G.K.Wertheim,V.Jaccarino,K.H.Wernick and D.N.E.Buchanan: Phys.Rev.Letters 12(1964) 24.
4) I.Vincze and I.A.Campbell: J.Phys.F:Metal Phys. 3(1973) 647.
5) W.E.Sauer and R.J.Reynik: *Mossbauer Effect and Methodology* (vol.4,Plenum Press,New York, 1968) 201.
6) L.H.Schwartz and D.Chandra: Phys.Stat.Sol.(b) 45(1971) 201.
7) C.E.Johnson,M.S.Ridout and T.E.Cranshaw: Proc.Phys.Soc. 81 (1963) 1079.
8) H.Yamamoto: Japan J.Appl.Phys. 3(1964) 745.

9) J.L.Walker,G.K.Wertheim and V.Jaccarino:Phys.Rev.Letters 6 (1961) 98.
10) T.De Nys and P.M.Gielen: Metallurg. Trans. 2(1971) 1423.
11) M.Hansen: *Constitution of Binary Alloys*(McGraw-Hill Company New York, 1958) 526.
12) I.R.Herbert,P.E.Clark and G.V.H.Wilson: J.Phys.Chem.Solids 33(1972) 979.
13) G.H.Lander and L.Heaton: J.Phys.Chem.Solids 32(1971) 427.
14) A.T.Aldred: Phys.Rev.B 14(1976) 219.
15) A.T.Aldred,B.D.Rainford,J.S.Kouvel and T.J.Hicks: *ibid.* 32 (1976) 228.
16) Y.Ishikawa,R.Tournier and J.Filippi: J.Phys.Chem.Solids 26 (1967) 1727.

§2 Magnetic properties of Cr-rich iron-chromium solid solutions

2.1 Introduction

The magnetic structure of Cr-Fe alloys varies sensitively with the change of iron content in the relatively dilute concentration range. For instance, when the iron content, X, is less than 0.02, a transition from paramagnetic(P) to incommensurable spin density wave state(I) occurs on cooling through a Néel temperature, T_N.[1-3] When X exceeds 0.023, the commensurable spin density wave state(C) exists stably instead of I phase below T_N. There is a characteristic triple point near the iron content X=0.02, where P-, I- and C-state coexist.[3,4] It is of interest to study the magnetic behavior of Fe atoms with the change in the magnetic structure of Cr matrix by using the Mössbauer effect which is highly sensitive to the local environment around Fe atoms.

According to susceptibility measurement on Cr-Fe alloys of the concentration X=0.02 to X=0.05, Fe atoms have an effective magnetic moment of 2.2 to 2.5 μ_B below T_N.[5] If the magnitude of magnetic moment remains unchanged even at low temperatures, the internal field about -8MA/m(100kOe) should be measured at Fe nuclei in the Mössbauer effect experiments. However, experimental values were at most -2.8MA/m(35kOe)[6-8] at 4.2K. There has been controversy on this subject. Herbert *et al*.[7] interpreted the small internal field in terms of the spin compensated state which is partially destroyed by the exchange field acting on the iron atom sites from the spin density wave of the Cr matrix.

In the Cr-Fe alloys of the concentration less than X=0.015, Katano and Môri[9] have confirmed a resistivity minimum which is

interpreted as an evidence for the Kondo effect. But the resistivity minimum was not detected for the more concentrated Fe samples, presumably because of the interference of the increased Fe atom clusters. In the concentration range, X=0.04 to X=0.4, the hyperfine field distribution has been studied using the Mössbauer effect by Shiga and Nakamura[10], who concluded that there are two states of iron atoms with a high internal field about 7.96MA/m (100kOe) or more and a low internal field about 2.8MA/m(35kOe), which are termed as magnetic and nonmagnetic Fe atoms, respectively. The latter was attributed to isolated Fe atoms, and was interpreted in terms of the Kondo effect. A Mössbauer effect study for the more dilute Fe content alloy and a measurement of the temperature dependence of the internal field are required for better understanding of the magnetic behavior of the Fe atoms. In the present section, systematic and detailed Mössbauer measurements on temperature dependence of the ^{57}Fe internal field are performed for the Cr-Fe alloys with X=0.006 to X=0.186. (It should be noted that the iron content, X, is described instead of the Cr content, x, in the present section, because the magnetic behavior of Fe atoms is of interest.)

2.2 Experimental procedure

By using an electric-arc furnace, 99.999% electrolytically pure chromium and 99.97% electrolytically pure iron were melted in an argon atmosphere to yield about 2 grams of net weight. Iron metal enriched to more than 90% in ^{57}Fe was appropriately added to the specimens to get good Mössbauer spectra. In order to ensure sufficient compositional homogeneity, specimens were

remelted three times followed by annealing at 1400K for 173ks (48h). The annealed specimens were filed to get fine powder to pass through a 400 mesh shieve. Hence, the mean diameter of the powder used was estimated as smaller than 40 μm. Ferromagnetic inclusions introduced through the filing process were removed carefully with a magnet. Powder samples sealed into an evacuated silica tube were annealed at 1273K for 3.6ks followed by quenching into iced water. The tube was crushed as soon as it was immersed into the water. Mössbauer spectra in the temperature range from 10K to 300K were obtained by using a CSA-202 cryogenic refrigeration system of Air Products and Chemicals, Inc., which controlled temperature within a fluctuation of ±0.5K by a combination of cold helium gas flows and an electric heater. Spectra in the temperature range from 1.7K to 4.2K were obtained with a conventional cryostat by pumping liquid helium. The temperature, 0.03K, was attained by adiabatic demagnetization of paramagnetic salt, KCr-alum. The latter two experiments were made at ISSP of the University of Tokyo.

Mössbauer spectra are numerically analyzed to see the local environmental effect by using a computer. A calculated spectrum is generally represented by the superposition of 63 spectra with the internal field,[11]

$$H(m,n)=H_{Fe}^{0}(1-am-bn)(1+c) \quad . \qquad (2.1)$$

Here m and n are the number of Cr atoms in the first and the second neighbouring shell, respectively, and H_{Fe}^{0} the internal field of pure iron at 0K, H_{Fe}^{0}=-27MA/m(340kOe). The relative amplitudes of the composite spectrum with $H(m,n)$ are given by the binomial distribution(eq.(1.3)). Representative values of

$P(m,n)$ calculated by eq.(1.3) are tabulated in Table 2.1 as a function of iron content. In the concentration range, $X<0.068$, an iron atom configuration with $m=8$ and $n=6$ (hereafter Fe(8,6) atom) occurs with a rather high probability compared with others, so that Fe(8,6) atoms can be distinguished from other configurations with a high certainty. Hence, in the later calculation and discussion, iron atoms in the matrix are classified into two groups:(1) Fe(8,6) atoms and (2) Fe(r) atoms which include all other Fe atom configurations with $m+n<14$.

Table 2.1 Probability, $P(m,n)$, of finding m nearest and n next nearest neighbours.

$p(m,n)$	X(Fe)						
	0.006	0.01	0.033	0.059	0.068	0.095	0.133
$p(8,6)$	0.932	0.870	0.625	0.427	0.373	0.247	0.136
$p(8,5)$	0.028	0.052	0.128	0.161	0.163	0.155	0.125
$p(7,6)$	0.038	0.07	0.171	0.214	0.218	0.208	0.166
$p(7,5)$				0.081	0.095	0.131	0.153

2.3 Results and discussion

2.3.1 Temperature dependence of the internal field

Mössbauer spectra were measured over a wide temperature range from 1.7K to 300K, and the mean internal field, $\bar{H}$, was eatimated as follows. Theoretical Mössbauer spectra for a variety of internal field values were calculated by superimposing six Lorentzian curves with intensity ratios 3:2:1:1:2:3, using a half width measured from a paramagnetic spectrum. Then, a relation curve was obtained between the full width of the half maximum(FWHM) and the internal field. The FWHM of the experimental spectra was converted into $\bar{H}$ by using the curve, as a rough approximation.

Figure 2.1 shows temperature dependence of $\bar{H}$ for the alloys

with the iron content X=0.006 and 0.010. These results depict clearly two step changes of $\bar{H}$ near the temperatures termed here as T_1 and T_2 . The former is approximately consistent with T_N proposed by many authors.[1,3,9] The gradual increase in $\bar{H}$ below a certain temperature named here nominally as T_3 will be explained in terms of the spin compensated state, as discussed in 2.3.4. The $\bar{H}$ changes saturate at about 20K with a saturation field of -2.2 to -2.4MA/m(27 to 30kOe). As an example, experimental spectra for X=0.006 at three different temperatures are drawn by dots in Fig.2.2. A solid line at the top(**a**) is well fitted by a Lorentzian curve with a half width of 0.35mm/s obtained above T_N. The solid line at the middle(b) is a spectrum calculated as a superposition of six Lorentzian curves with a unique internal field H=-0.44MA/m(5.5kOe), showing a good fit to the experimental data. However, experimental spectra obtained at temperatures lower than T_3(∿140K) including spectrum at 14K(c) can not be represented by a single sextuplet spectrum with a unique internal field, suggesting the existence of the hyperfine field distribution of iron atoms from site to site. Since $P(8,6)$=0.932 for X=0.006 (Table 2.1), the average internal field $\bar{H}$=-2.2MA/m estimated from the FWHM of the experimental spectrum may be safely attributed to the isolated Fe(8,6) atoms. But, the calculated spectrum ((the curve No.1 in Fig.2.2)) for the unique internal field H=-2.2MA/m shows a deviation from the experimental data, in particular, at the vicinity of the spectrum center. This suggests coexitence of the Fe atoms with a lower internal field which should be naturally attributed to the Fe(r) atoms. Trial and error calculations result in the solid curves No.2

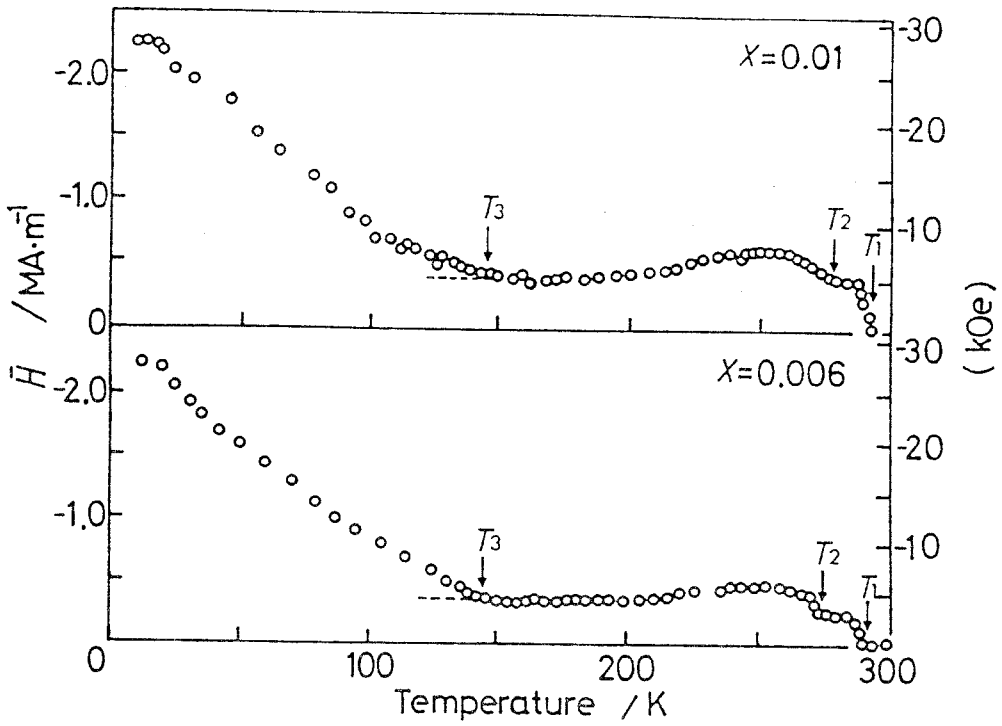

Fig.2.1 Temperature dependence of the mean internal field, $\bar{H}$, for $Cr_{1-X}Fe_X$ alloys with X=0.006 and 0.01.

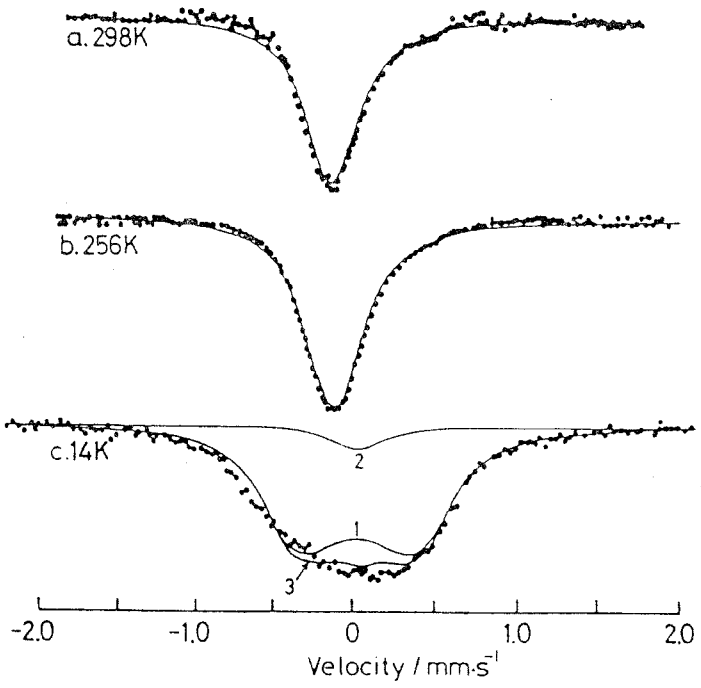

Fig.2.2 Mössbauer spectra measured at several temperature for the alloy with the iron content X=0.006. Solid curves are computer fits assuming a unique internal field: (a) H=0, (b)H=-0.44MA/m(5.5kOe), (c)-1 H= -2.2MA/m(27kOe),(c)-2 H=-0.44MA/m(5.5kOe),(c)-3 curve 1+ curve 2.

with H=-0.44MA/m(5.5kOe) for the Fe(r) atoms. The solid curve No.3 represents the sum of the curve No.1 and the curve No.2, showing a satisfactory agreement with experimental data. A slight disagreement still observed may be due to the rather complex hyperfine field distribution in the ISDW structure of Cr matrix than in the purely antiferromagnetic structure.

The two step changes in $\bar{H}$ are also observed at temperatures 230-280K for the alloy with X=0.033 and X=0.059 in Fig.2.3, for which the P-C phase transition at T_N has been confirmed by several workers.[3,4] These curves show different features with those in Fig.2.1 in two points: (1) the $\bar{H}$ changes around T_2 are much large and sharp in comparison with the lower Fe content samples of Fig.2.1, and the very sharp change may be due to a first order phase change which is accompanied by the appearance of the C-phase.[4,5] (2) $\bar{H}$ shows a rapid increase below a certain temperature named here T_4 which shifts to higher temperatures with increasing Fe content, being roughly coincident with the Curie temperature T_C obtained by the magnetization measurement[17] around X=0.18(Fig.2.6). Thus T_4 is related to the magnetic ordering temperature of the Fe spins. The experimental spectra of X=0.033 measured above T_3(~150K), as well as the case of lower Fe content alloys, are interpreted as that iron atoms have a single internal field as shown in Fig.2.4. The solid lines are calculate with H=0 for T=290K, H=-0.4MA/m(5kOe) for T=252K and H=-0.96MA/m(12kOe) for T=232K. There is an internal field distribution at the Fe nuclei at temperatures lower than T_3 (Fig. 4.2(d)). Solid curves No.1 and No.2 are the calculated spectra with H=-2.46MA/m (31kOe) for Fe(8,6) atoms and H=-1.35MA/m

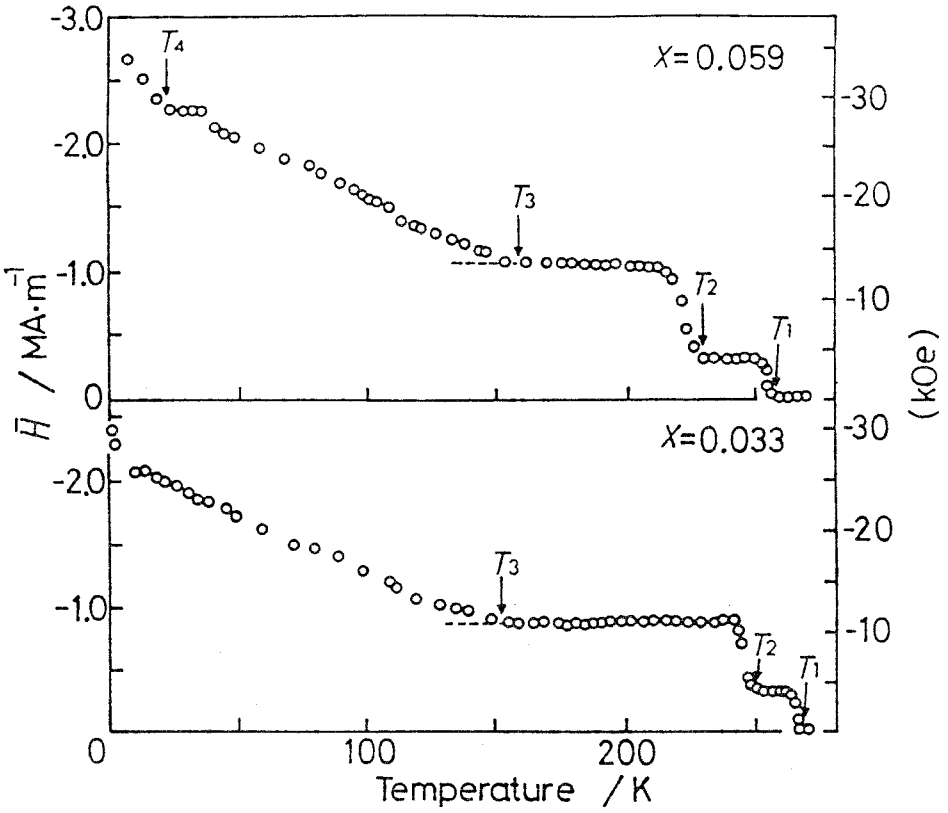

Fig.2.3 Temperature dependence of the mean internal field, $\bar{H}$, for $Cr_{1-X}Fe_X$ alloys with the iron content X=0.033 and 0.059.

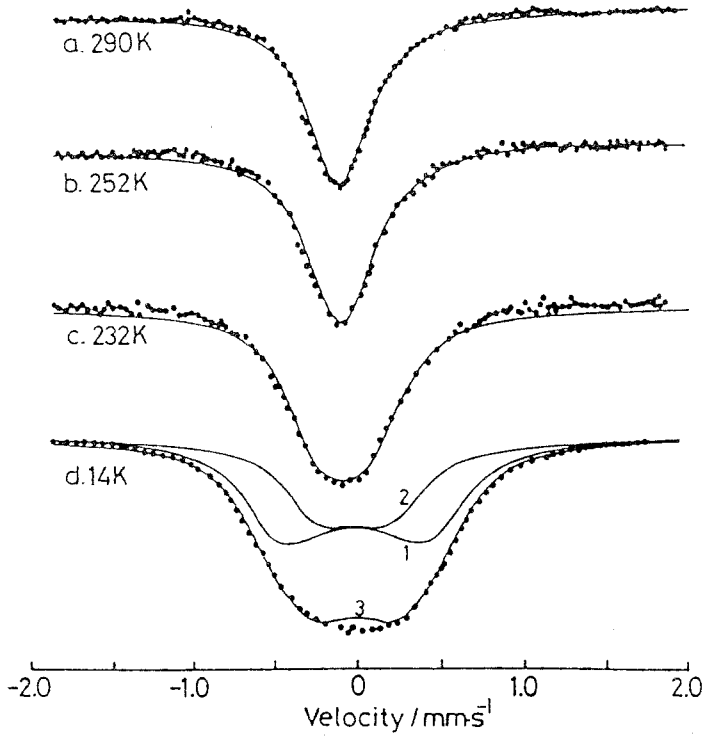

Fig.2.4 Mössbauer spectra measured at various temperatures for the alloy with X=0.033. Solid curves are computer fits assuming a unique internal field: (a) H=0, (b) H=-0.4MA/m(5kOe), (c) H=-0.96MA/m(12.1kOe), (d)-1 H = -2.46MA/m(31kOe), (d)-2 H=-1.35MA/m(17.6kOe), (d)-3 curve 1+curve 2.

(17.6kOe) for Fe(r) atoms, respectively. The solid curve No.3 represents the sum of these two, and agrees very well with the experimental data. In comparison with the case of X=0.006 (Fig.2.2 (c)), a better agreement between the calculation and the experiment may be due to the rather simple internal field distribution in this alloy which has a purely antiferromagnetic structure at low temperatures. If the temperature is further lowered below 14K, the whole aspect of the spectrum changes very little as shown in Fig.2.7(a), and the internal field of the Fe(8,6) atoms also changes little with the value H=-2.4MA/m(30kOe) at 1.7K. These facts indicate that, in the concentration ranges $X \leq 0.033$, the internal field of the isolated Fe atoms is substantially independent of temperature when $T \leq 14$K, and also independent of Fe content.

As a representative example of further Fe concentrated alloys, the result for X=0.095 is shown in Fig.2.5. The $\bar{H}$ change

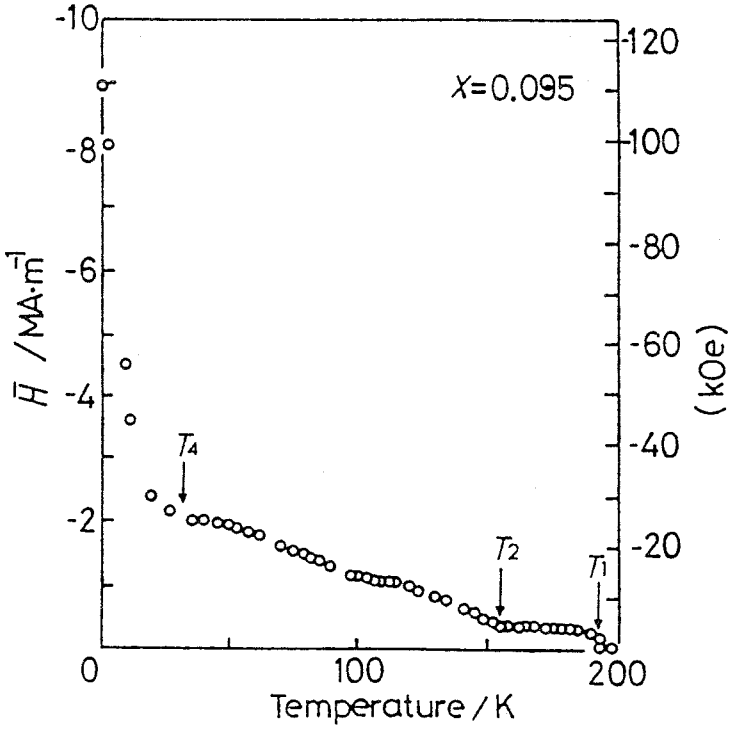

Fig.2.5 Temperature dependence of the mean internal field, $\bar{H}$, for the alloy with X=0.095.

just below T_2 is very slow and may be termed as a second order phase change, which is consistent with the result of AC calorimetry[4]. The $\bar{H}$ change just below T_4 is very sharp, and the spectrum corresponding to Fe(r) atoms(Fig.2.7(c),No.2 curve) exhibits a six-peak appearance which is characteristic of the ferromagnetic iron atoms. The average internal field $\bar{H}$ at 1.7K for the alloy lies on the line of eq.(1.6) extrapolated from the ferromagnetic $Cr_{1-X}Fe_X$ alloy region for $X \geq 0.15$(Fig.2.8).

2.3.3 Magnetic transition temperatures

Transition temperatures, T_1, T_2, and T_4, are plotted in Fig.2.6 as a function of iron concentration to compare with the Néel temperature, T_N, and the Curie temperature, T_C, determined by many other different methods. There two trends in the concentration dependence of T_N reported hitherto: electrical resistivity measurements by Katano and Môri(▽)[9], Arajs(△)[12] and Loegel(◑)[13] have reported Néel temperatures higher about 20K than those by X-ray diffraction by Mori *et al.*(□)[3], AC calorimetry by Suzuki(○)[4] and electrical resistivity by Arajs(⊠)[14]. This discrepancy may be due to experimental conditions such as sample preparation, and the experimental method how to determine T_N. However, the present study confirms clearly two transition temperatures T_1 and T_2 in the same sample, which are coincident with the higher and the lower temperatures of T_N, respectively mentioned above. Although many recent studies support that single crystals undergo the P-I transition in the concentration range of less than X=0.02 and the P-C transition in more than X=0.025, respectively, there are some reports which have proved the existence of the

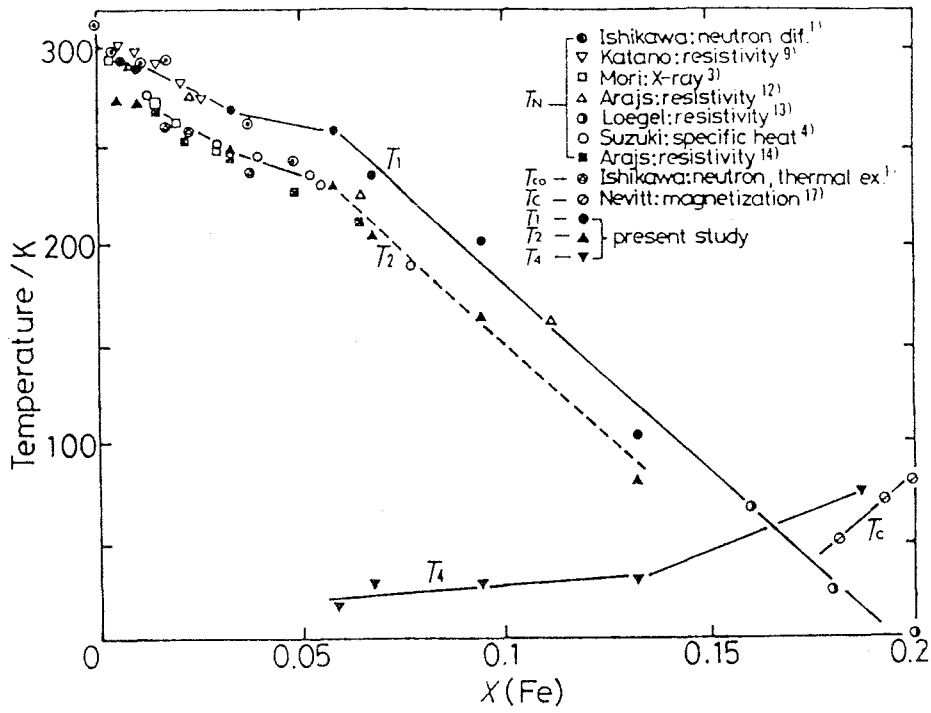

Fig.2.6 Magnetic transition temperatures as a function of the iron content.

two-stage transition such as P-C-I or P-I-C. In single crystals prepared by the strain annealing method, Ishikawa *et al.*[1] have confirmed by neutron diffraction and thermal expansion measurements that the P-I and I-C phase transition takes place at T_N (◉) and T_{Co} (◬), respectively, in the iron content X=0.02 to 0.04. Edwards and Fritz[15] have observed the P-I-C transition for a single crystal with X=0.028 under the application of hydrostatic pressure. In addition, Bacon *et al.*[16] have found the P-C-I transition for coarse powder of pure chromium annealed at 1263K after being heavily crushed. These experiments suggest that the history of sample preparation or the existence of strain affect considerably the magnetic transition of pure Cr and Cr-Fe alloys. In the present study, two transition temperatures, T_1 and T_2, are clearly detected in the wide concentration ranges from X=0.006 to X=0.133. The result shows that the magnetic phase transition

of P-C-I and P-I-C take place for the case of fine powder with the Fe content $X<0.01$ and $0.03<X\leq0.133$, respectively.

2.3.3 Internal field at low temperatures

In Fig.2.7, experimental spectra observed at 1.7 K are shown by dots for several alloys. Values of the mean internal field $\bar{H}$ estimated from the FWHM of these spectra are designated by open circles in Fig.2.8. The dotted line stands for an extrapolation of the empirical relation(eq.(1.6)),

$$\bar{H}(\mathrm{MA/m})=18.7(1-X)-26.8.$$

which is obtained in the previous section for the concentration range $0.15\leq X\leq 1.0$, where most parts of the iron atoms behave ferromagnetically at 4.2K. Present data show a large deviation from the equation when X is less than 0.07. According to the recent idea proposed by Friedel and Hedman[18], closely paired iron

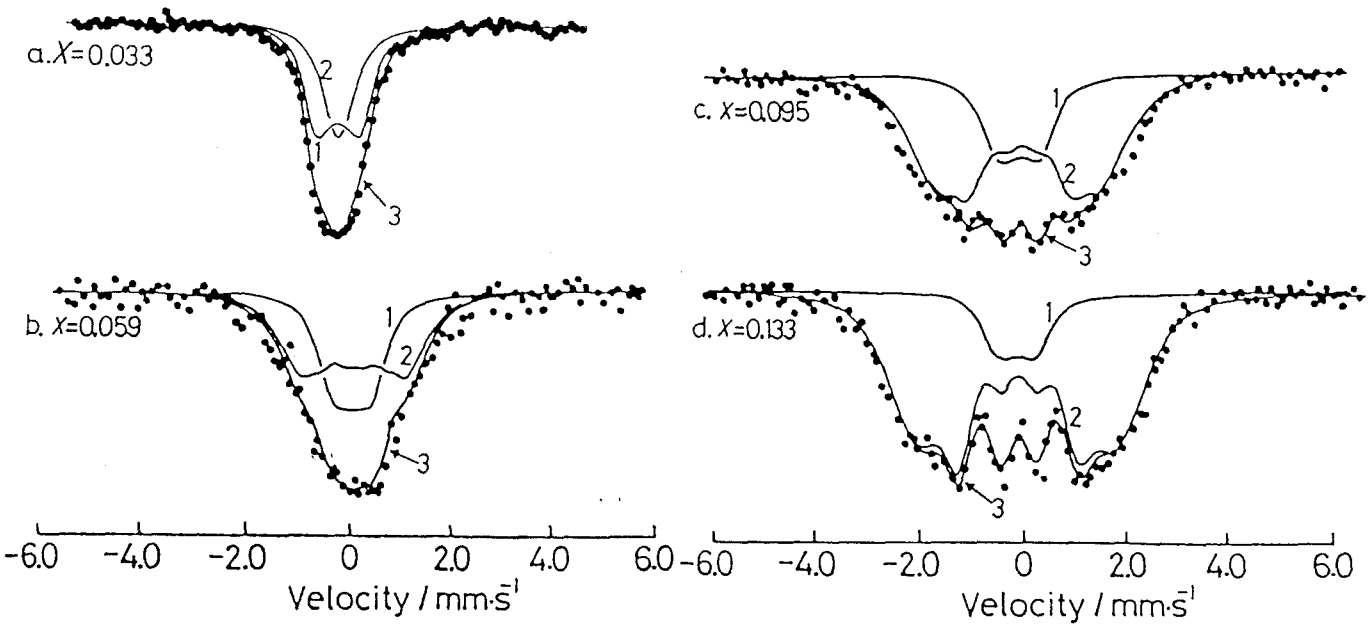

Fig.2.7 Mössbauer spectra measured at 1.7K for $Cr_{1-X}Fe_X$ alloys. Solid curves 1 and 2 are computer fits for the Fe(8,6) and the Fe(r) atom configurations, respectively. The curve 3 is a sum of the curve 1 and the curve 2.

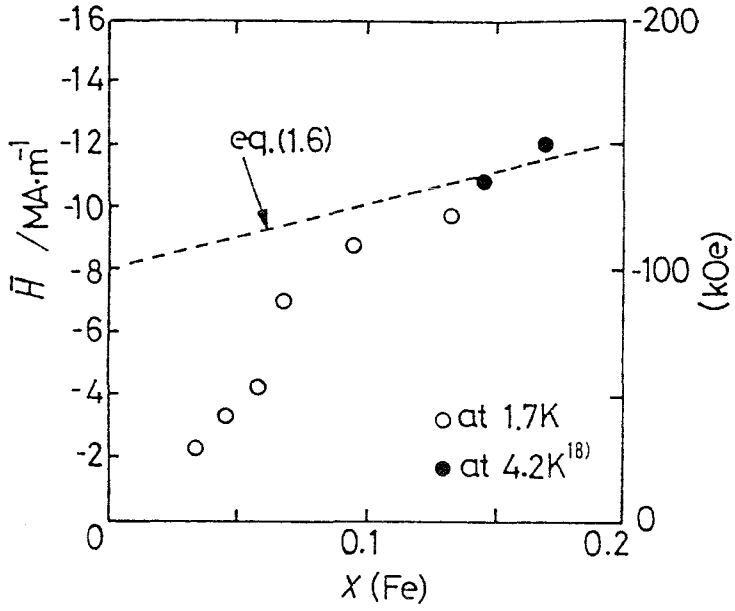

Fig.2.8 The mean internal field, $\bar{H}$, at 1.7K as a function of the iron content.

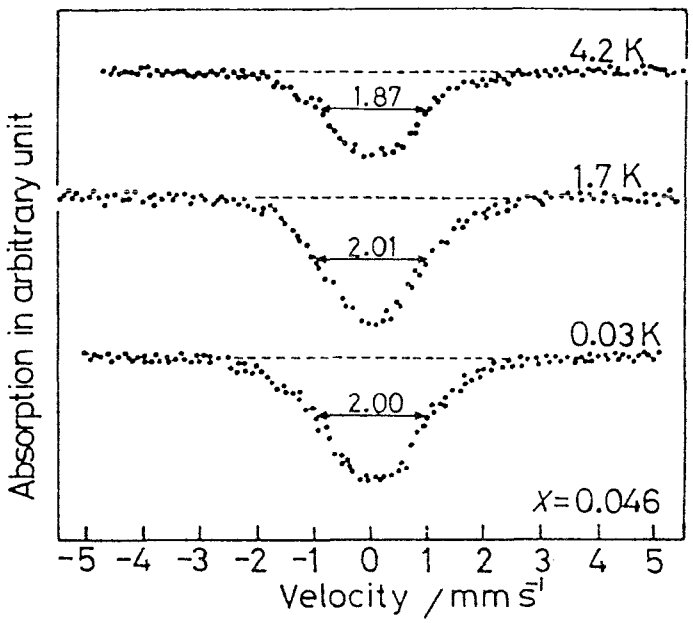

Fig.2.9 Mössbauer spectra obtained at very low temperatures for the alloy of X=0.046

atoms in the purely antiferromagnetic Cr matrix behave superparamagnetically at least down to liquid helium temperature. If so, it is expected from eq.(1.6) that the internal field for the iron atom pairs increases more than -8 MA/m(100 kOe), when the temperature is further lowered below 4.2K. In order to check this, measurements at very low temperatures are performed for the X=0.046 sample in which the population of the iron atom pairs is estimated to be about 20% from eq.(2.2). In Fig.2.9 the FWHM of the spectrum shows a slight increase of about 7%, when the temperature is lowered from 4.2K to 1.7K. An increase in the FWHM is scarcely observed for further decrease of temperature down to 0.03K, where $\bar{H}$ is obtained as -3.7MA/m(49kOe). The results stress that the internal field of most Fe atoms in the antiferromagnetic Cr matrix almost saturates at 1.7K, and they are not ferromagnetic even at 0.03K. Present results do not support Friedel's idea mentioned above. Experimental spectra in Fig.2.7

are analyzed by assuming two groups of Fe atoms, Fe(8,6) and Fe(r), as mentioned in 2.2. The ratio, Fe(8,6)/Fe(r), is calculated from eq.(1.3). Computations are performed separately on these two configurations, assuming that the internal field of Fe(r) atoms is given by eq.(2.1), whereas that of Fe(8,6) atoms is independent of the equation. First, under the condition, $H(8,6)=0$, iteration parameters, a, b, and c, are determined. Next , these parameters are fixed and the $H(8,6)$ value is iterated to find the minimum of $\Sigma\rho^2$, and finally parameters, a, b, and c, are redetermined. The solid lines No.1 and No.2 in Fig.2.7 stand for the calculated spectra which correspond to Fe(8,6) atoms and Fe(r) atoms, respectively. The curve No.3 represents the sum of these two. Calculated spectra show a good agreement with the experimental data. Available parameters are summarized in Table 2.2. The parameters, a and b, are substantially independent of X. On the contrary, the parameter, c , shows an abrupt decrease when X becomes smaller than 0.06, which results in a rather small

Table 2.2 Parameters in eq.(2.2) to give the best-fit spectra to the experimental data, as shown in Fig.2.7.

Parameters	X(Fe)				
	0.033	0.059	0.068	0.095	0.133
a	0.065	0.065	0.065	0.063	0.057
b	0.05	0.05	0.05	0.05	0.05
c	-0.212	-0.053	0.04	0.02	0.02
H(8,6)/MA m^{-1}	-2.39	-2.31	-2.47	-2.55	-2.39

internal field for Fe(r) atoms in the concentration range $X \leq 0.033$. Concentration dependence of Mössbauer pattern observed is interpreted as follows.

(1) When $X > 0.07$, Fe(r) atoms occupy more than 50% of the existence probability and have a large internal field of more than -8MA/m(100kOe) at 1.7K, so that the whole spectrum is broad and exhibits a ferromagnetic aspect. On the other hand, the internal field of the isolated Fe(8,6) atoms is about -2.4MA/m(30kOe), and is independent of the iron content. The result has a strong similarity to those obtained by Shiga and Nakamura[10] who have confirmed the coexistence of the magnetic and nonmagnetic iron atoms.

(2) When $X < 0.05$, the probability for Fe(r) atoms decreases less than 50%, and the internal field of these atoms also shows a sharp decrease, so that the whole spectrum is chiefly determined by the isolated Fe(8,6) atoms which have a low internal field of -2.4MA/m(30kOe).

It should be noted that Fe(r) atoms have a very low internal field as well as Fe(8,6) atoms in the dilute Fe content regions, $X < 0.06$. If Fe(r) atoms have a localized magnetic moment of about $1.5\mu_B$ as suggested by magnetization measurements, the internal field of these Fe atoms should amount to -10 MA/m which is not obtained experimentally. Though the reason for the small internal field of Fe(r) atoms in the dilute concentration ranges ($X < 0.06$) is unclear, the present result does not support the consideration presented by Friedel and Hedman[18] that Fe atom pairs are superparamagnetic in the antiferromagnetic Cr matrix.

2.3.4 Temperature dependence of H due to the Kondo effect

In the present section, discussion will be limited to the X=0.033 sample, because the probability of finding Fe(r) atoms is not large. According to the magnetization measurement due to Ishikawa *et al.*[5], Fe atoms in the specimen have an effective magnetic moment of 2.4 μ_B below T_N. Herbert *et al.*[7] have found that an exchange field H_{Cr-Fe}=17.9MA/m(225kOe) acts on the Fe atom site from the Cr matrix. If Fe spins are assumed to be paramagnetic at temperatures below T_N, the temperature dependence of the internal field $H(T)$ is given by Brillouin function

$$H(T)=H_{sat}B_S(gS\mu_B H_{Cr-Fe}/k_B T)\ . \qquad (2.2)$$

Here the saturation internal field, H_{sat}, equals to -8.7MA/m(110kOe) due to eq.(1.6). The calculated result of eq(2.2) is represented by a dotted line in comparison with experimental points for the X=0.033 sample in Fig.2.10. Neutron diffraction measurements on 2.3%Fe[2] and 3.76%Fe[3] samples indicate that the appearance of C-phase is accompanied by a sharp increase in the magnetic moment of the Cr matrix of about 60% of its saturation value. The sharp increase in $\bar{H}$ at T_2 for X=0.033 is qualitatively consistent with the neutron experiment results. Equation (2.2) predicts that the internal field should increase rapidly if the temperature is lowered below 200K. The experiment shows that $\bar{H}$ is almost constant in the temperature range 150K to 240K, followed by a slow increase for further decreasing temperature. The discrepancy between the experimental result and eq.(2.2) may be explained by an assumption that the localized magnetic moment of Fe atoms shrinks with decreasing temperature as predicted

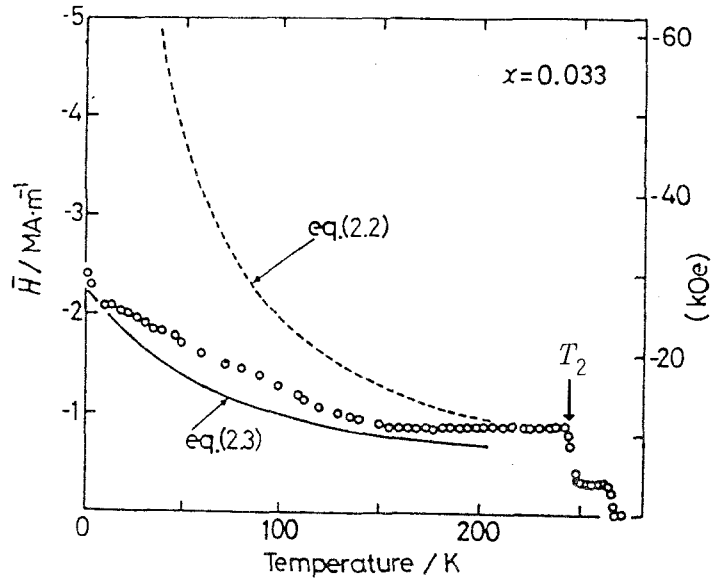

Fig.2.10 Comparison between the calculated and the experimental internal field as a function of temperature for X=0.033

by the Kondo effect. According to Dworin,[19] an approximate expression for the temperature dependence of the internal field, $H_K(T)$, of Fe atoms in the Kondo state is

$$H_K(T) = H_{sat}\, B_S(g\mu_B S H_{Cr-Fe} / k_B (T+T_K)), \qquad (2.3)$$

where H_{sat} is a saturation value of the internal field in the case that the spin compensated state is destroyed by a large magnetic field and T_K is the Kondo temperature. Herbert *et al*.[7] estimated T_K=60K from the temperature dependence of the internal field by using eq.(2.3). Here T_K is estimated as follows. The susceptibility of the impurity magnetic moment in the Kondo state with spin S is at $T \ll T_K$,[21]

$$\chi_{imp}(0) = \frac{g^2 \mu_B^2 S(S+1)}{3 k_B T_K} . \qquad (2.4)$$

When the kondo state is partly destroyed by the exchange field, H_{Cr-Fe}, which acts on the Fe atom site from the Cr matrix, the magnetic moment, μ_K, of Fe is given by

$$\mu_K = \chi_{imp}(0)\, H_{Cr-Fe} . \qquad (2.5)$$

Then,

$$\mu_K = \frac{g^2 \mu_B^2 S(S+1) H_{Cr-Fe}}{3 k_B T_K} . \qquad (2.6)$$

Iron atoms should have the localized magnetic moment, $\mu_{Fe}=g\mu_B S$, for the case that the Kondo state is fully destroyed. The internal field at ^{57}Fe nuclei is proportional to the localized magnetic moment at the Fe atom site (eq.(1.7)), then one can set

$$\frac{\mu_K}{\mu_{Fe}}=\frac{H_K(0)}{H_{sat}} \quad . \tag{2.7}$$

Here, $H_K(0)$ is replaced by the experimental value of $H(8,6)$= -2.4MA/m(30kOe) at 1.7K, and H_{sat}=-8.7MA/m(110kOe). Then, $\mu_K=0.28\mu_{Fe}$ is obtained. Substitution of μ_K and μ_{Fe} into eq.(2.6) gives T_K as

$$k_B T_K=1.2(S+1)g\mu_B H_{Cr-Fe} \tag{2.8}$$

and T_K=73K is obtained. The solid line in Fig.2.10 stands for the calculated result of eq.(2.3) for T_K=73K and H_{Cr-Fe}=17.9MA/m, showing a qualitative agreement with the experimental data at low temperatures.

2.4 Conclusion

Temperature and concentration dependence of the internal field of ^{57}Fe in Cr-Fe alloys has been measured in the temperature range from 1.7K to 300K, and in the iron content range from X=0.006 to X=0.133. Computer analysis of the Mössbauer spectra reveals the following things.

(1) Isolated Fe atoms have a low internal field of about -2.4MA/m (30kOe) which is independent of Fe content in the concentration range, $0.006 \leq X \leq 0.133$, and independent of temperature at those lower than 14K. Temperature dependence of the low internal field is interpreted in terms of the Kondo effect. The Kondo temperature of Fe atoms in the antiferromagnetic Cr matrix is estimated as 73K.

(2) Fe atom clusters have a large internal field (> 7MA/m (88kOe)) and behave ferromagnetically in the concentration ranges $X > 0.07$ at 1.7K. The ferromagnetic feature of Fe atom clusters disappears gradually with decreasing Fe content at less than $X < 0.06$.

(3) The magnetic phase transition of P-C-I or P-I-C is found in the concentration range $0.006 \leq X \leq 0.133$.

References

1) Y.Ishikawa, S.Hoshino and Y.Endoh: J.Phys.Soc.Japan 22(1967) 1221.
2) A.Arrot and S.A.Werner: Phys.Rev. 153(1967) 624
3) M.Mori ,Y.Tsunoda and N.Kunitomi: Solid State Commun. 18 (1976) 1103.
4) T.Suzuki: J.Phys.Soc.Japan 41(1976) 1187.
5) Y.Ishikawa, R.Tournier and J.Filippi: J.Phys.Chem.Solids 26 (1965) 1227.
6) R.B.Frankel and N.A.Blum: *ibid.* 34(1973) 1565.
7) I.R.Herbert,P.E.Clark and G.V.H.Wilson: *ibid.* 33(1972) 979.
8) T.Shinjo,K.Okada,T.Tanaka and Y.Ishikawa: J.Phys.Soc.Japan 37(1974) 877.
9) S.Katano and N.Môri: *ibid.* 46(1979) 1265.
10) M.Shiga and Y.Nakamura: *ibid.* 49(1980) 528.
11) G.K.Wertheim,V.Jaccarino,J.H.Wernick and D.N.E.Buchanan.: Phys.Rev.Letters 12(1964) 24.
12) S.Arajs and G.R.Dunmyre: J.Appl.Phys. 37(1966) 1017.
13) B.Loegel:J.Phys.F 5(1975) 497.
14) S.Arajs: Phys.Scr. 8(1973) 109.
15) L.R.Edwards and I.J.Fritz: AIP Conference Proc. 18(1973) 401.
16) G.E.Bacon and N.Cowlam: J.Phys.C 2(1969) 238.
17) M.V.Nevitt and A.T.Aldred: J.Appl.Phys. 34(1963) 463.
18) J.Friedel and L.E.Hedman: J.de Phys. 39(1978) 1225.
19) B.B.Schwartz, D.J.Kim,R.B.Frenkel and N.A.Blum: J.Appl.Phys. 39(1968) 698.
20) A.Yoshimori: Prog.Theor.Phys. 55(1976) 67.

Chapter 3. Phase decomposition of Iron-Chromium Solid Solutions

§3. Phase diagram

3.1 Introduction

Figure 3.1 shows a part of the Fe-Cr phase diagram in which the miscibility gap lies below the σ phase region. An alloy heated within the miscibility gap decomposes into α- and ά-solid solution which are termed as *the Fe-rich phase* and *the Cr-rich phase*, respectively. Williams and Paxton[2] first studied by means of hardness measurements and reported that the critical temperature, T_{Cr}, of the miscibility gap is about 830K, and that there is an anomalous bulge around $x=0.8$. Williams[3] later made a further experiment on the miscibility gap by means of electrical resistivity measurements in which the bulge was not confirmed. Another systematic study was proposed by Köster and Kienlin[4] who summarized their own data and other author´s ones measured by differnt methods,

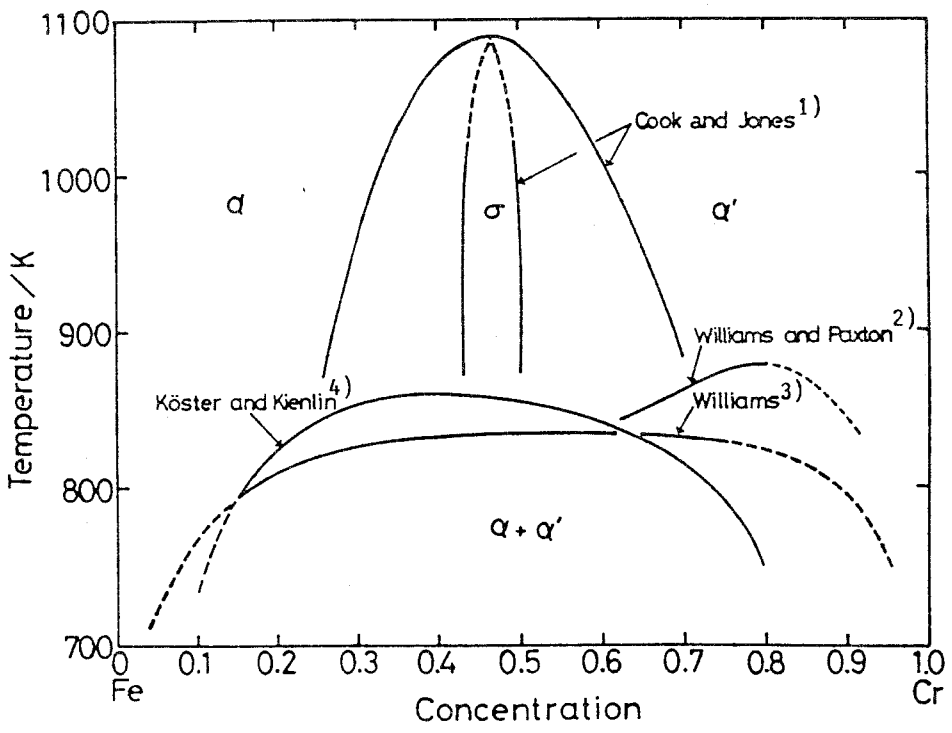

Fig.3.1 Partial phase diagram of the Fe-Cr binary system.

those are, magnetization measurements,[5] vickers-hardness measurements,[6] specific heat[7] and chemical anslysis,[8] and constructed the miscibility gap shown in the figure. There is a distinct discrepancy between results proposed by Williams[3] and by Köster *et al.*,[4] in particular, at the upper and at the Cr-rich boundaries of the miscibility gap. The Cr content of the Cr-rich phase was determined by Fisher *et al.*[8] and Williams[3] with chemical analysis of the chemically extracted residues from the alloys aged for long times around 750K. The former obtained a result of 79-83 at%Cr, whereas the latter 87at%Cr. The discrepancy is, perhaps, caused by the impurity of specimen used and the inaccuracy of correction which is inevitable when second phases such as carbides, nitrides and inclusions coexist with the Cr-rich phase within the aged alloys. Because the Cr-rich phase is paramagnetic[9] at room temperature, one can determine accurately its Cr content by measuring the isomer shift with the Mössbauer spectroscopy. The iron-rich and the upper boundary of the miscibility gap are obtainable by measuring the internal filed which is proportional to the Cr content of the ferromagnetic Fe-Cr alloys. It is expected that the Mössbauer spectroscopoy is more effective and convenient method than any other conventional techniques for the study of the miscibility gap of this alloy system. However, there has been little systematic study on the subject by this method. It is main purpose of this section to clarify the miscibility gap by means of the Mössbauer spectroscopy.

3.2 Experimental procedure

Sample preparations and Mössbauer measurements are the same

as those described in §1. Foil specimens for Mössbauer measurements, about 0.02x15x15mm^3 in dimensions, were initially solution treated at temperatures 1000K to 1300K, and then aged at desired temperatures. A quick temperature drop of about 10K happened when a specimen was put into the furnace because of the latter's rather small heat capacity. but it recovered within 15s to the desired temperature. When a high accuracy is requisite for the internal field measurement, a single sample is aged sequentially with a holding time of 60s or 120s in order to avoid sample-to-sample variations. The total aging time is a sum of the holding time of the batch. Electrical resistivity measurements were done with a conventional four-terminal method on heating at a rate of 1K/min. X-ray measurements were performed on the aged specimens to check the formation of the σ phase by using monochromatic CuK_α radiation.

3.3 Results and discussion

3.3.1 Determination of the miscibility gap

a. Isochronal aging

The as-quenched alloys are isochronally aged for 180ks(50h) at various temperatures of 750-1100K, and their mean internal fields, $\bar{H}$, are measured at room temperature. Open circles in Fig.3.2 show an representative example of $\bar{H}$ as a fucntion of aging temperature for the alloy of x=0.363. An accuracy for the value $\bar{H}$ is estimated about ± 0.15MA/m(2kOe), which corresponds to the compositional fluctuation of 1 at%Cr due to eq.(1.5). Thus if the compositional change of more than ±1 at%Cr takes place within alloys

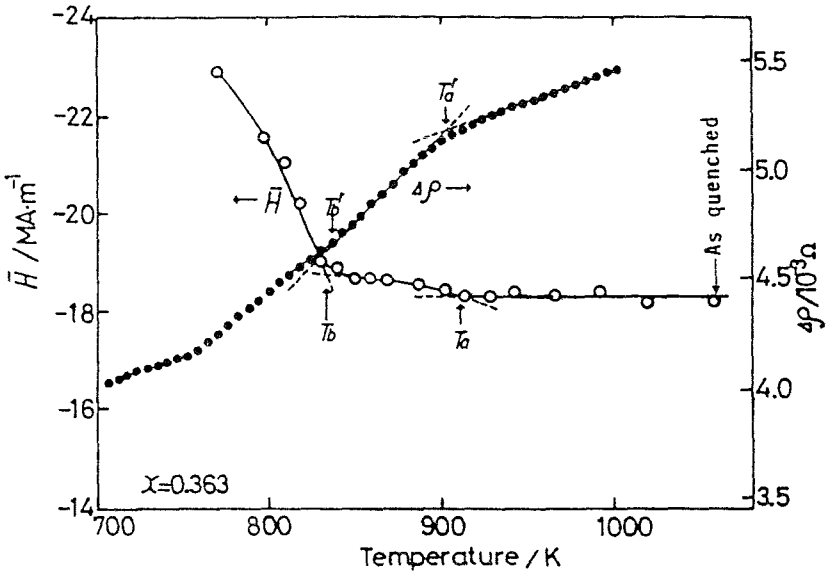

Fig.3.2 Mean internal field, $\bar{H}$, of specimens aged for 180ks(50h) at various temperatures, and resistivity change, $\Delta\rho$, on heating for an $Fe_{0.637}Cr_{0.363}$ alloy.

during aging, it may be detectable. When the aging temperature is higher than 910K, little change in $\bar{H}$ is obtained in comparison with the quenched state. As the aging temperture is lowered below a temperature denoted here as T_a, a slight increase in $|\bar{H}|$ is confirmed. When the temperature is further decreased, a sharp increase in $|\bar{H}|$ takes place below a temperature named here as T_b. These transition temperatures T_a and T_b obtained by the $\bar{H}$ measurements on the isochronally aged alloys are plotted by solid circles and open circles, respectively, in Fig.3.3 as a function of x. Comparison of the present result with Fig.3.1 indicates that T_b agrees with the miscibility gap obtained by Williams and Paxton[2] within a fluctuation of ±10K in the concentration range from x=0.3 to x=0.7. The temperatures T_a are much higher than the miscibility gap obtained by Köster and Kienlin,[4] and do not agree with the solubility limit of the σ phase. X-ray diffraction

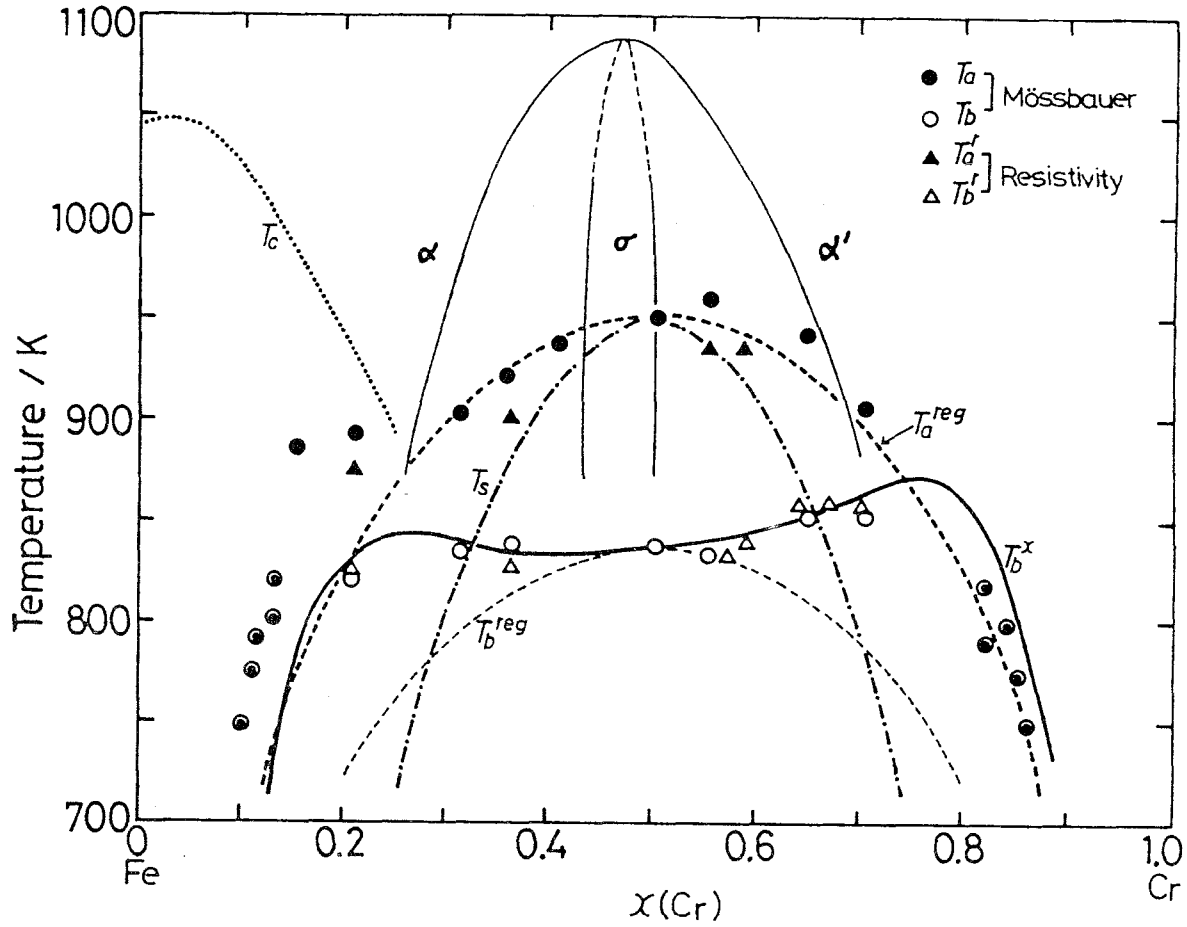

Fig.3.3 Proposed phase diagram of the Fe-Cr binary system.

measurements performed on the same specimen used for the Mössbauer effet confirmed that the formation of the σ phase is limited to the specimens aged at temperatures above 950K in the case of the aging time of 180ks(50h). Therefore the direct relation between T_a and the σ formation can be denied. As discussed later in section 3.3.2, T_a is responsible for the metastable miscibility gap of this system.

b. Electrical resistivity measurement

The electrical resistivity measurement[3] on the 75at%Cr alloy denied the existence of the anomolous bulge of the miscibility gap found by the hardness measurements[2] around x=0.8. Present

Mössbauer study again suggests that there is a small bulge of the miscibility gap around $x=0.7$. Electrical resistivity measurements are also carried out here in order to campare with the Mössbauer results. Solid circles in Fig.3.2 stand for an typical example of the resistivity change $\Delta\rho$ for $x=0.363$. Close examination reveals that the temperature coefficient of the resistivity change varies slightly at the temperatures, T_a^r and T_b^r. The latter is plotted by open circles in Fig.3.3 as a function of x, showing good agreement with the transition temperatures, T_b, obtained by the Mössbauer effect. Temperatures, T_a^r's, which are plotted by solid triangles, show rough agreement with the Mössbauer result T_a, though having a tendency to be 10-30K lower than the latter. When x exceeds 0.7, only T_b^r is detective, and T_a^r becomes vague as seen in Fig.3.4. However, the Mössbauer spectroscopy points out that there is compositional changes within solid solutions during aging at temperatures higher than T_b^r (Fig.3.5): Mössbauer spectra obtained at temperatures higher than 910K (**a,b**) are single peaks with the FWHM of 0.32mm/s. The first detectable change in the Mössbauer spectra with decreasing temperature is recognized on the alloy aged at 905K(c) through the broadening of the peak width:FWHM=0.43mm/s. The spectra obtained below 890K (**d-f**) show that the ferromagnetic components increase with decreasing aging temperature. The width of these spectra measured at the base line, Γ_B, is plotted in Fig.3.6 as a function of aging temperature. Two step changes in Γ_B are clearly recognized on the figure as well as the case of the lower Cr content alloys (*cf.* Fig.3.2). These results prove that the Mössbauer effect is more effective and sensitive than the resistivity measurement.

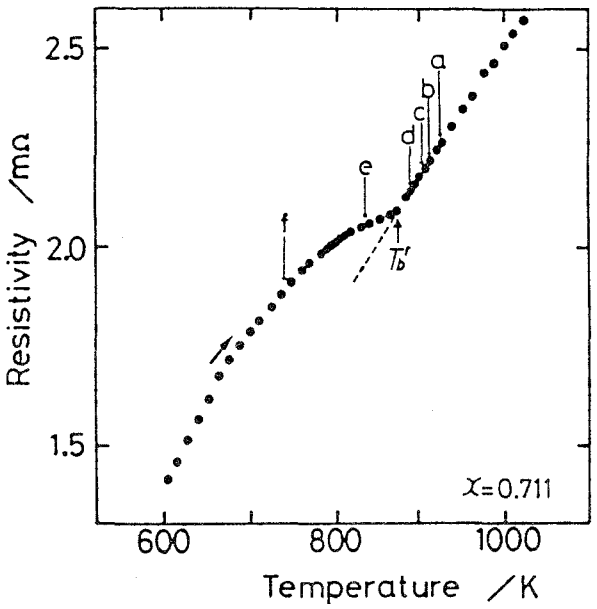

Fig.3.4 Resistivity change on heating at a rate of 1K per minute for an $Fe_{0.289}Cr_{0.711}$ alloy.

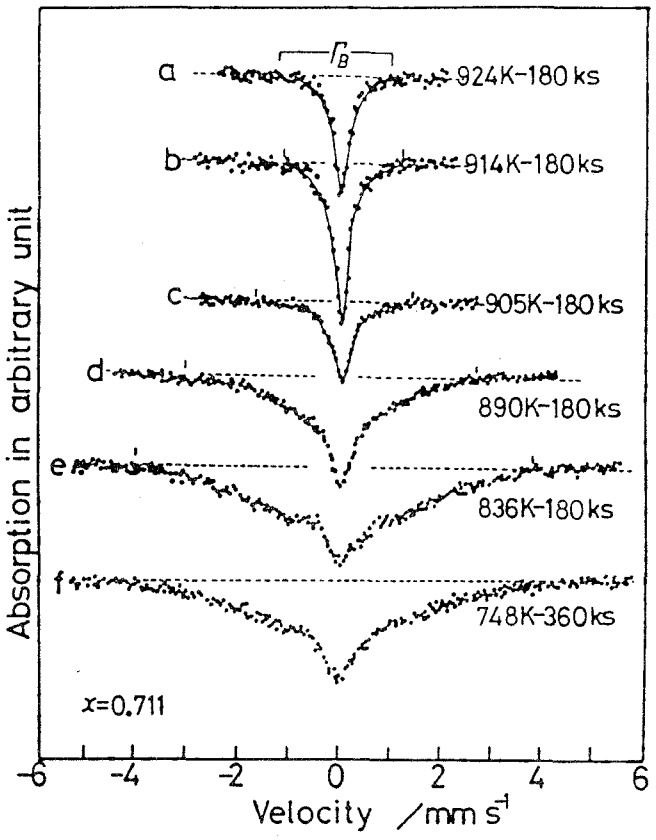

Fig.3.5 Mössbauer spectra measured at room temperature for an $Fe_{0.289}Cr_{0.711}$ alloy aged at various temperatures.

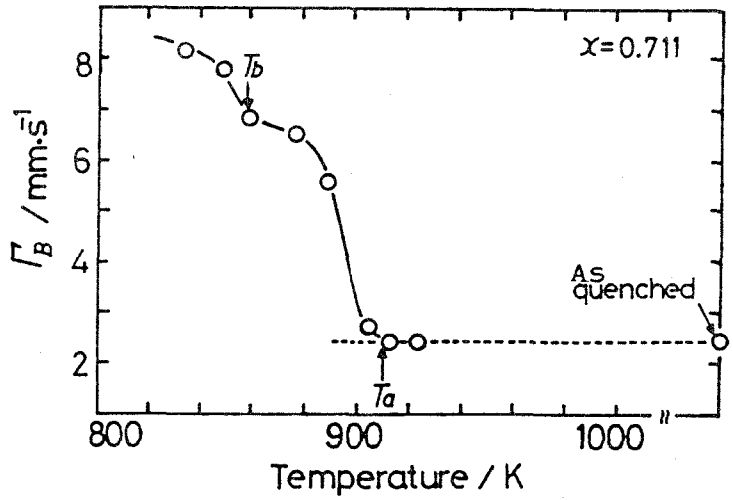

Fig.3.6 Peak width, Γ_B, at the bottom of the Mössbauer spectra as a fucntion of aging temperature for an $Fe_{0.289}Cr_{0.711}$ alloy.

c. Composition of the Fe-rich phase and the Cr-rich phase

The limit of miscibility gap at the Fe-rich and the Cr-rich side can be determined by finding the concentrations of the decomposition products in equilibrium with each other at a given temperature within the gap. Figure 3.7 shows changes in $\bar{H}$ for three alloys with the original compositions, x=0.21, 0.363, and 0.556. With increasing aging time, $\bar{H}$ of these alloys shows a gradual increase which means development of the concentration change within the matrix. After a very prolonged aging time of about 11.34Ms (3150h, log$t$=7.1), $\bar{H}$'s of these three alloys concentrate on a value of -24.6±0.2MA/m. No more increase in $\bar{H}$ is confirmed for further increased aging time within an experimental error of ±0.15MA/m for alloys with x=0.21 and 0.556. Therefore, one can conclude that the decomposition has substantially been completed after 11.34 Ms at 748K. Fig.3.8 shows Mössbauer spectra obtained at room temperature for various alloys aged for up to 18 Ms(5000h). Each of these spectra consists of two parts: (1) ferromagnetic sextuplet peaks due to the matrix, that is, the Fe-rich phase and (2) a paramagnetic peak designated by arrows due to the Cr-rich phase. In addition to the nearly same mean internal fields of these four ferromagnetic spectra, their finestructures observed at the outermost peaks do not vary considerably from sample to sample. The facts also indicate that the decomposition has reached a final state. Then, the Cr content of the final Fe-rich phase at 748K is estimated 9 at%Cr from the internal field value (-24.6MA/m) due to eq.(1.5). The isomer shift measurement may be another available means for determining the composition of the Fe-rich phase. Representative examples of the partial

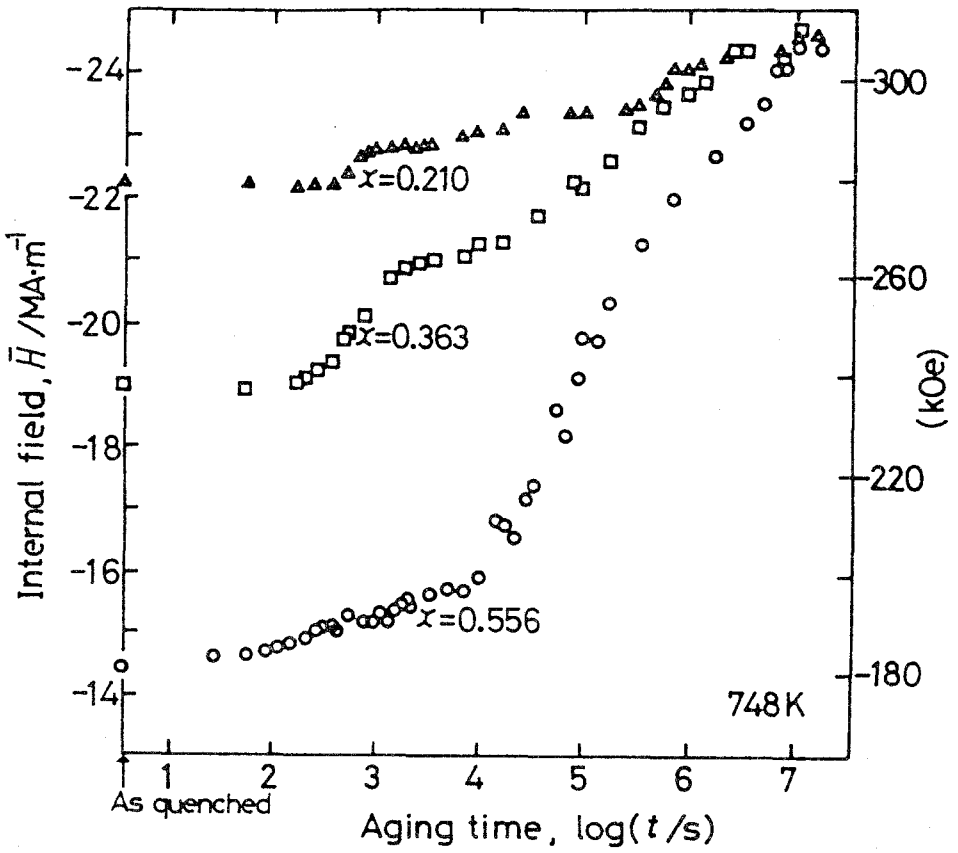

Fig.3.7 Mean internal field, $\bar{H}$, measured at room temperature as a function of aging time during aging at 748K for $Fe_{1-x}Cr_x$ alloys.

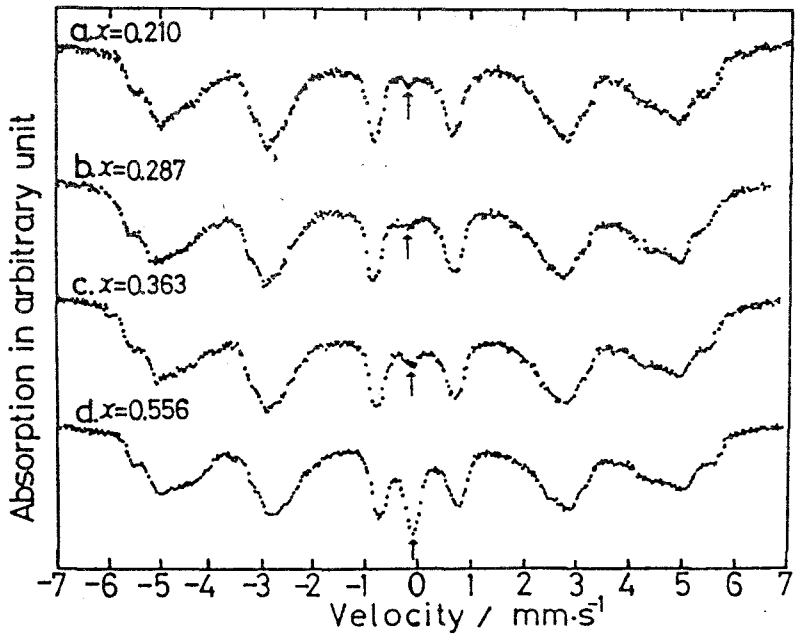

Fig.3.8 Mössbauer spectra measured at room temperature for $Fe_{1-x}Cr_x$ alloys aged at 748K for long times.(cf. Fig.1.1,P11) a,b,d:18Ms(5000h) aging, c:11.34Ms(3150h) aging.

Mössbauer spectra measured in the velocity range from -1.5mm/s to 1.5mm/s are shown in Fig.3.9 for the aged alloys with x=0.287, 0.363 and 0.556. The isomer shifts, IS_{Fe}, for the Fe-rich phase obtained from the center of gravity of the outside two peaks P_{Fe} are -0.012, -0.013 and -0.012 for x=0.287, 0.363, and 0.556 respectively. According to the experimental relation between IS and x shown in Fig.1.6, these values correspond to the Cr content of 12±1 at%. Finally, the composition of the Fe-rich phase x_{Fe} at 748K is concluded to be 10±2 at%Cr, if values estimated from the internal field and the isomer shift measurement are combined together. As for the composition of the Cr-rich phase, it is estimated from the isomer shift, IS_{Cr}, which is obtained from the peak position of the paramagnetic peak P_{Cr} in Fig.3.9. Values of IS_{Cr} are -0.126, -0.124 and -0.125 for the aged alloy with x=0.287, 0.363, and

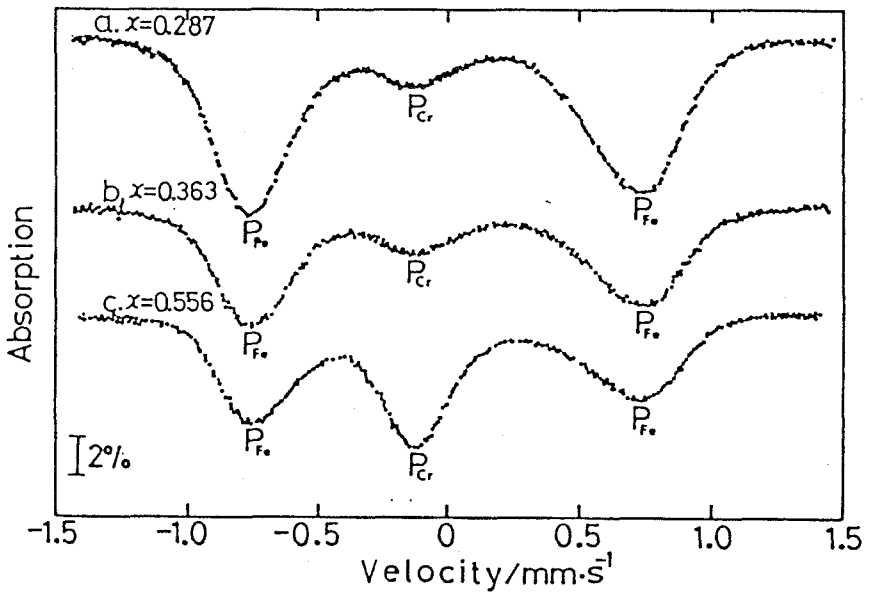

Fig.3.9 Partial Mössbauer spectra measured in the velocity range from -1.5 to 1.5 mm/s at room temperature for $Fe_{1-x}Cr_x$ alloys aged at 748K for (a)18Ms(5000h), (b)11.34Ms(3150h) and (c)18Ms(5000h). Letters P_{Fe} and P_{Cr} indicate absorption peaks associated with the Fe-rich phase and the Cr-rich phase, respectively.

Table 3.1 Mean internal field, $\bar{H}_{Fe}$, isomer shift, IS_{Fe}, and Cr content, x_{Fe}, of the Fe-rich phase, and isomer shift, IS_{Cr}, and Cr content, x_{Cr}, of the Cr-rich phase formed in $Fe_{1-x}Cr_x$ alloys aged at various temperatures.

x	Aging temp./K	Fe-rich phase		Cr-rich phase	Cr content		Method*	Author
		$\bar{H}_{Fe}$/mms^{-1}	IS_{Fe}/mms^{-1}	IS_{Cr}/mms^{-1}	Fe-rich phase x_{Fe}	Cr-rich phase x_{Cr}		
0.21	748	-24.7	———	———				
0.287	748	-24.8	-0.012	-0.126	0.10	0.86	M	
0.363	748	-24.5	-0.013	-0.124				
0.556	748	-24.4	-0.012	-0.122				Present
0.556	773	-24.1	-0.012	-0.123	0.11	0.85		
0.556	791	-24.0	-0.010	-0.119	0.12	0.82	M	
0.363	798	-22.2	-0.019	-0.122	0.14	0.84		
0.556	808	-23.7	-0.016	-0.118	0.13	0.81		
0.365	745				0.16	0.87	C	Williams[3]
0.24	748				0.12	———	M	Chandra[9]
0.30	755				0.15	0.79 - 0.83	C	Fisher[8]

* M ; Mössbauer effect C ; Chemical analysis

0.556, respectively. Substitution of IS_{Cr} obtained here into eq.(1.10) gives 86±1 at%Cr for the composition of the Cr-rich phase formed at 748K. Compositions of the Fe-rich phase and the Cr-rich phase determined in a similar way for various aging temperatures are compiled in Table 3.1 together with the values of $\bar{H}_{Fe}$, IS_{Fe}, and IS_{Cr}. Other investigaters' results are shown in comparison too. The present result for the Fe-rich phase (x_{Fe}=0.1) at 748K agrees well with that obtained by Chandra[9] (x_{Fe}=0.12) by means of the Mössbauer effect. The Mössbauer results suggest that the Cr content of the Fe-rich phase is slightly lower than those obtained by Williams[3] and Fisher *et al.*[8] by means of chemical analysis. For the composition of the Cr-rich phase, the present (x_{Cr}=0.86), and the Williams' result[3] (x_{Cr}=0.87) agree with each other. These two are more credible than those obtained by Fisher *et al.*[8] (x_{Cr}= 0.79-0.83) who used the specimens including carbon and nitrogen 10 to 40 times as large as those used here. There have been reported no available data to be compared with the present results for the compositions of these phases at higher aging temperatures. The present data are plotted by a symbol ⊙ in Fig.3.3. Particular features of the miscibility gap proposed here are as follows: (1) a double miscibility gap in the concentration range, $0.2 \leq x \leq 0.7$. (2) a parabolic feature for the upper and flatness with a small bulge around x=0.7 for the lower.

3.3.2 Calculation of the miscibility gap

The strictly regular solution approximation expresses the free energy change, ΔG, on mixing of pure Fe and pure Cr to yield

an alloy with the Cr content x as

$$\Delta G=(1-x)x\,W+RT\{(1-x)x\ln(1-x)+x\ln x\}, \qquad (3.1)$$

$$W=NZ(V_{Fe-Cr}-\tfrac{1}{2}(V_{Fe}+V_{Cr})),$$

where W is the interaction parameter, $V_{Fe(,Cr,Fe-Cr)}$ binding energy of an Fe-Fe(,Cr-Cr,Fe-Cr) bond, N Avogadro's constant and Z co-ordination number. Assuming that W is independent of x, the miscibility gap and the spinodal curve are given by the condition

$$\frac{\partial \Delta G}{\partial x}=(1-2x)W+RT\{-\ln(1-x)+\ln x\}=0 \qquad (3.2)$$

and

$$\frac{\partial^2 \Delta G}{\partial x^2}=2x(1-x)W-RT=0\ , \qquad (3.3)$$

respectively. The critical temperature, T_{cr}, of the gap is that point at which $\frac{\partial^2 \Delta G}{\partial x^2}=0$ at $x=0.5$, thus

$$W=2R\,T_{cr}\ . \qquad (3.4)$$

The interaction parameter is evaluated empirically if T_{cr} is known.

a. Concentration dependence of the interaction parameter

There is a problem of which the value of T_a or T_b should be selected as T_{Cr}. First, substitute T_{Cr} in eq.(3.4) by T_b =835k for x=0.50, and then W=13.9kJ/mol is obtained. A thin dotted line, T_b^{reg}, in Fig.3.3 shows the calculated result of eq.(3.2) for the value W obtained here. Large discrepencies are recognized between the calculation and the experimental points(T_b). The observed discrepancy may be explained here by considering concentration dependence of W. Assume that W is the sum of the constant term, W_c(=13.9kJ/mol), and the concentration dependent term, W_x, as

$$W=W_c+W_x\ . \qquad (3.5)$$

Because the experimental miscibility gap is roughly symmetric to x=0.5, it is tacitly assumed that

$$W_x=A\,|x-B|^n. \qquad (3.6)$$

Here A is a constant, n an exponent and $B \sim 0.5$. Then the miscibility gap is expressed by the condition:

$$\frac{\partial \Delta G}{\partial x}=(1-2x)W_c+\{(1-2x)+\frac{nx(1-x)}{|x-B|}\}W_x+RT\{-\ln(1-x)+\ln x\}=0. \quad (3.7)$$

Comparison of eq.(3.7) with eq.(3.2) suggests that the temperature difference, ΔT, observed between the experimental(T_b) and the calculated results(T_b^{reg}) at a given concentration is given by

$$\{(1-2x)+\frac{nx(1-x)}{|x-B|}\}W_x+R\,\Delta T\{-\ln(1-x)+\ln x\}=0 \quad (3.8)$$

Values of ΔT are obtainable directly from Fig.3.3 as a function of x. Parameters A , B and n are determined by the following procedures: (1) First select any value for B between 0.47 and 0.50, (2) assume that n equals 2, (3) and find the value of ΔT from Fig.3.3 as a function of x. (4) Then determine A and n from eq.(3.6) by the least-square fitting to the obtained relation between W_x and x. (5) Use the calculated value of n and repeat calculations from (3) again and again until a consistent value of n is obtained. The iterative calculations result in a set of parameters: A=-261kJ/mol, B=0.49 and n=4.95. The thick solid line, T_b^x , in Fig.3.3 is the result of the above calculation(eq.(3.7)) by using these values, showing good-fit to the experimental points, T_b. The result of B=0.49 accounts qualitatively for the asymmetric feature of the experimental miscibility gap, and the existence of the bulge around x=0.7. But, the treatment seems to involve a problem because physical meanings of eq.(3.6) are not clear at present.

b. Metastable miscibility gap

Next, replace T_{Cr} in eq.(3.4) by T_a=950K for x=0.5, then W=15.8 kJ/mol is obtained. A thick dotted line, T_a^{reg}, in Fig.3.3 is calculated from eq.(3.2) with respect to the value of W obtainde here, and

shows good agreement with the experimental values, T_a, in the concentration range $0.3 \leq x \leq 0.7$, and the experimental solubility limit at the Cr-rich side of $x \sim 0.8$. The line also agrees well with T_b^{reg} at temperatures lower than 820K. But, there is large discrepancies between T_a^{reg} and T_b^{reg} in the center of the miscibility gap, that is, the concentration regions corresponding to the σ and (σ+α) regions.

These results may be interpreted as follows. There is no theoretical reason and the experimental findings for that the σ phase is unstable at temperatures within the miscibility gap. So that, the σ and the (σ+α) phase regions found at high temperatures could be stretched down to the room temperature if the process of the formation of σ phase was fast enough. But, since the alloys are usually quenched or cooled rapidly from the single α-phase region, the σ phase formation is suppressed. If the alloys are reheated or aged at temperatures below 830K, the σ phase formation is quite difficult[14] because of the large difference in the crystal lattice form and chemical bonding state between the σ phase (tetragonal)[13] and the bcc parent matrix. Therefore, the metastable state is expected to take place. Because the interaction parameter of the α-solid solution is positive, the phase separation is the most probable at low temperatures below T_b where the σ phase formation is difficult. These considerations are, of course, based on the assumption that the miscibility gap does not represent a real equilibrium but the metastable phase diagram. Most likely, the σ phase formation needs the activation energy for the lattice transformation in addition to that for diffusion, while the phase separation needs only the latter.

If the aging temperature is between T_b and T_a, competition between the phase separation and the σ phase precipitation is expected to take place because the latter is now possible.[14] But, the former will occur prior to the σ phase formation, since it takes very long incubation time for the latter, for example, 252ks(70h) on aging at 873K.[14] Changes in the average internal field, $\bar{H}$, observed in the temperature range, $T_a - T_b$(Fig.3.2), may be ascribed to such phase separation, though the general aspects seem to be slightly different from the phase separation at temperatures below $T_b \approx 830$K. Figure 3.10 represents time dependences of $\bar{H}$ on aging at temperatures above and below T_b for the alloy of $x=0.556$. The increase in $\bar{H}$ for the 878K-aging saturates quickly after ∿360s($\log t = 2.6$), and the saturation value is only about 0.8MA/m (10kOe) larger than the internal field of the as-quenched alloy. The increment of the internal field corresponds to the decrease in the average Cr content of 4 at%. Even if the aging time is increased up to 720ks($\log t = 5.9$),

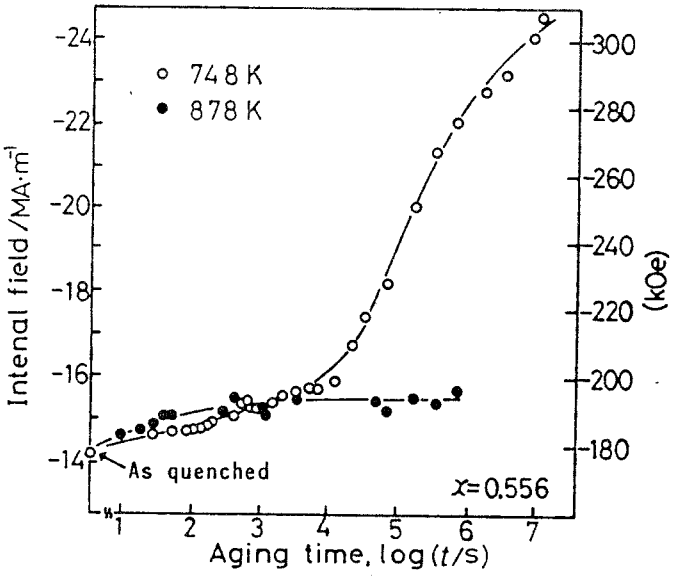

Fig.3.10 Comparison of the mean internal field change during aging at temperatures below and above the apparent critical temperature, T_b (≈830K), for an $Fe_{0.444}Cr_{0.556}$ alloy.

an indication of the paramagnetic peak is not confirmed, as shown in Fig.3.11(a). In contrast to this, the 748K-aging, in spite of the lower aging temperature, is accompanied by the considerable increase in H and the appearance of the paramagnetic peak after the 720ks-aging(bottom of Fig.3.11(b)). These facts are interpreted by that the phase separation above T_b(830K) is heavily suppressed and unable to undergo the complete transition: it is involved by the slight deviation of the atomic distribution from the randomness of the as-quenched alloy. These features may be referred to as the *clustering* of constituent atoms rather than the phase decomposition for the practical purpose. The concentration change attending the clustering is so small that previous studies by means of the conventional techniques have failed to detect the metastable miscibility gap T_a.

If an attention is paid on the iron rich side of the phase diagram(Fig.3.3), it is noticed that the experimental miscibility gap deviates to lower Cr contents from the calculated

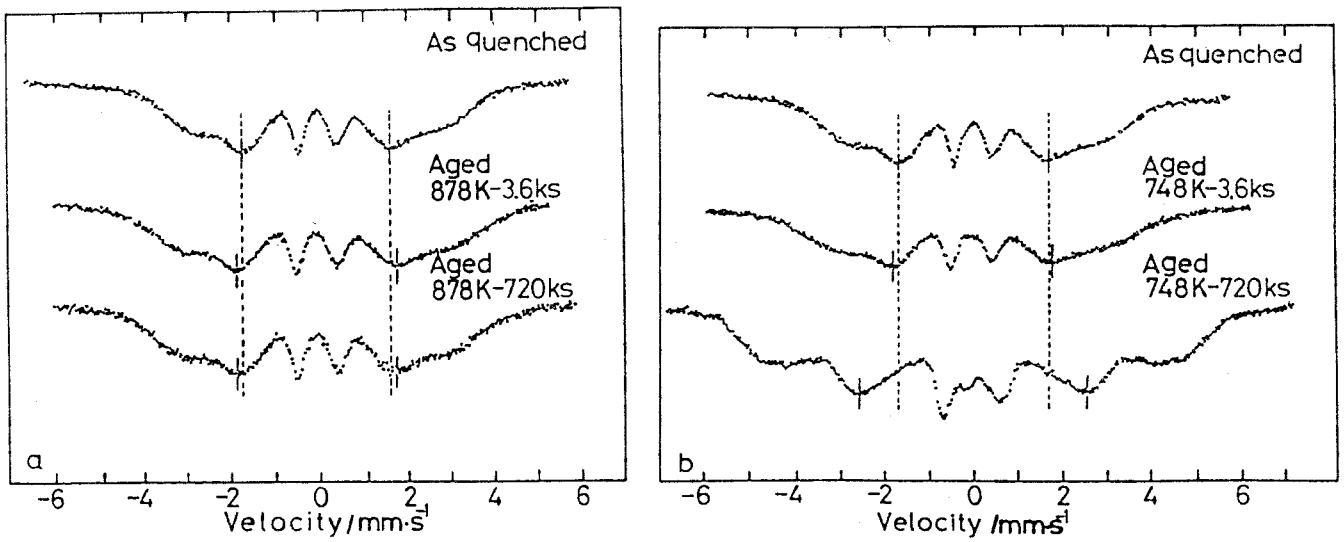

Fig.3.11 Comparison of the room temperature Mössbauer spectra of an $Fe_{0.444}Cr_{0.556}$ alloy aged at 878K(a) and 748K(b), showing an indication of the paramagnetic peak only for the latter.

result of T_a^{reg}. The deviation takes place in the concentrations of less than $x \approx 0.25$ where the Curie temperature, T_C, intersects the T_a^{reg} line. The result is consistent with the theoretical consideration treated by Nishizawa *et al*.[15] who have emphasized that the magnetic free energy term has an influence to expand the miscibility gap or solid solubility.

If the calculated line, T_a^{reg}, is accepted as the metastable miscibility gap of this system, then the corresponding spinodal curve defined by eq.(3.3) is calculated as a chained line, T_s, in Fig.3.3. Note that one of the spinodal concentrations, x_s, is 0.27 at 748K.

3.4 Conclusion

The Mössbauer effect proves itself to be more effective and convenient than other conventional techniques to study the miscibility gap of an Fe-Cr system in which only the compositional change is accompanied. Experimental findings to be noted are summarized as follows on the basis of the assumption that the miscibility gap represents the metastable phase diagram of this system.

(1) The metastable miscibility gap which has not been found in the previous studies with traditional methods is determined by the Mössbauer effect measurement, and is confirmed to be expressed by the regular solution approximation. Its critical temperature, T_{Cr}, is about 950K, being about 120K higher than the previous results.

(2) On aging at temperatures below T_{Cr} and above 830K within the miscibility gap, the phase separation takes place prior to the σ phase formation. However, the concentration change attended

is so minute that it may be referred as the clustering of the constituent atoms. The aging at temperatures below 830K, which has been believed to be the critical temperature, is involved by the typical features of the concentration change attending the phase decomposition, that is, the mixture of two phases with different compositions.

(3) The solubility limits of the miscibility gap at 748K, that is, the concentrations of the Fe-rich and Cr-rich phase, are estimated as 10 at%Cr and 86 at%Cr, respectively, through the isomer shift and internal field measurements, and are confirmed to show good agreement with the calculated result based on the regular solution approximation. Slight discrepancies observed between the experimental and the calculated result in the iron-rich side of the miscibility gap are interpreted in terms of the effect of the magnetic free energy term treated theoretically by Nishizawa *et al.*[15]

References

(1) A.J.Cook and F.W.Jones: J.Iron Steel Inst. 183 (1943) 217.
(2) R.O.Williams and H.W.Paxton: *ibid.* 185 (1957) 358.
(3) R.O.Williams: Trans.Met.Soc.AIME 212 (1958) 497.
(4) W.Köster and A.von Kienlin: Archiv Eisenhüttenwes. 12 (1956) 793.
(5) Y.Imai and K.Kumada: Sci.Rep.Res.Inst.Tôhoku Univ. A.5 (1953) 218, 520.
(6) K.Bungardt and W.Spyra: Archiv Eisenhüttenwes. 12 (1956) 777.
(7) H.Masumoto, H.Saito and M.Sugihara: Sci.Rep.Res.Inst.Tôhoku Univ. A.5 (1953) 203.
(8) R.M.Fisher, E.J.Dulis and K.G.Caroll: Trans.AIME (J.Metals) 97 (1953) 690.

(9) D.Chandra and L.H.Schwartz: Metallurg.Trans. 2 (1971) 511.
(10) H.Kuwano and Y.Morooka: J.Japan Inst.Metals 44 (1980) 202.
(11) R.A.Swalin: *Thermodynamics of Solids*(John Wiley & Sons, New York, 1972) 2nd ed. P.148.
(12) T.Nishizawa: Bullet.Japan Inst.Metals (in Japanese) 12(1973) 189.
(13) K.Kumada: *ibid*.2 (1963) 261.
(14) E.Baerlecken and H.Fabritius: Archiv Eisenhüttenwes. 11 (1955) 679.
(15) T.Nishizawa,M.Hasebe and M.Ko: Acta Met. 27 (1979) 817.

§4 Mechanism of the Phase Decomposition

4.1 Introduction

Classical theories for the phase separation of solid solutions describe that the spinodal curve is uniquely defined as a locus of the second derivatives of the free energy G with respect to the solute concentration x: $\partial^2 G/\partial x^2 = 0$.[1,2] In the previous section, the spinodal curve of Fe-Cr binary system is calculated on the basis of the above definition by using critical temperature obtained experimentally. The result predicts that one of the spinodal concentrations at 748K is 27 at%Cr for the system. According to the classical spinodal theory, it is expected that phase decomposition due to the nucleation and growth (*N-G process*) and the spinodal decomposition (*S process*) take place outside and inside the spinodal line, respectively, within the miscibility gap. Conventional nucleation theory describes that precipitation nuclei, the composition of which is the same with that of the final stable phase, separate from the matrix after an elapse of incubation time[3]. One of the final stable phases is the Cr-rich phase, and is paramagnetic at room temperature as mentioned in §3. On the other hand, the S process is accompanied by the spontaneous growth of the inherent concentration fluctuation within solid solutions in a moment of the start of aging, because there is no energy barrier for the decomposition. The Cr-rich phase is expected to appear after the considerable development of the decomposition reaction. Hence, one of the best ways to distinguish these two types is to examine the precipitation of the Cr-rich phase in the early stages of the decomposition. Nys and Gielen[4] made the Mössbauer effect

measurement on the decomposed alloys and confirmed that a paramagnetic peak due to the Cr-rich phase appears after the 1.5Ms (410h) aging at 748K for the 20%Cr sample. However, the peak was not observed for the 30%Cr sample aged for 0.9Ms(250h) an 3.8Ms (1050h) at 743K. They concluded that the former decomposes via N-G and the latter via S process. The result seem to agree with predictions of the classical spinodal theory. However recent non-linearized spinodal theory due to Langer[5,12,13], computer simulations based on the kinetic Ising model due to Sur *et al.*[6] and Morro *et al.*,[7] and those based on the cluster kinetic due to Binder[8,9] *et al.*had a suspect about the fixed location of the spinodal curve and its physical meaning: they emphasized that the spinodal curve defined in the classical spinodal theory has no physical significance and the boundary between N-G and S process is vague. Katano and Iizumi[10,11] studied the decomposition kinetics of the 24, 32, and 40%Cr sample by means of neutron scattering, and concluded that the decomposition of Fe-Cr alloys is well described by the recent spinodal theory due to Langer[12,13] and computer simulations[6-9] mentioned above on the whole. However, neutron scattering measurements and most of computer simulations mainly treat a time evolution of the structure factor, $S(k,t)$ (k:wave number vector), which is the Fourier transform of the correlation function of the local concentration of solute atoms. The measurement of $S(k,t)$ has an advantage for examination of the concentration periodicity. But it overlooks the nucleation and growth process of the precipitate phases. In contrast to $S(k,t)$, the internal field obtained by the Mössbauer spectroscopy is highly sensitive to the local concentration change accompanied

by the precipitation of new phases. It measures concentration profiles in the real space in contrast to the neutron scattering which looks for that in the Fourier space. Because these two techniques are complementary each other, systematic Mössbauer study is highly needed here to clarify the phase separation of Fe-Cr alloys. Transmission electron microscope observation usually gives a visual, direct evidence for the precipitation of the decomposition products. Lagneborg[14] confirmed that general precipitation of spherical Cr-rich phases is discernible already after the shortest aging time of 3.6ks(1h) at 748K for an Fe=30%Cr alloy. He also confirmed that there was no incubation time of the hardness change on aging at 748K for the alloy. Blackburn and Nutting[15] have reported that the Cr-rich phase is disk-like at 748K, and that there is an incubation time of about 54ks(15h) for the hardness change of an Fe-21%Cr alloy. Based on these experimental results, Lagneborg[14] had a conclusion that 21%Cr and 30%Cr locate outside and inside the spinodal curve at 748K, respectively. However, there is a question about his conclusion because he did not perform hardness measurements and transmission electron microscope observations for aging times shorter than 3.6ks, and because hardness is not so sensitive to detect small concentration change in the early stages of the decomposition. More systematic and detailed studies by means of the recent advanced techniques are needed to understand kinetics of the phase decomposition from the microscopic view point.

In the present section, Mössbauer spectroscopy is applied to clarify the early-stage decomposition of solid solutions with the aid of numerical analysis by a computer and the microstructure observation by an electron microscope.

4.2 Experimental procedure

Specimens and the Mössbauer effect measurement are the same with those described in the previous section. In addition to the computer calculation to see the local environmental effect, Mössbauer data are closely analyzed by using a computer to obtain (a) a difference between two Mössbauer spectra (*difference spectrum*) and (b) the probability curve for the internal field distribution (*P(H) curve*).

a. Difference spectrum

It is very difficult to catch a smallest change in the Mössbauer spectrum by naked eyes, when the aging time is very short. It may be useful to obtain a difference between two spectra in such a case. By fitting a quadratic equation to the experimental background, the calculated background is first subtracted from the whole experimental spectrum. After the area below the background for the aged specimens is equalized to that of the as-quenched one, the latter is subtracted from the former to get a difference-spectrum. In another case, the spectrum synthesized assuming a random solid solution is subtracted from a synthesized one corresponding to the decomposed alloy which is calculated by assuming a deviation from the random= atomic distribution.

b. P(H) curve

The numerical method proposed by Hesse and Rübartsch[16] is used to obtain the P(H) curve. The internal field range from 0 to 26.5MA/m(333kOe) is divided into fifty equal intervals, ΔH=0.53 MA/m(6.7 kOe) : $H_j = j\,\Delta H$, j=0 to 50. The experimental spectrum, $S(x_i)$ is expressed by the equation:

$$S(x_i) + \varepsilon_i = \Sigma P(H_j) L_6(H_j, x_i). \qquad (4.1)$$

Where x_i is the channel number or velocity, $L_6(H_j, x_i)$ the sextuplet of Lorentzian curve, ε_i the error. The unknown parameter $P(H_j)$ is numerically calculated by means of the least square fit to satisfy a condition,[16,17]

$$\frac{\partial}{\partial P} \sum_i \{(P_{i-1} - P_i + P_{i+1})^2 + \gamma^{-1} \Sigma \varepsilon_i^2\} = 0 \qquad (4.2)$$

The smoothness of the P(H) curve obtained is influenced by the selection of the parameter γ in particular at the lower internal field regions of less than -10MA/m(125kOe). An optimum value of γ is selected among various values of 0.1 to 1000 by a trial-error calculation for the as-quenched alloy to give the minimum square error deviation from the experimenta data. It is confirmed that γ=100 is the most favorable for the present case.

4.3 Results and discussion

4.3.1 Rate-controlling process

a. Incubation time

Classical theories for the phase separation predict that the solid solution heated at temperatures inside the miscibility gap will decompose via N-G and S process outside and inside the spinodal line, respectively. A rough distinction of these two mechanisms may be achieved by examining the incubation time for the change in the matrix composition during aging. As mentioned in §1, the average internal field, $\bar{H}$, measures the average Cr content of solid solutions within an accuracy of ±1%Cr. Figures 4.1(a) and (b) show changes in $\bar{H}$ measured at room temperature as a function of aging time at 748K. For alloys of x=0.21 to x=0.363

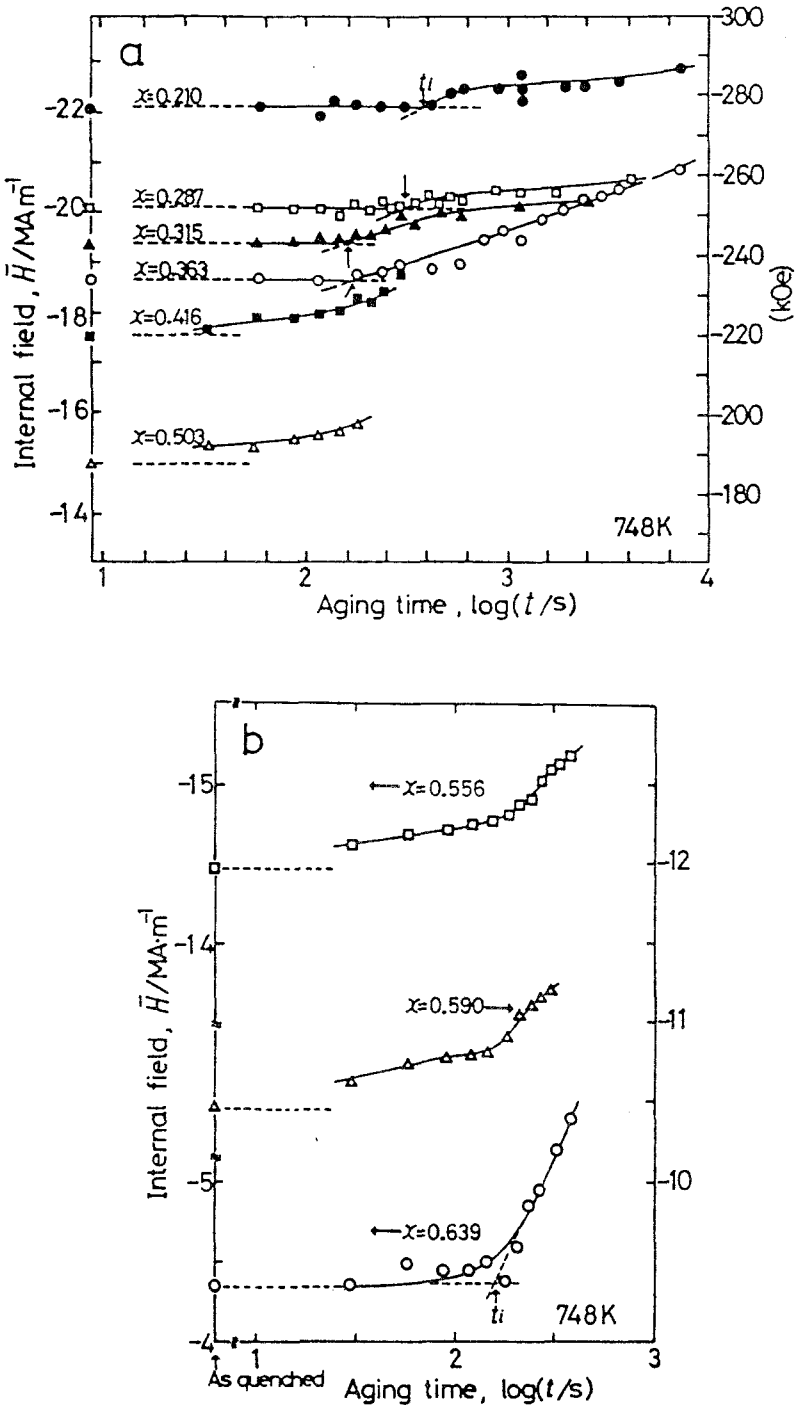

Fig.4.1 Average internal field, $\bar{H}$, as a function of aging time at 748K for various $Fe_{1-x}Cr_x$ alloys. The incubation time t_i is clearly confirmed for alloys with x=0.21-0.363 and 0.639. Lines are handwritten through experimental points.

and x=0.639, there is an incubation time, t_i, which is defined here as the time interval in that no significant change in $\bar{H}$ is measured within an experimental error of ±0.16MA/m (2kOe). These results do not support the conclusion by Lagneborg[14] that the 30%Cr sample decomposes via S process because of no incubation time for the hardness change at 748K. For alloys of x=0.416 to x=0.556, t_i is indistinguishable on the $\bar{H}$ vs. t_i plot, because $\bar{H}$ shows an increase already after 30s of the aging time. For an closer examination, the fraction transformed, y, defined by

$$y=\frac{\bar{H}_t-\bar{H}_0}{\bar{H}_\infty-\bar{H}_0} \qquad (4.3)$$

is plotted against the aging time in Fig.4.2. Here $\bar{H}_0$, $\bar{H}_t$, and $\bar{H}_\infty$ are the mean internal field at the beginning, the elapsed time t and the completion of the phase decomposition. The value of H_∞ for the 748K-aging has been measured in §3. $\bar{H}_\infty=\bar{H}_{Fe}$=-24.6MA/m (307kOe). As seen in the figure, a linear relationship is obtained between y and t for each alloy. The extrapolation of each line intersects the time axis at a minus point. Hence it is concluded that the decomposition takes place so fast that the incubation time is substantially absent from these alloys. The concentration dependence of t_i is summarized as shown in Fig.4.3. With increasing x, t_i decreases linearly in the concentration range x=0.2 to x=0.38. Because t_i=0 for x=0.42, it is expected that there is an "apparent" boundary around x=0.4 where transition from N-G to S process takes place. According to Feder *et al.*[3,18], the incubation time is expressed as

$$t_i=\frac{-4\,k_B T}{\beta^*\left(\partial^2\Delta G^0/\partial r^2\right)|_{r^*}} \qquad (4.4)$$

where ΔG^0 is the standard free energy change associated with the

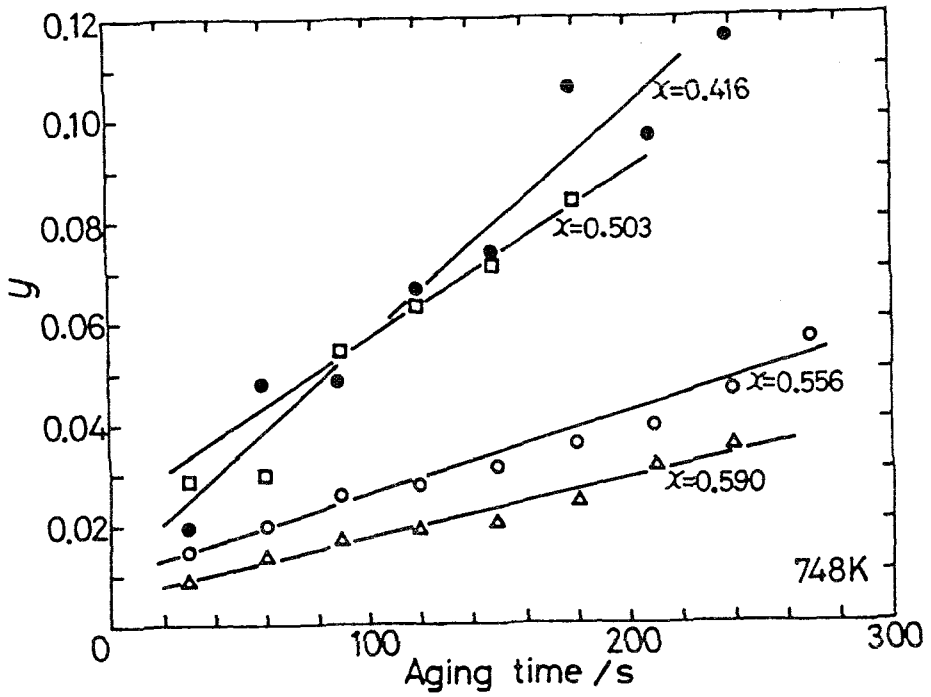

Fig.4.2 Fraction transformed, y, as a function of aging time at 748K for various $Fe_{1-x}Cr_x$ alloys. The extrapolation of each linear line intersects the time axis at $t<0$.

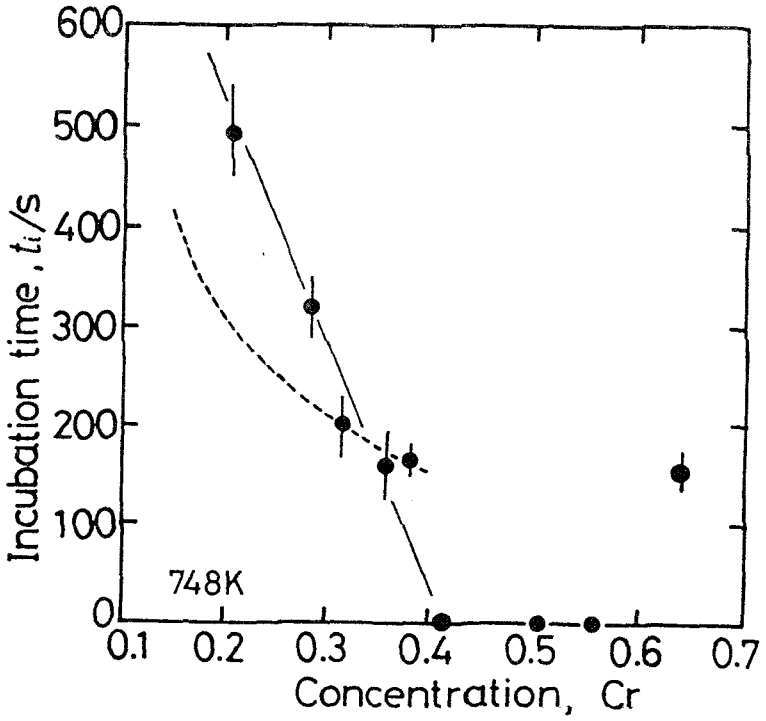

Fig.4.3 Incubation time, t_i, for the 748K-aging as a function of Cr content. A dotted line is calculated from eq.(4.7). A solid line is handwritten through the experimental points.

formation of spherical embryo with the size r, and β^* the frequency factor, *i.e.*, the rate at which single atoms join the critical nucleus with the size r^*. ΔG and β^* are given by[3]

$$\Delta G^0 = \frac{4}{3}\pi r^3 \Delta G_V + 4\pi r^2 \gamma_s \ , \tag{4.5}$$

and

$$\beta^* = D S^* x / a^4 . \tag{4.6}$$

Here D is the diffusivity of the constituent atoms, S^* the area of the nucleus, ΔG_V the volume free energy change attending the formation of clusters, γ_s the interfacial energy between the cluster and the matrix, and a the lattice constant. From eq.(4.5), is obtained

$$\left.\frac{\partial^2(\Delta G^0)}{\partial r^2}\right|_{r^*} = -8\pi\gamma_s \ . \tag{4.7}$$

and by substituting it with β^* into eq.(4.4),

$$t_i = \frac{k_B T \Delta G_V a^4}{8\pi^2 D_0 x \gamma_s^3} \exp\left(\frac{Q}{RT}\right) . \tag{4.8}$$

Here D_0 is the diffusion coefficient, Q the activation energy for diffusion of solute atoms, k_B the Boltzmann constant. Figure (4.4) shows the time and temperature dependence of the transformed fraction, y , for x=0.363. The incubation time for temperatures of 753-813K is measured at the intersection between these curves and the time axis. Logarithmic values of the term, t_i / T, are plotted against $1/T$ in Fig.4.5. A linear line is obtaind by the least square fit to these experimental points as shown in the figure:

$$\ln (t_i / T) = \frac{24500}{T} - 34.3. \tag{4.9}$$

The slope of the linear line evaluates Q in eq.(4.8) as 204 kJ/mol, which is consistent whith the activation energy for diffusion of Cr atoms (=203kJ/mol) in an Fe-26 at%Cr alloy

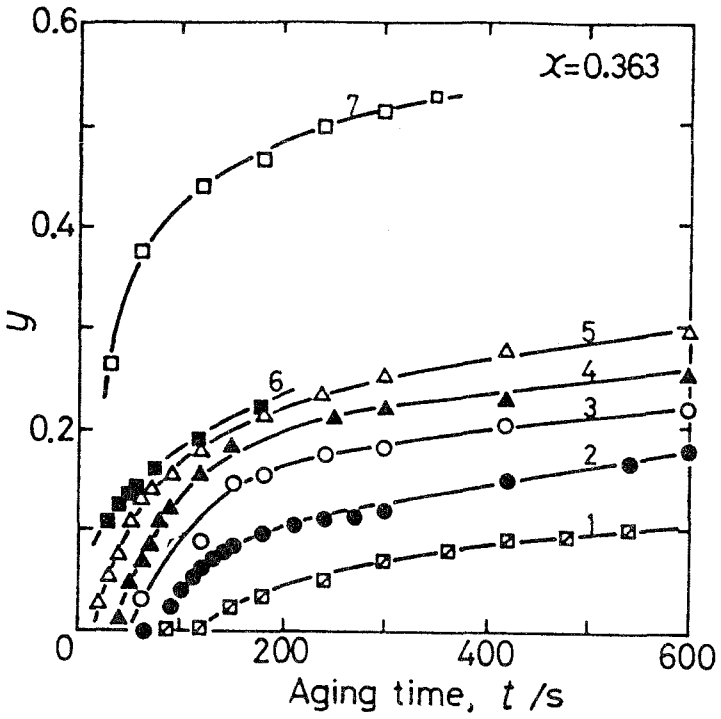

Fig.4.4 Transformation fraction, y , as a function of aging time and temperature for an $Fe_{0.637}Cr_{0.363}$ alloy. 1-753K, 2-773K, 3-783K, 4-798K, 5-813K, 6-823K, 7-833K.

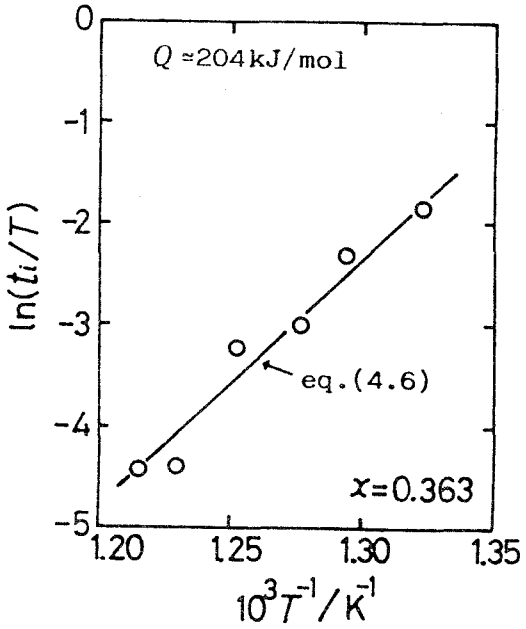

Fig.4.5 $\ln(t_i/T)$ vs. $1/T$ plot for an $Fe_{0.637}Cr_{0.363}$ alloy.

measured by Paxton and Kunitake[19] using ^{51}Cr tracer.

Then, next consider the concentration dependence of the incubation time. Equation (4.8) is rewritten in a form

$$t_i = \frac{\Phi}{x} \quad , \text{ and}$$

$$\Phi = \frac{k_B T \Delta G_V^2 a^4}{8 \pi^2 D_0 \gamma_s^3} \exp\left(\frac{Q}{RT}\right) \quad . \tag{4.10}$$

Equation (4.10) gives Φ=61.4s for T=748K and x=0.363. Assuming that values of ΔG_V, a, D_0, γ_s, and Q are independent of x, t_i is calculated by eq.(4.10) as shown by a dotted line in Fig.4.3. A qualitative agreement between the calculation and the experiment seems to be obtained, but the former must be improved to fit the latter's linear relation by taking account of parameter changes. For instance, the activation energy for diffusion, Q,

increases with decreasing x.[19] Finally it should be emphasized that eq.(4.4) derived by the clssical nucleation theory accounts for the temperature and concentration dependence of the incubation time in the concentration range $x \leq 0.38$.

b. Johnson-Mehl plot

The experimental data of $\bar{H}$, which have been already shown in Fig.3.7, are rearranged in Fig.4.6 by using the Johnson-Mehl equation,

$$\log \log \frac{1}{1-y} = n \log k + n \log t - \log 2.3, \qquad (4.11)$$

where, n is the time exponent and k the rate constant. The Johnson-Mehl plot for $x=0.210$ consists of three parts with different time exponents, n. Because n is approximately 1.5, the first stage of the phase decomposition is interpreted as the diffusion-controlled growth of fixed numbers of particles.[1] The Cr-rich precipitates are confirmed by an transmission electron microscope at the aging time of 36ks($\log t = 4.6$) in the second stage (See Photo.1(b)), though they are invisible in the first stage probably because of their small sizes and low

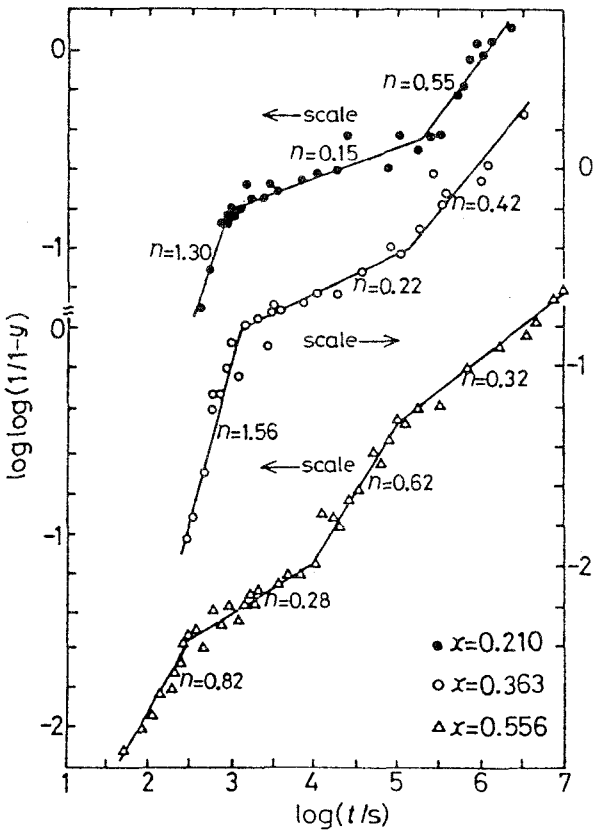

Fig.4.6 Johnson-Mehl plots for the the 748K-aging of $Fe_{1-x}Cr_x$ alloys with x=0.21, 0.363, and 0.556.

volume fractions. The present result is consistent with the conclusions for the 20%Cr alloy by Nys and Gielen[4], and Lagneborg[14] that it decomposes via N-G process around 748K.

The figure also suggests that the decomposition process of the alloy with x=0.363 should be explained by the same mechanism as that for the alloy of x=0.21, because the Johnson-Mehl plot has a close resemblance to one for the latter. The Cr-rich phase precipitation is confirmed by the transmission electron microscope after 600s ($\log t$=2.8) in the first stage of the plot (See Photo.2(b), P.89). These results are quite interesting in the sense that N-G process is not restricted outside the spinodal line defined in the classical theory (the spinodal concentration is about 0.27 at 748K), but takes place within the spinodal region. This aspect is qualitatively consistent with the computer simulation due to Binder *et al*.[9] who proposed that the structure factor outside the spinodal line is indistinguishable from what will be expected by the non-linear spinodal theory due to Langer,[12] and that the decomposition kinetics inside the spinodal line is described by the nucleation theory.

The Johnson-Mehl plot for x=0.556 consists of four stages, and n for the first stage is considerably smaller than 1.5. Accordingly, its decomposition process seems to be somewhat different from that of the lower Cr content alloys cited above. The Cr-rich phase is observed after the prolonged aging time of 108ks(30h, $\log t$=5) (See Photo.3(d), P.99) which coincides with the onset of the fourth stage of the Johnson-Mehl plot. The the time is also coincident with that where the concentration fluctuation

characteristic of the S process develops to a maximum (See Fig.4.10). It is clear that the decomposition process of the alloy has a different feature from that of the lower Cr content alloys mentioned above. Finally, note that the Johnson-Mehl plot suggests that the kinetics changes apparently between the concentraration of x=0.363 and x=0.556, supporting the result obtained by the incubation time measurements.

c. *Activation energy*

The activation energy of the initial-stage decomposition is evaluated by the rate-constant method. Generally, the rate constant k in eq.(4.11) obeys the Arrhenius type equation,

$$k = \nu \exp(-A_r/RT) \qquad (4.12)$$

where ν is the frequency factor, and A_r the activation energy which controls the reaction rate. Data in Fig.4.4 are rearranged by the Johnson-Mehl plot as shown in Fig.4.7. Because values of n are about 1.5 for the first stages of aging at temperatures from 753K to 813K, the mechanism of decomposition at these

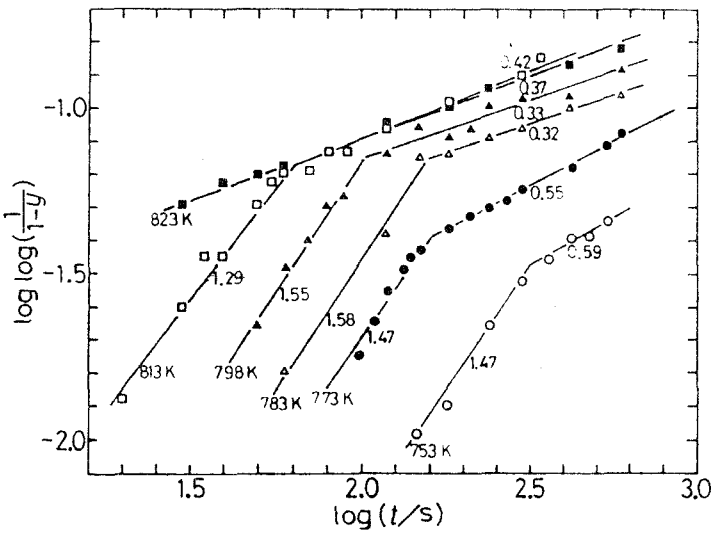

Fig.4.7 Johnson-Mehl plots as a function of aging temperature for an $Fe_{0.637}Cr_{0.363}$ alloy. Figures represent the time exponent n.

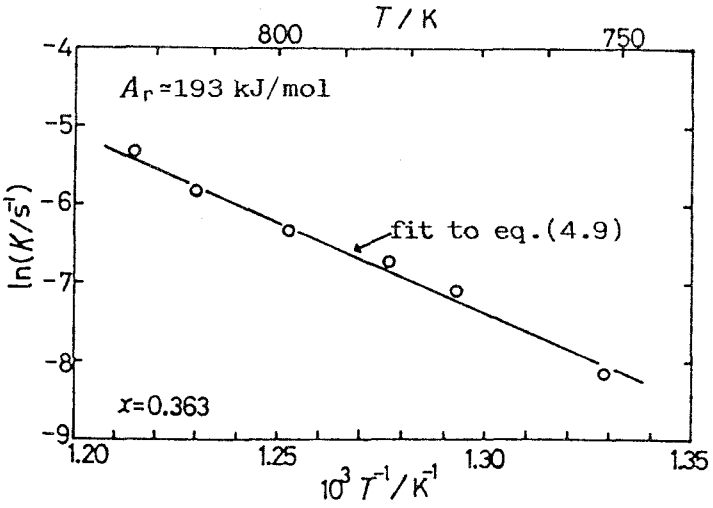

Fig.4.8 Logarithm of the rate constant, k , as a function of $1/T$ for an $Fe_{0.637}Cr_{0.363}$ alloy.

temperatures is expected to be the same as that at 748K. Logarithms of k obtained by the least square fit for the first stage of these Johnson-Mehl plots are shown as a function of $1/T$ in Fig.4.8, which ensures that experimental data are represented by eq.(4.12). The slope of the linear line gives the activation energy, A_r=193±3kJ.mol, which is roughly consistent with the value, Q=204kJ/mol, obtained by the incubation time measurement. Accordingly, it is concluded that the first stage of the growth process of precipitates is controlled by the diffusion of Cr atoms as well as their nucleation in the alloy of x=0.363.

d. Concentration fluctuation

The spinodal decomposition is accompanied by a gradual growth of the concentration deviation from the average composition. The alloy decomposed via S process is considered to be composed by small regions the average composition of which varies from region to region. It is easily predicted that the corresponding Mössbauer spectrum will have a peakwidth broader than that of the as-quenched alloy with a random distribution of constituent atoms. For the N-G process, little or only trifle broadening of the halfwidth will be expected. Because the innermost peaks of the Mössbauer spectrum are sharp and symmetrical, the accurate measurement of their peakwidth will permit us to catch a smallest change in the compositional fluctuation. Figure 4.9 shows two typical examples of x=0.363 and 0.556. The half width, Γ_e, of the left peak is shown in Fig.4.10 as a function of aging time. For x=0.556, Γ_e increases gradually with increasing aging time, having a maximum around $\log t$=5.2(50h). The time is consistent with that where the absorption around zero velocity

begins to develop (See Fig.4.9, 108ks(30h)), which means the formation of a paramagnetic phase. When the aging time becomes longer than 180ks(50h), Γ_e decreases gradually in inverse proportion to the increase in the absorption around zero velocity. Such features of the change in Γ_e are an evidence for the evolution of the compositional fluctuation characteristic of the

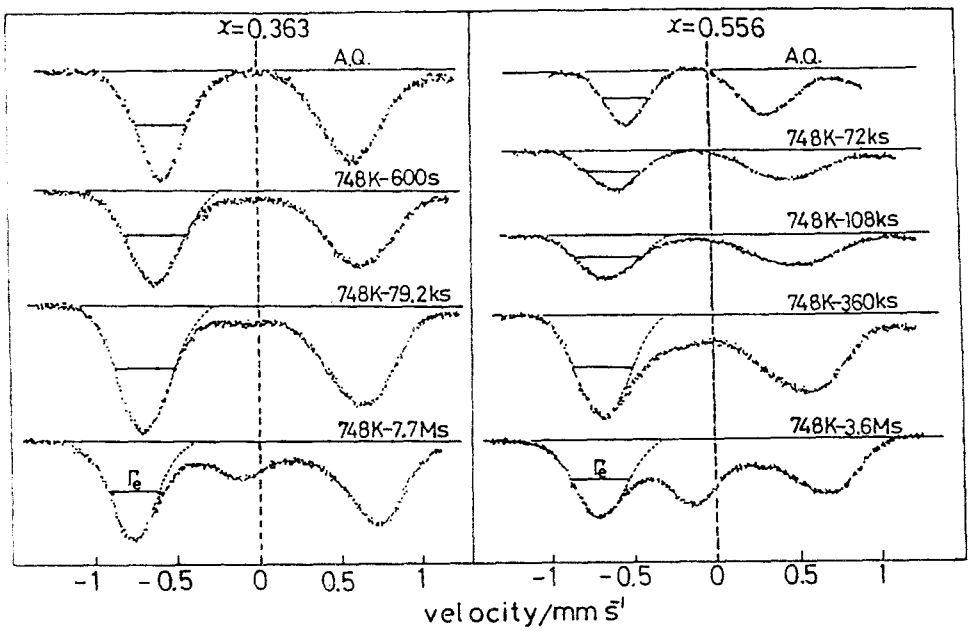

Fig.4.9 Partial Mössbauer spectra near zero velocity showing the change in the half width, Γ_e, during aging at 748K. *A.Q.* represents the as-quenched alloy.

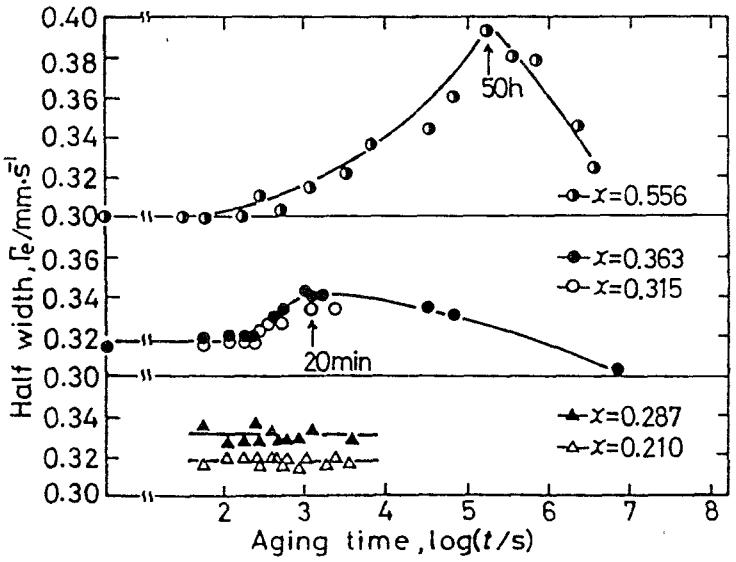

Fig.4.10 Half width, Γ_e, illustrated in Fig.4.9 as a function of aging time at 748K for various $Fe_{1-x}Cr_x$ alloys.

S process.

In spite of the previously obtained results that the alloys with x=0.21 to 0.363 decompose via N-G process at 748K, the increase in Γ_e takes place for x=0.315 and 0.363 like x=0.556. However, the time evolution of Γ_e for the former attains a maximum at rather short aging time ($\log t$≈3.2, t=20min) with a rather low height compared with the latter alloy. As will be mentioned in the later part, the Cr-rich precipitates are clearly observed after the 600s-aging by the transmission electron microscope (See Photo.2(b)), so that the above result suggests that the precipitation is accompanied by the increase in the concentration fluctuation similar to the S mechanism. In the case of the lower Cr content alloys of x=0.21 and 0.287, changes in Γ_e are negligibly small. According to Katano and Iizumi[11], a time evolution of the neutron scattering intensity of alloy with 32%Cr and 40%Cr showed a typical spinodal behavior expected in the recent spinodal theory due to Langer[12]. In contrast, the feature became less pronounced in the 24%Cr sample. These facts mean that concentration fluctuation in the matrix develops significantly in the alloys with $x \geq 0.32$, but only slightly for $x \approx 0.24$. The present Mössbauer results mentioned above are qualitatively consistent with the neutron scattering experiment.

4.3.2 Computer analysis and microstructure change

Experimental results hitherto obtained strongly suggest that the decomposition kinetics of alloys with x=0.21 to 0.363 somewhat differs from that of the alloy of x=0.556: N-G process is expected for the former and S process for the latter. It is needed to get a direct evidence for the formation of the cr-rich

phase for the sake of clear distinction of these two mechanisms. Neutron scattering experiments, which have proposed S mechanism for the 32%Cr sample, did not include any information about the time when the precipitates appear, their size and volume fraction. The present section intends to disclose these subjects by using Mössbauer spectroscopy with the help of transmission electron microscopy.

(a) *The alloy with chromium concentration, x=0.21*

The effect of aging on the Mössbauer spectrum appears clearly on the shape of the outermost peaks as well as the shift of their positions toward outside, as seen in Fig.4.11. However, the paramagnetic peak associated with the Cr-rich phase is not observed even after the 108ks(30h)-aging. It is probably due to the low volume fraction of the phase. The difference spectrum which is defined as

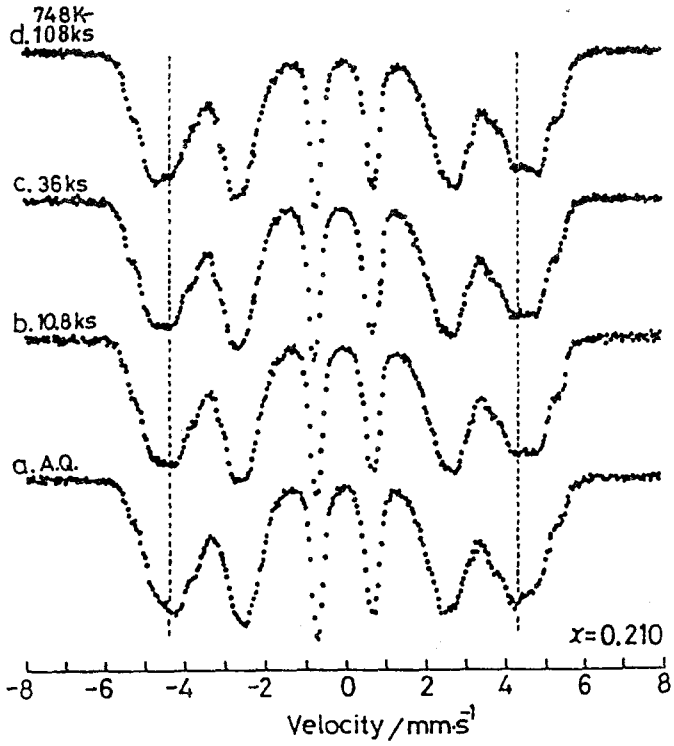

Fig.4.11 Mössbauer spectra at room temperature of an $Fe_{0.79}Cr_{0.21}$ alloy quenched from 1273K(a) and then aged at 748K for various times(b,c, and d).

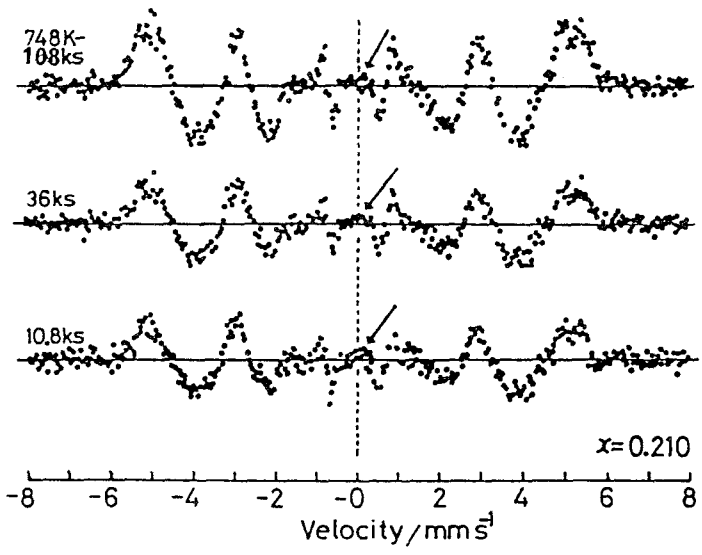

Fig.4.12 Difference-spectrum of an $Fe_{0.79}Cr_{0.21}$ alloy. Arrows show a weak appearance of the paramagnetic peak.

(the aged-alloy spectrum minus the as-quenched alloy spectrum) is shown in Fig.4.12 which indicates that an absorption peak associated with paramagnetic phases exists around zero velocity (arrows) after the 10.8ks(3h)-aging already, though it is very small. Transmission electron micrographs corresponding to the above annealing times are shown in Photo.1. Uniform precipitation of fine particles is observed when the aging time is longer than 36ks(10h). They are invisible at 10.8ks(3h). This result suggests that the difference spectrum is more sensitive to recognize the precipitates than transmission electron microscopy. According to Kelly and Nicholson,[20,21] the volume fraction, f_T, of spherical particle with diameter, d, and the mean free distance, Λ, is expressed by

$$f_T=\frac{\pi}{6}\left(\frac{d}{\Lambda}\right)^2, \tag{4.13}$$

where the subscript, T, means transmission electron microscopy. Values of f_T are shown in Fig.4.13 as a function of aging time: $f_T \simeq 0.02, 0.05, 0.12$ for t=36ks($\log t$=4.56), 108ks($\log t$=5.03), 360ks($\log t$=5.56), respectively. Another way of estimating the volume fraction is to

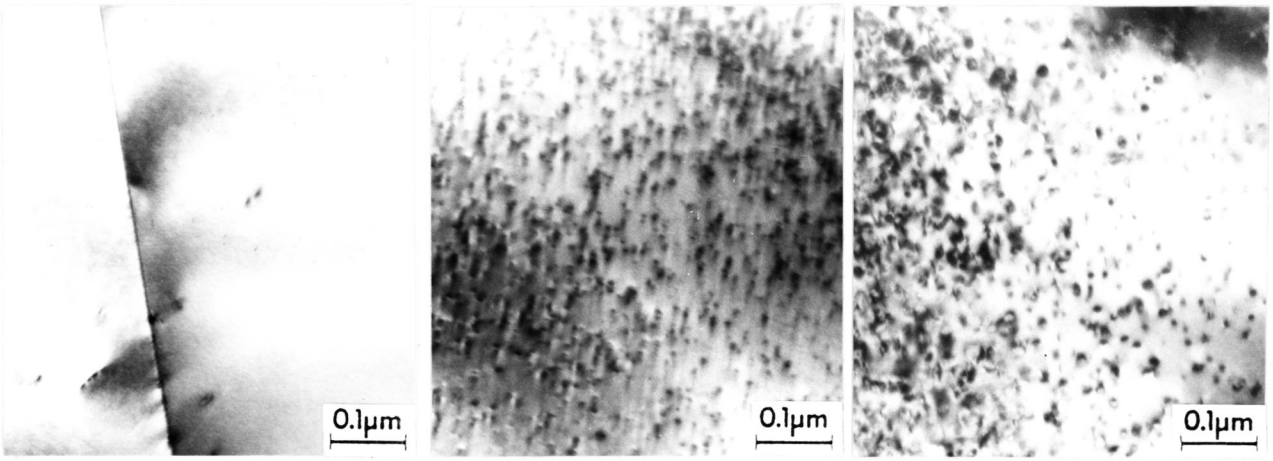

(a) Aged 10.8ks (3h) (b) Aged 36ks (10 h) (c) Aged 108 ks (30h)

Photo.1 Transmission electron micrograghs of an $Fe_{0.79}Cr_{0.21}$ alloy aged at 748K, showing the Cr-rich precipitation in (b) and (c).

use the lever relation,

$$f_L = \frac{x_0 - x_t}{x_{Cr} - x_{Fe}} \qquad (4.14)$$

Here the subscript, L , represents the lever relation, and x_{Cr} , x_{Fe} , x_0, x_t are the concentration of the Cr-rich phase, that of the Fe-rich phase, the initial average matrix concentration, the average matrix concentration after an aging time, t . The values of x_t are obtained by substituting the measured values of $\bar{H}$ into eq.(1.5) as a function of aging time. Values of f_L are plotted along with f_T in Fig.4.13 which indicates good agreement between these values for the prolonged aging time of about 360ks($\log t$ =5.6). Therefore one can conclude that fine precipitates observed in Photo.1 are the Cr-rich phase, though their compositions and lattice structure have not been directly determined by electron microscopy. The short-time aging shows a tendency to give lower values of f_T compared with f_L. The average diameter of the Cr-rich phase is about 11 nm for the 30ks-aging (Photo.1(a)). One of the possible reasons for the discrepancy between f_T and f_L is that there may be many invisible precipitates which have much smaller sizes than the average. It is likely that more accurate and careful observations by the electron microscope are needed to estimate f_T closely in the early stages of the decomposition. Attention should be paid on the point that the Mössbauer effect is more sensitive and convenient than electron microscopy to detect the

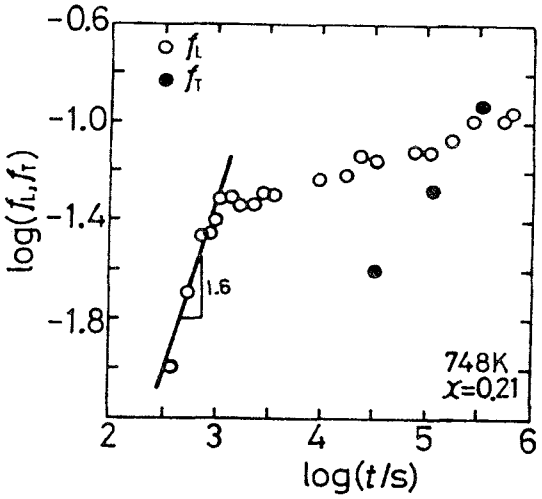

Fig.4.13 Volume fractions, f_L and f_T , of the Cr-rich phase as a function of aging time for an $Fe_{0.79}Cr_{0.21}$ alloy.

Cr-rich phase even when its volume fraction is very small. The fact that the slope of $\log t$ vs. $\log f_L$ plot is about 1.5 in the initial stage suggests that the growth of precipitates is controlled by diffusion because the precipitate volume, V_p, will increase with $t^{3/2}$ when the radius increases with $t^{1/2}$, supporting the result obtained previously by the Johnson-Mehl plot. In summary, those facts that (1) the incubation time for the matrix concentration change exists, (2) the Johnson-Mehl plot gives $n \sim 1.5$ in the initial stage following to the completion of the incubation period, (3) the Cr-rich phase is confirmed at 10.8ks(3h) and 36ks (10h) of the aging time by Mössbauer spectroscopy and transmission electron microscopy, respectively and (4) development of the concentration fluctuation in the matrix is negligible lead to a conclusion that the alloy has typical features of the decomposition predictable by the nucleation and growth theory.

(b) The alloy of x=0.363

(i) Internal field distribution curve and difference spectrum

Figure 4.14 shows experimental Mössbauer spectra (dots) of x=0.363 in the as-quenched state(a), and the aged state for various aging times at 748K ((b) to (e)). It is very difficult to distinguish the spectrum changes due to the aging by naked eyes, except for a slight increase in absorption around zero velocity for aging times of more than 600s. Solid lines represent best-fit curves obtained by computing the internal-field distribution curves shown in Fig.4.15. The maximum of the distribution curve seen around H=-17 MA/m(214kOe) for the as-quenched state(a) shifts to higher $|H|$ when the aging time increases more than 240s. This implies that the aging is accompanied by the increase in the mean internal field, $\bar{H}$.

It should be noted that the increase in the probability of the zero internal field occurs at 240s, and roughly coincides with the beginning of the shift of the probability curve. The former means precipitation of the paramagnetic phases. Values of $P(0)$ are plotted in Fig.4.16 as a function of aging time. It is evident that $P(0)$ increases sharply after a duration of 200-300s which agrees with t_i=190s for x=0.363 obtained previously in 4.3.1a. Figure 4.17 depicts that the paramagnetic peak is clearly recognized in the difference specra for the aging times longer than 360s, though it is absent or vague at 120s. The height of the paramagnetic peak, h_0, is compared with $P(0)$ in Fig.4.16. After a duration of about 200s, h_0 also shows a rapid increase followed by a gradual increase for the longer aging time of more than 500s. General trend of the time dependence of h_0 and $P(0)$ has a close similarity. The time when the paramagnetic peak is first recognized is much shorter than the case of x=0.21, and is included within the first stage of the Johnson-Mehl plot.

Since the paramagnetic peak is clearly measured at 480s in the initial stage aging, detailed discussions will be, hereafter, concentratred on the aging time. The experimental Mössbauer spectra of the 480s-aged and the as-quenched alloy are repeated in Figs.4.18(a) and (b), respectively. A solid line(b_2) in Fig.4.18(b) is the spectrum calculated by assuming the random atomic distribution, showing good fit to the experimental data, which is also checked by the comparison of two difference spectra defined by ($a-b_1$) and ($a-b_2$) in Fig.4.18(c). The distance between the A and Á peak is about 9.3mm/s which is equivalent to the average internal field of -23MA/m(289kOe), and is comparable with the internal field of the

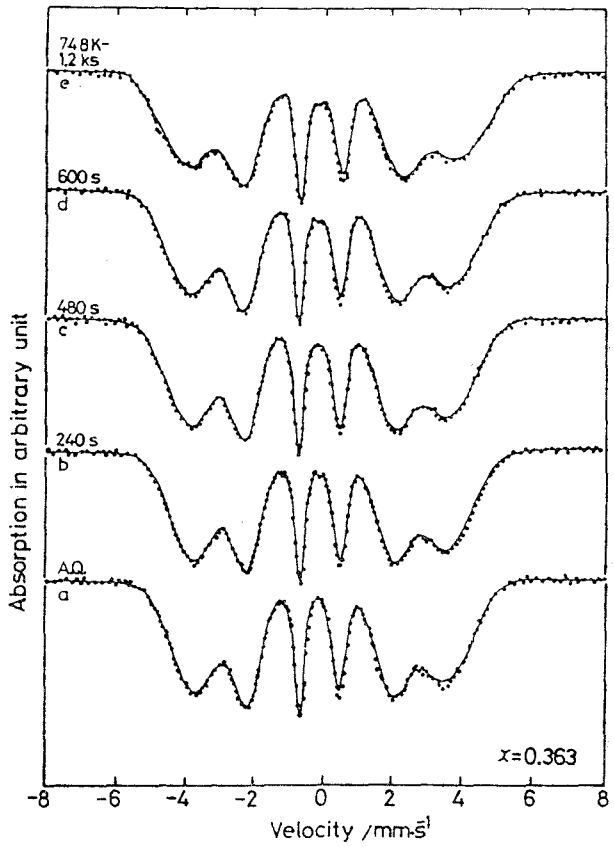

Fig.4.14 Mössbauer spectra at room temperature(dots) of an $Fe_{0.637}Cr_{0.363}$ alloy quenched from 1273K(a) and then aged at 748K for various times (b-e), and computer fits (solid lines) to yield the internal field distribution curves shown in Fig.4.15.

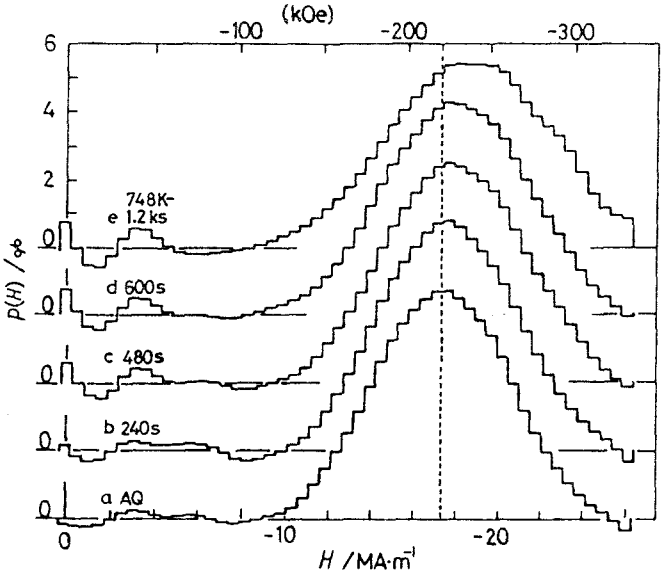

Fig.4.15 Internal field distribution curves of an $Fe_{0.637}Cr_{0.363}$ alloy quenched from 1273K(a) and then aged at 748K for various times (b-e).

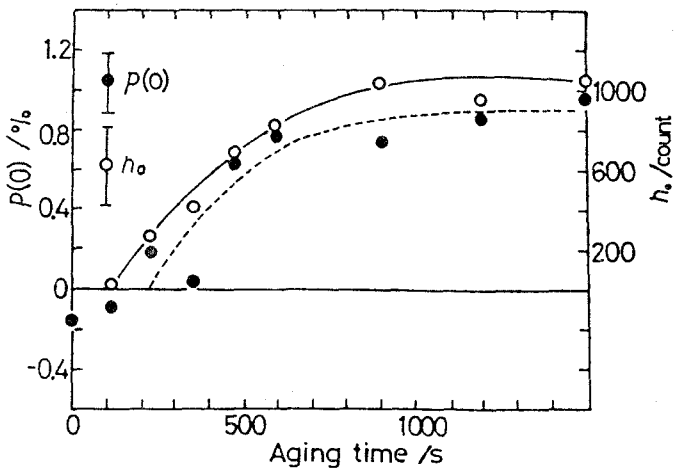

Fig.4.16 Probability of the zero internal field, $P(0)$, and the height of the paramagnetic peak, h_0, in Fig.4.17 as a function of aging time for an $Fe_{0.637}Cr_{0.363}$ alloy.

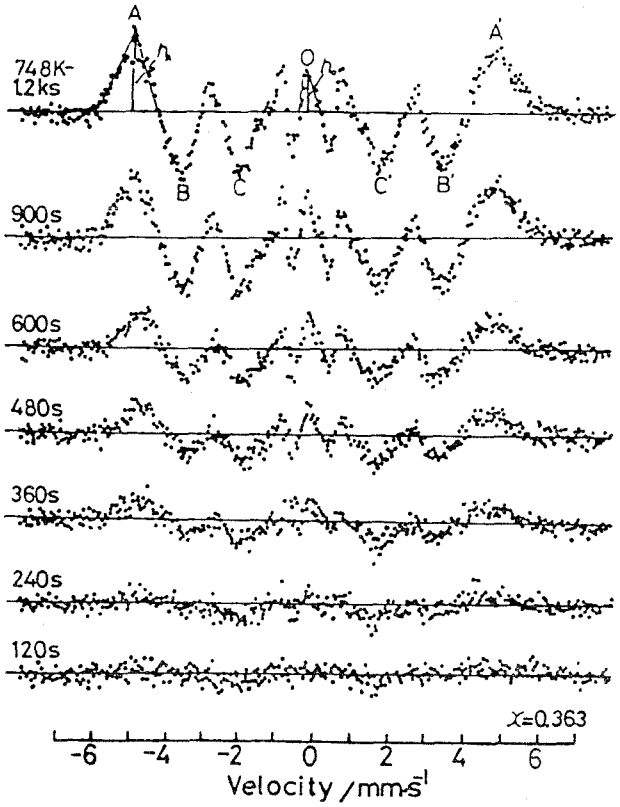

Fig.4.17 Difference spectra of an $Fe_{0.637}Cr_{0.363}$ alloy aged at 748K, showing the paramagnetic peak designated O for the aging time longer than 360s.

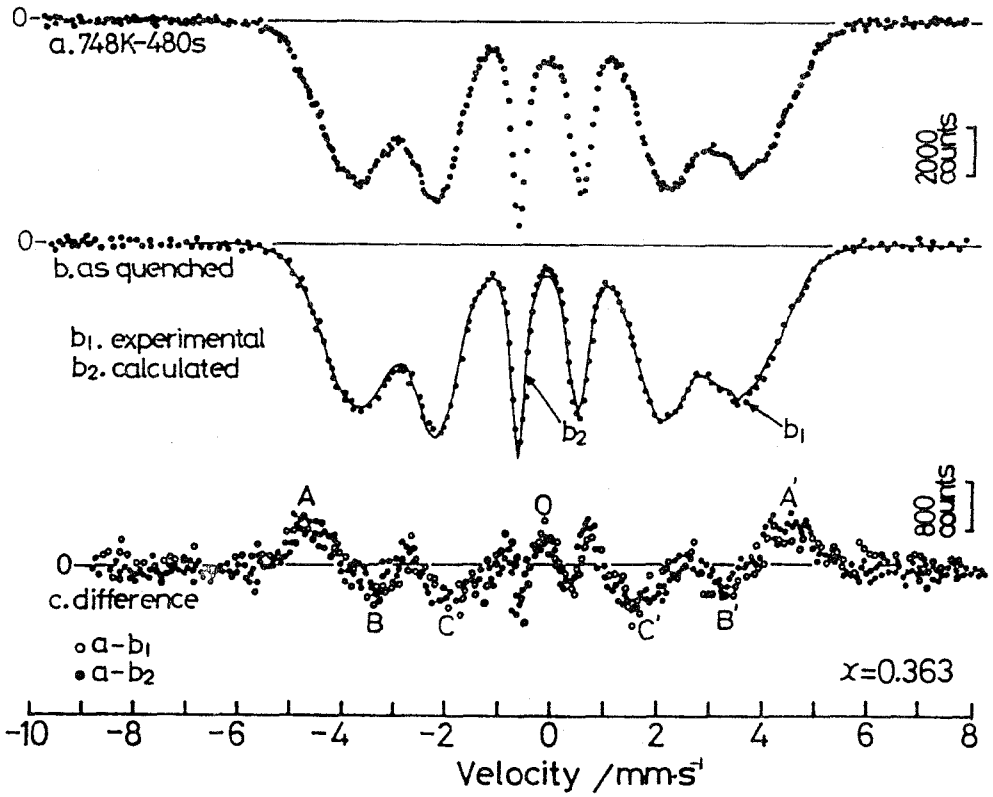

Fig.4.18 Mössbauer spectra of an $Fe_{0.637}Cr_{0.363}$ alloy aged at 748K for 480s(a), quenched from 1273K(b_1) and computer fits(b_2), and difference spectra (c) defined by ($a-b_1$) for open circles and ($a-b_2$) for soild circles.

final Fe-rich phase(-24.5MA/m). The fact strongly suggests that Fe-rich clusters coexist with the Cr-rich phase in the beginning of the decomposition already, being consistent with descriptions of the nucleation and growth theory. Figure 4.19(a) shows the internal field distribution curves of both the 480s-aged (P_A) and as-quenched sample(P_Q) for the comparison. The difference of ($P_A - P_Q$) in Fig.4.19(b) points out that the aging is accompanied by an increase in $P(H)$ in the field range from -20 to -25MA/m(region A) and at $H=0$, and a decrease in $P(H)$ in the range from -5 to -20 MA/m. The change in region A is induced by the increase of Fe atom configurations with internal fields higher than the average. Since the hatched area B is roughly equal to the hatched area A, it may be reasonable to consider that the atom configurations in the region B transform into those in the region A, which will be realized by the replacement of Cr atoms with Fe atoms. Then, the decreased probability in the field region C may be related with the increase in $P(0)$, if we assume that the replaced Cr atoms agglomerate to form Cr-rich clusters. In other words, it is speculated that atom configurations belonging to the field region C act as the nucleation site for the Cr-rich phase precipitation.

(*ii*) *Computer simulation*

The computational method to see the local environmental effect has proved itself to be effective to synthesize a spectrum of the as-quenched state (e.g., Fig.4.18(b)). The method may be also available to synthesize a spectrum of the decomposed state if probabilities $P(m,n)$ are modified as follows. Since the method to compute the probability of the internal field distribution also gives good fit to the as-quenched spectrum (e.g., Fig.4.14(a)),

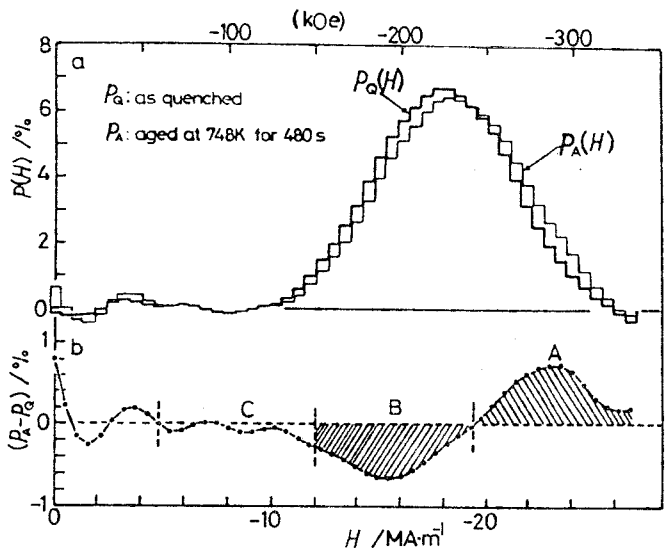

Fig.4.19 (a) Comparison of the internal field distribtution curves between the as-quenched ($P_Q(H)$) and the aged state ($P_A(H)$) of an $Fe_{0.637}Cr_{0.363}$ alloy. (b) the difference defined by ($P_A(H)-P_Q(H)$).

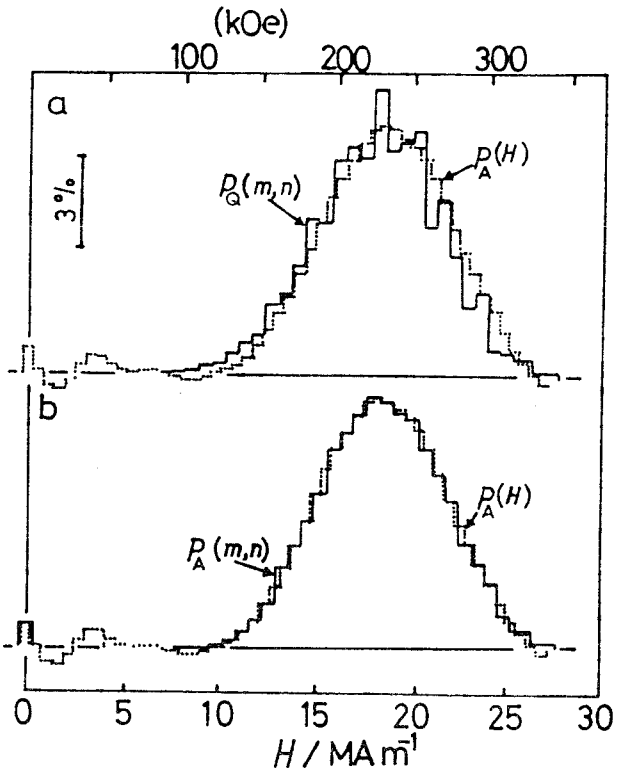

Fig.4.20 $P(m,n)$ values for the as-quenched (Q) and the aged state (A) of an $Fe_{0.637}Cr_{0.363}$ alloy in comparison with the internal field distirution curve, $P_A(H)$.

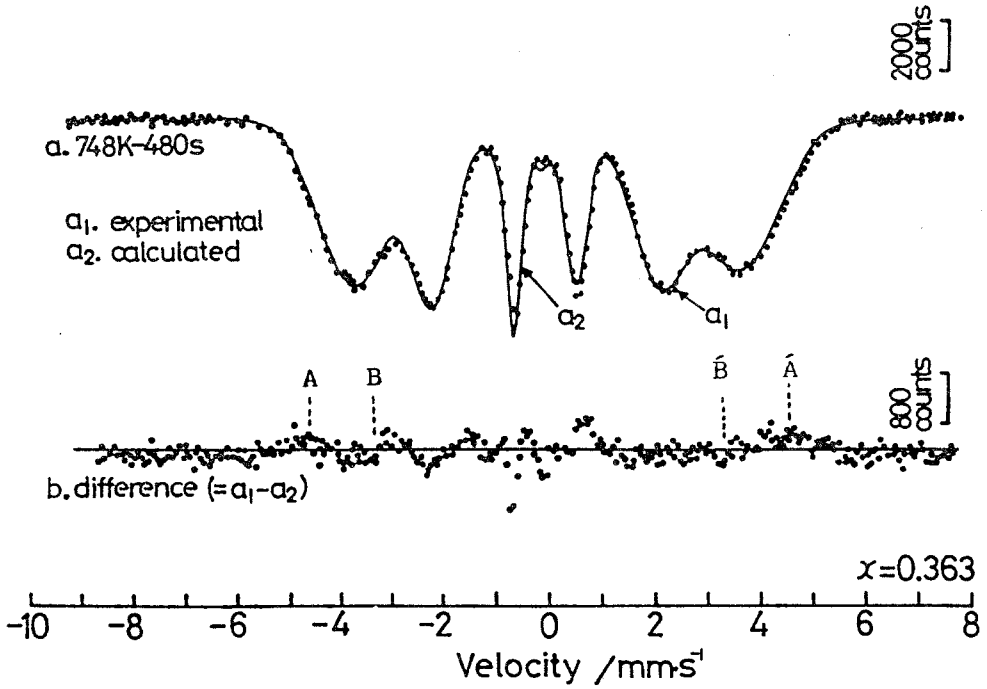

Fig.4.21 (a) Comparison of the spectrum synthesized by taking consideration of the local environment effect(a_2) with the experimental Mössbauer spectrum(a_1) of the decomposed $Fe_{0.637}Cr_{0.363}$ alloy. (b) Difference spectrum defined by (a_1-a_2).

the internal field probabilities $P(m,n)$ and $P(H)$ are comparable with each other. However, there is a problem that the intervals between $P(m,n)$'s which are given by eq.(1.1) vary from value to value in contrast to the equal division of ΔH(=0.53MA/m) in the method to compute the internal field distribution curves. Therefore, $P(m,n)$ values are first recalculated to have nearly equal intervals($\sim$ 0.66MA/m) comparable with ΔH. The resultant values (hereafter $P_Q(m,n)$) are compared with those of $P_A(H)$ in Fig.4.20(a), which are calculated from the 480s-aged spectrum. It is easily understood that the figure has a qualitatively similar meaning with Fig.4.19(a) which has revealed the change in the internal field distribution due to the short-time aging. Next, $P_Q(m,n)$ values are modified point by point to compensate discrepancies with the $P_Q(H)$ curve, which yields $P_A(m,n)$ shown in Fig.4.20(b). The procedure taken is qualilitatively equivalent to the description that the amount corresponding to the decrements in the field region B is transferred to the region A, and that corresponding to those in the region C is accumulated at H=0 (*cf.* Fig.4.19). In the actual calculation, $H(8,6)$ which has the lowest internal field among other values given by eq.(1.1) is replaced by zero because it has small probability, $P(8,6)\simeq 0$, for the as-quenched state of x=0.363. The change in the average concentration which will arise from the neglect of the mass conservation in the above procedure is estimated about 1.5 at%Cr, and is negligible. The spectrum synthesized by using these values of $P_A(m,n)$ is represented by a solid line(a_2) in Fig.4.21(a) along with the experimental one(a_1). (Other parameters in eqs.(1.1) and (1.2) are those obtained previously in 1.3.1.) The difference, (a_1-a_2), in Fig.4.21(b) compared with Fig.4.18(c) clearly shows the collapse

of the peaks at the A(A′) and B(B′) sites, which proves a good agreement of the synthesized spectrum to the experimental data in the high velocity ranges. Values of $P(m,n)$ for the as-quenched state and those corresponding to the decomposed state are shown in Fig.4.22 as a function of $(m+n)$, *i.e.*, the sum of the number of Cr atoms in the first(m) and the second(n) nearest shell. As has already been stated in 1.3.1, because single Cr atom in the next nearest neighbour shell should correspond to 0.7 Cr atoms in the nearest neighbour shell, $(m+n)$ should be replaced by $(m+0.7n)$ if the influence on the Fe internal field is considered. But the correction do not affect significantly the general feature of the figure. The figure, essentially, has the same meaning with Fig.4.19(a), but is more intuitive than the latter for understanding atomic rearrangements accompanied by the decomposition. The histogram is nearly symmetric to $(m+n)=5$ in the as-quenched state, with $P(8,6)\approx 0$. The center of gravity of the histogram is a measure of the average concentration. The phase decomposition involves the increase in the concentration regions

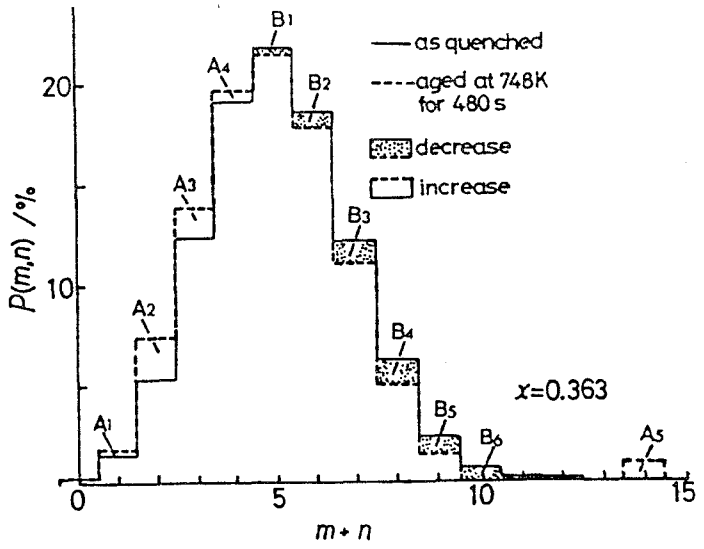

Fig.4.22 Comparison of the probability histograms of $P(m,n)$ between the as-quenched state and the aged state of an $Fe_{0.637}Cr_{0.363}$ alloy. Note a remarkable increase in $P(m,n)$ at $m+n=2$.

richer in Fe than the average (designated as A_1 -A_4) and the decrease in those poorer in Fe (designated as B_1 -B_6) in addition to the increase in $P(8,6)$ which corresponds to the formation of the Cr-rich phase. As a consequence, the histogram becomes asymmetric after the decomposition. The precipitation of the Cr-rich phase requires agglomeration of Cr atoms to the nucleation sites. The decrease of B_i's suggests that the Cr atoms to participate the formation of the phase are mainly supplied from the atom configurations with $m+n$=5 to 13. These atom configurations will be enriched in Fe after the precipitation, which will result in the increase in the Fe-rich regions denoted by A_1 -A_4 . Among A_i's, the remarkable increase in $P(m,n)$ at $m+n$=2 (designated as A_2) should be noted because it means the preferential increase in the Fe-rich configutations with two Cr atoms in the first and the second nearest neighbour shell. The configurations correpond to the final Fe-rich phase, since the internal field of -23MA/m which is estimated from eq.(1.1) for $m+n$=2 is roughly equal to that of the phase(=-24.6MA/m) obtained previously. The computer simulation suggests that the Fe-rich regions coexists with the Cr-rich regions in the early stages of the aging already.

(*iii*) *Transmission electron microscopy*

The transmission electron micrograph of the as-quenched alloy is shown in Fig.2(a), in which no precipitate associated with the phase decomposition is observed within the grains. Overall precipitation of fine particles with the diameter of about 10 nm is clearly recognized at 600s of the aging time already, as seen in Photo.2(b). The time is within the first

stage of the Johnson-Mehl plot (Fig.4.6), and is delayed slightly from the first appearance of the paramagnetic peak in the difference specra (Fig.4.17). The particles gradually grow with increasing aging time as seen in Photos.2(c) and (d). The volume fraction, f_T, of these particles, which is estimated from eq.(4.13), is plotted in Fig.4.23 along with f_L based on the lever relation (eq.(4.14)). Values of f_T are 0.02, 0.12, 0.15 at

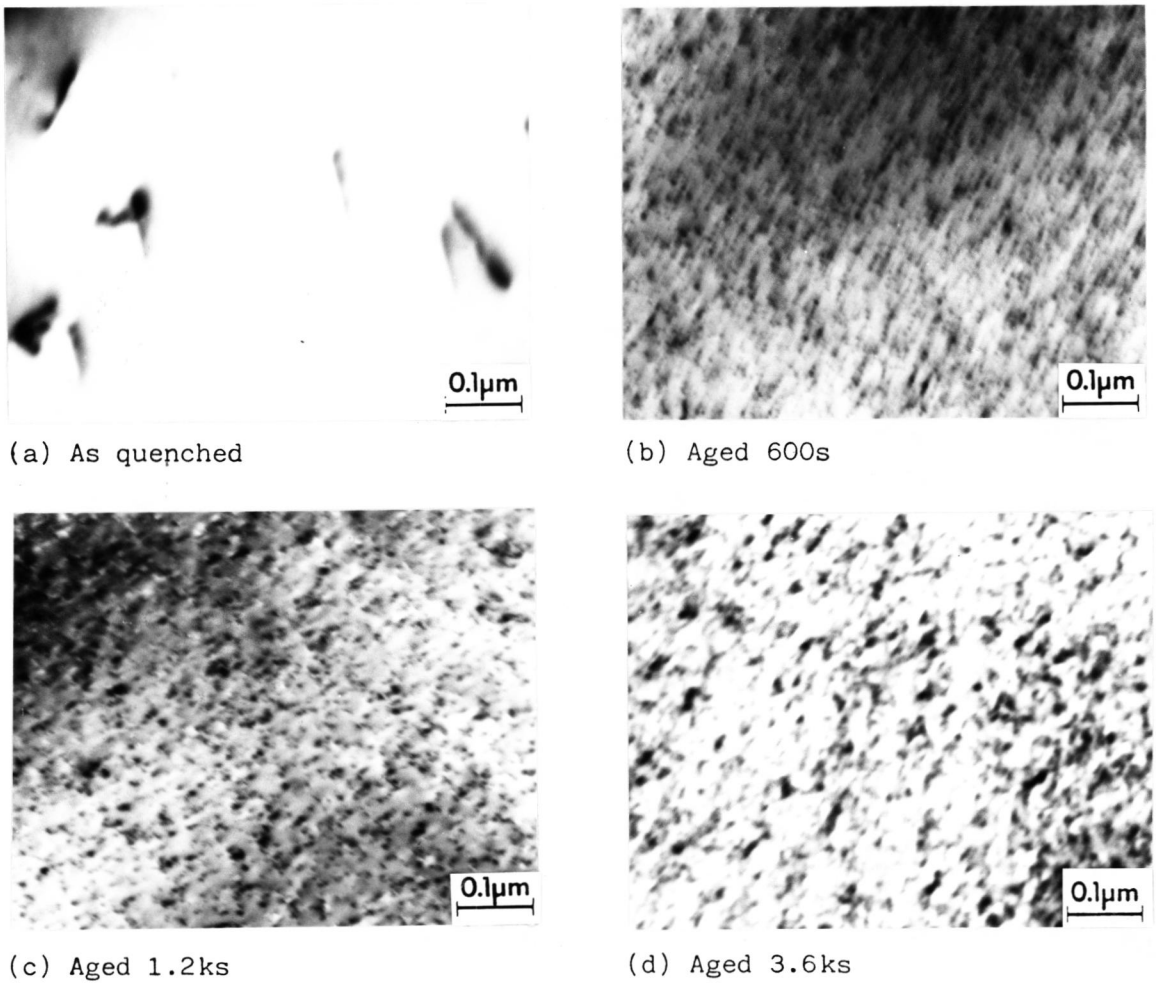

(a) As quenched (b) Aged 600s

(c) Aged 1.2ks (d) Aged 3.6ks

Photo.2 Transmission electron micrographs of an $Fe_{0.637}Cr_{0.363}$ alloy quenched from 1273K (a) and then aged at 748K (b-d), showing the Cr-rich phase for aging times of more than 600 s.

t=600s, 1.2ks, 3.6ks, respectively. Though f_T is about a half of f_L at 600s, it agrees well with the latter for aging times of more than 1.2ks($\log t \approx 3$). These particles seem to be visible by the electron microscope when $f_L \geq 0.05$. Mössbauer spectroscopy proves itself to be more sensitive than electron microscopy in detecting the particles in the early stages of the decomposition, because the paramagnetic peak is measured at 360s already(Fig.4.17). The slope of the $\log f_L$ vs. $\log t$ is about 1.5, which supports the result obtained by the Johnson-Mehl plot that their growth is controlled by the lattice diffusion. These features are quite similar to the case of x=0.21 cited previously. It may be reasonable to identify these particles as the Cr-rich phase from the avobe experimental result, though their composition and structure are not determined by electron microscopy.

In summary, those results that, (1) the matrix concentration varies after the elapse of incubation time of about 200s(Fig.4.1), (2) the paramagnetic phase appears immediately after the completion of the incubation time (Figs.4.15,4.17), (3) the Johnson-Mehl plot has the time exponent $n \approx 1.5$ in the initial stages of the aging times of less than 1ks (Fig.4.6), and (4) overall precipitation of fine particles occurs after a aging time as short as 600s(Photo. 2b), indicate that the alloy of x=0.363 decomposes by N-G process at 748K as well as

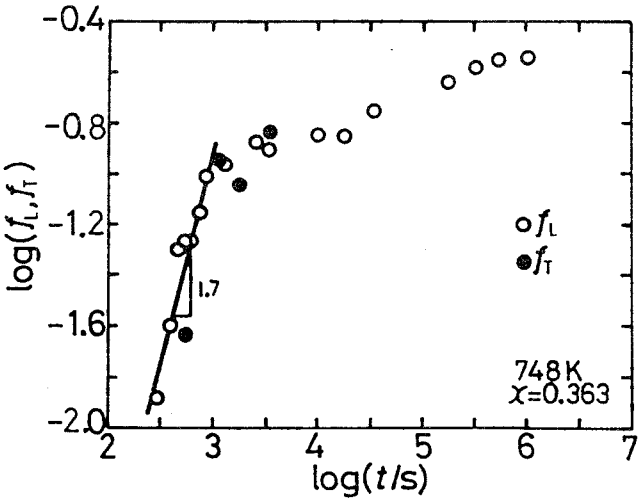

Fig.4.23 Volume fractions, f_L and f_T, of the Cr-rich phase in an $Fe_{0.637}Cr_{0.363}$ alloy, showing good agreement between the lever relation (L) and the electron microscope observation (T).

the alloy of x=0.21. But, in cotrast to these results, the fact that the decomposition is accompanied by the development of the concentration fluctuation in the matrix(Fig.4.10) is rather characterized by S procees, being qualitatively consistent with the neutron scattering experiment that the time evolution of the neutron scattering intensity of the 32%Cr alloy showed typical spinodal behavior at 773K. It is therefore concluded that two modes of decomposition, N-G and S process, coexist in the case of x=0.363, though the former is predominant.

(c) *The alloy of x=0.556*

(*i*) *Internal field distribution curve and difference spectrum*

The experimental spectra for x=0.556 are shown by dots in Fig.4.24. When the aging time is less than 600s, the change in the spectum is hardly distinguishable with the naked eyes. However, when the time becomes longer than 3.6ks, the broadening of the second and fifth peak is clearly recognized. The internal field distribution curves of these spectra are depicted in Fig.4.25, the corresponding synthesized spectra being drawn by solid lines in Fig.4.24. It is evident that the distribution curves become gradually broader with increasing aging time. These mean that the deviation from the compositional homogeneity develops slowly with the aging time. The broadening of the internal field distribution curve is accompanied by the gradual displacement of the location of its maximum to higher values of $|H|$, meaning the increase in the average internal field. However, it should be noted that these changes in the distribution curve do not involve the increase in the probability at H=0 or H=-24.6MA/m, when the aging time is less than 3.6ks. This implies that there is no sign of

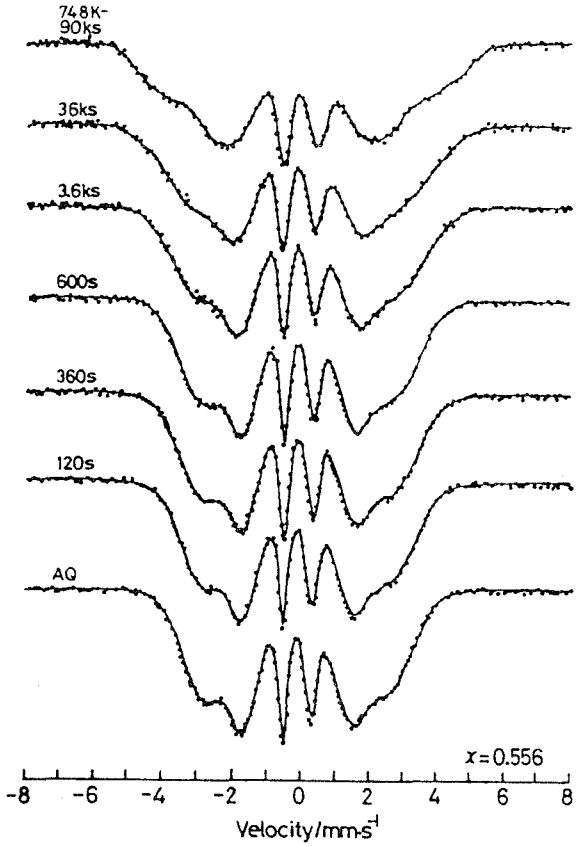

Fig.4.24 Experimental Mössbauer spectra(dots) and computer fits(solid line) as a function of aging time at 748K for an $Fe_{0.444}Cr_{0.556}$ alloy.

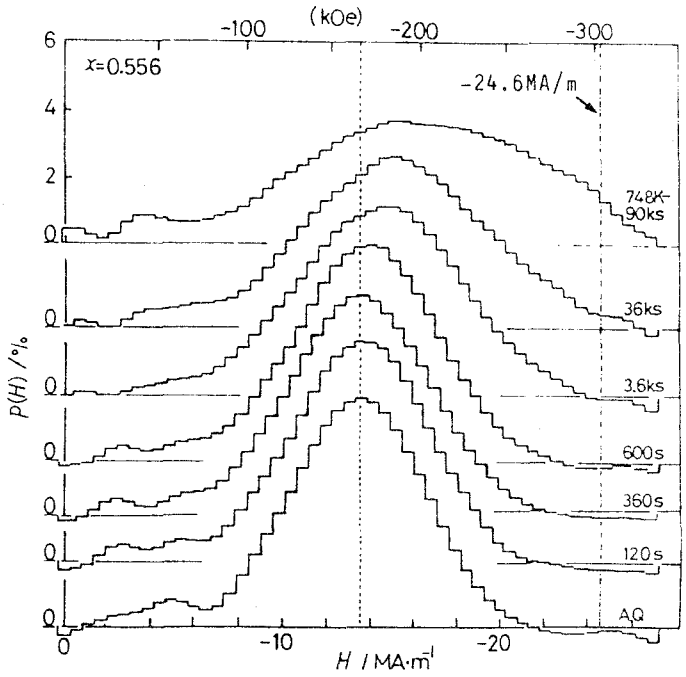

Fig.4.25 Internal field distribution curves corresponding to the Mössbauer spectra illustrated in Fig.4.24.

precipitation of the Cr-rich phase or the Fe-rich phase regardless of the considerable development of the concentration fluctuation in the matrix. These circumstances differ significantly from the case of the alloy of x=0.363. A noticeable increase in $P(0)$ is measured after the prolonged aging time of 90ks.

Figure 4.26 shows various difference spectra in which the first indication of the spectrum change is weakly confirmed around the velocity of ±3.5 mm/s at 60s. With increasing aging time, the outermost peaks designated as A and Á increase their amplitudes, and displace their positions outside, similar trends being observed on the inner peaks. However, there is no sign of the paramagnetic peak around zero velocity at least until 36ks of the aging time. It

is observed after the prolonged aging time of about 90ks. These results are consistent with those obtained from the internal field distribution curves. The above result contrasts strikingly with the case of x=0.363 in which the paramagnetic peak is recognized at the short aging time of 360s, and suggests that the decomposition mode of the x=0.556 alloy is characterized by S process.

The distance between two outermost peaks, $\overline{AA'}$, is plotted in Fig.4.27 for the comparison between x=0.556 and x=0.363. Dotted lines in the figure represent distance between the first and the sixth peak of the room temperature Mössbauer spectra

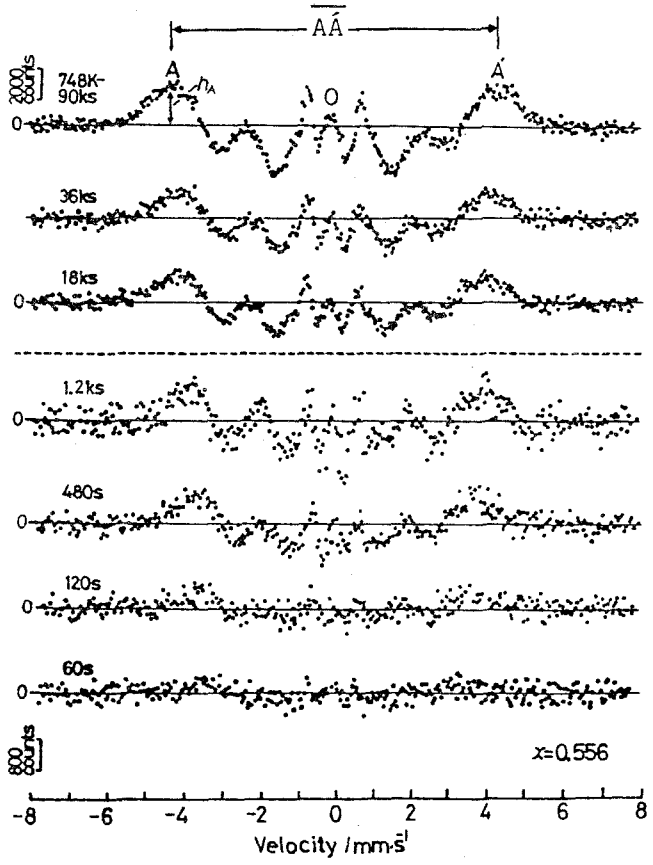

Fig.4.26 Difference spectra of an $Fe_{0.444}Cr_{0.556}$ alloy aged for verious times. Note that a paramagnetic peak labeled O appears after 90 ks.

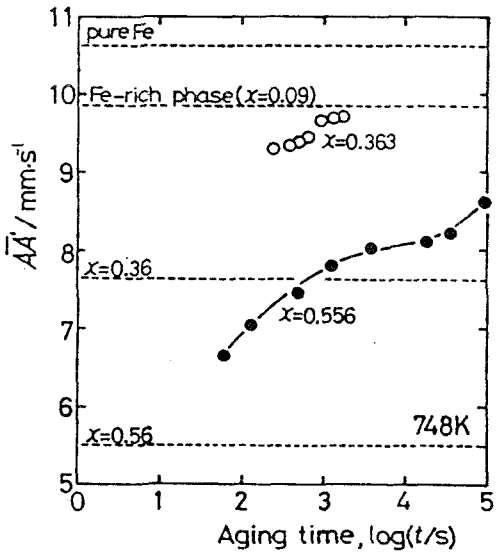

Fig.4.27 Distance, $\overline{AA'}$, between two outermost peaks in the difference spectra (Figs. 4.17, 4.26) as a function of aging time.

of pure iron, the Fe-rich phase and alloys of x=0.36 and 0.56. As for the alloy of x=0.556 aged for 60s($\log t \simeq 1.8$), $\overline{AA'}$ is about 6.7mm/s which corresponds to the average internal field of -17MA/m(214kOe). The latter is converted into the average Cr content of x=0.45, assuming that eq.(1.5) holds for the decomposed alloys. Therefore, the extreme of the concentration fluctuation deviats at most 10 %Cr from the average at the beginning of the decompostion. The value $\overline{AA'}$ tends to increase very slowly with increasing aging time, which is interpreted in terms of the slow growth of the amplitude of the concentration fluctuation wave. It takes very long aging time for $\overline{AA'}$ to reach the composition of the final Fe-rich phase(x_{Fe}=0.09). On the other hand, the alloy of x=0.363 has a rather large value of $\overline{AA'}$ at the beginning of the decompositon:$\overline{AA'}$=9.3mm/s for t=240s($\log t \simeq 2.4$). The former corresponds to the average internal field of -23MA/m (289kOe) which is near the value of -24.6MA/m(309kOe) of the Fe=rich phase. In other words, the matrix concentration change starts with the formation of iron-rich regions whose concentration (estimated about x=0.16 from eq.(1.5)) is rather near that of the final state and becomes equivalent to the latter after the short aging time of $\sim$1.2ks ($\log t \simeq 3.1$). These features are characterized by the N-G mechanism, and are different considerablly from the case of x=0.556 which shows the spinodal behavior.

(*ii*) *Computer simulation*

Since the initial-stage decomposition is of interest and the difference spectrum becomes relatively sharp after 600s, the corresponding spectrum is examined closely as illustrated

in Fig.4.28(a). The aging time is comparable with 480s in the case of x=0.363 discussed in the former subsection. A solid line(b_2) in Fig.4.28(b) is a spectrum calculated to give the best fit to the experimental data(b_1) of the as-quenched state, by using parameters, a=2.03MA/m(25.5kOe), b=1.35MA/m(17kOe), and H_0=-26.3 MA/m(330kOe), on the assumption of the random atomic distribution. The agreement between these spectra is good in the higher velocity ranges, but slightly poor around the spectrum center. Hence the following discussion will be limited in the higher velocity ranges. Since the method for computing the internal field distribution gives a good-fit spectrum to the same experimental

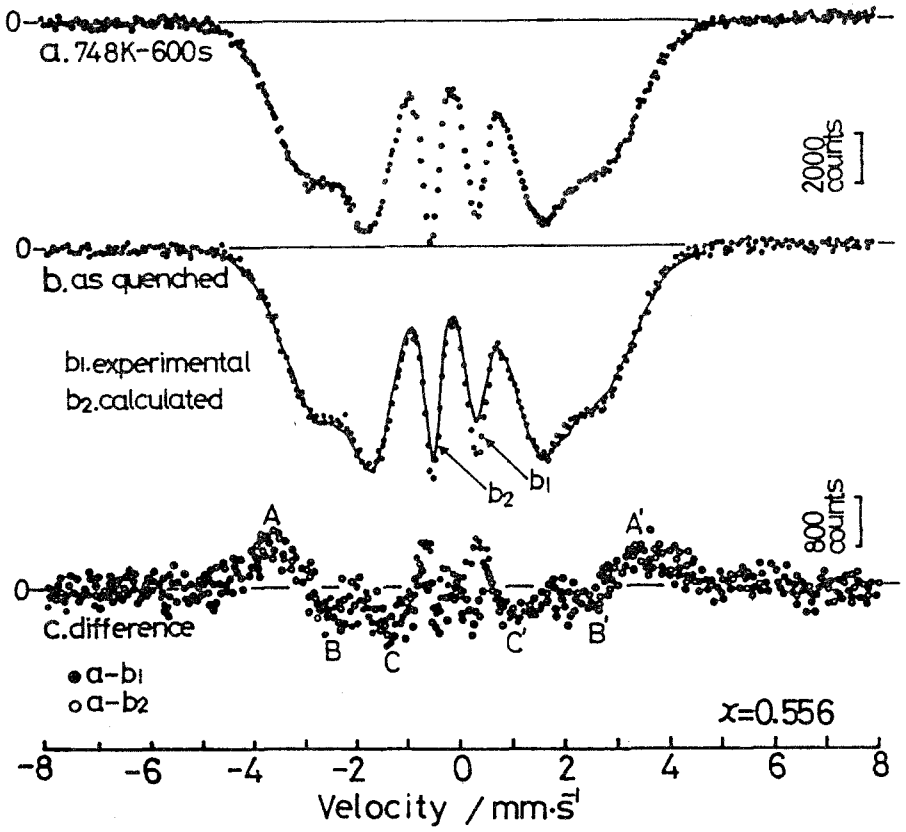

Fig.4.28 (a)Mössbauer spectra of an $Fe_{0.444}Cr_{0.556}$ alloy aged at 748K for 600s, (b_1)quenched from 1273K, (b_2)calculated on the assumption of the random atomic distribution and (c)difference spectrum defined by ($a-b_1$) for solid circles and ($a-b_2$) for open circles.

data(*cf.* Fig.4.24), the probabilities of $P(H)$ and $P(m,n)$ are comparable with each other, if corrections are made in the same way as cited in 4.3.2(b). In Fig.4.29(a) are shown the values of $P_Q(m,n)$ in the as-quenched state after the correction, together with the internal field distribution curve($P_A(H)$) of the 600s= aged alloy. Discrepancies observed between these two curves are interpreted as the change in the atomic configuration accompanied by the decomposition. Values of $P_Q(m,n)$ are modified point by point to compensate the discrepancies to yield $P_A(m,n)$ as shown in Fig.4.29(b). The spectrum synthesized by using these values of $P_A(m,n)$ is represented by a solid line in Fig.4.30 (a_2), which shows good fit of the calculation to the experimental data (a_1). The good fitness is confirmed by disappearance of the peaks at the A(A´) and the B(B´) site of the difference spectrum defined by (a_1-a_2) in Fig.4.30(b)(cf.Fig.4.28(c)). The values of $P_A(m,n)$ thus obtained represent probabilities to find m and n Cr atoms at the 1st and the 2nd nearest shell of an Fe atom in the decomposed state, respectively. Figure 4.31 depicts the change in $P(m,n)$ attending the phase decomposition as a function of $(m+n)$. The maximum of $P(m,n)$ at $(m+n)=8$ in the as-quenched state (labeled by the subscript,Q) shows a slight displacement to the lower values of $(m+n)$ after the decomposition (labeled A): it involves the increase in $P(m,n)$'s at $(m+n)=4$ to 7, and the decrease in those at $(m+n)=8$ to 10. The former means that the probabilities of concentration regions in which the Fe content is higher than the average increase after the decomposition. The increments in $P(m,n)$ at $(m+n)=5$ to 7 are about equal. There is no indication of remarkable increase in $P(m,n)$ at $(m+n)=2$ or 3.

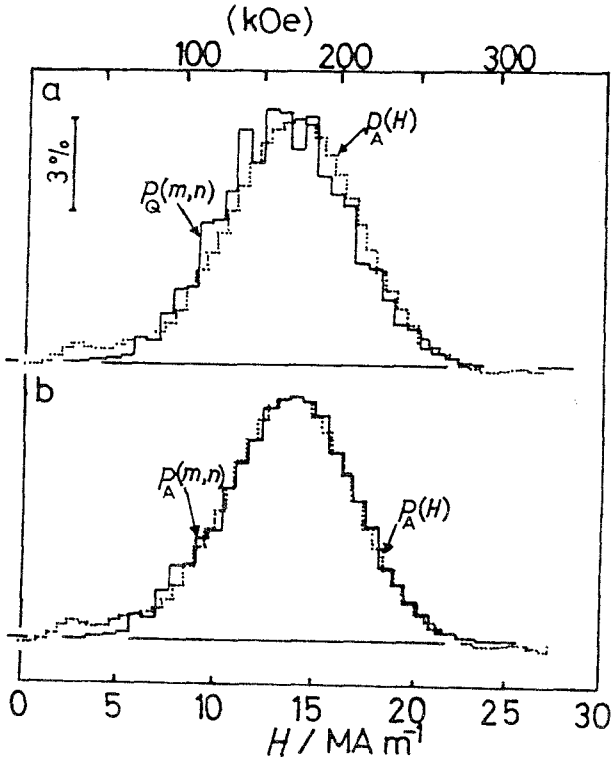

Fig.4.29 $P(m,n)$ values in the as-quenched (Q) and the aged state(A) of an $Fe_{0.444}Cr_{0.556}$ alloy, compared with the internal field distribution curve ($P_A(H)$) of the 600s-aged sample.

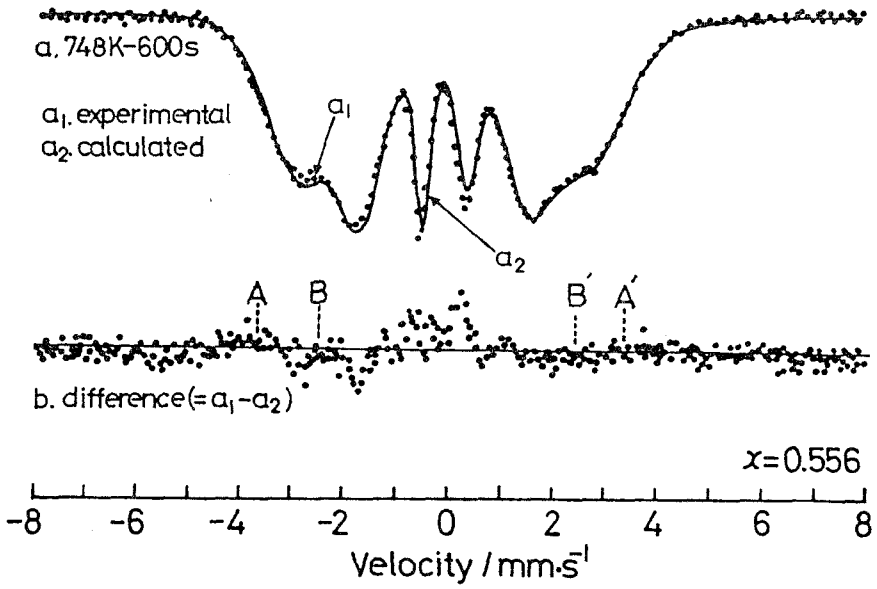

Fig.4.30 (a) Comparison of the Mössbauer spectrum synthesized by taking consideration of the local environment effect(a_2) with the experimental one (a_1) of the decomposed $Fe_{0.444}Cr_{0.556}$ alloy. (b) Difference spectrum defined by (a_1-a_2).

The figure means that the concentration profile after the decomposition is characterized by the slight deviation from the random atomic distribution in the as-quenched state, without being accompanied by the formation of Fe atom clusters. The aspect of the concentration change is one of distinctive features of the spinodal decomposition, and is significantly different from the case of x=0.363 in which the preferential increase in $P(m,n)$ is confirmed around $(m+n)=2$, which implies the formation of Fe atom clusters (*cf.* Fig.4.22). The computer simulation supports the experimental findings that the alloy of x=0.556 decomposes via S process in the early stage of the aging.

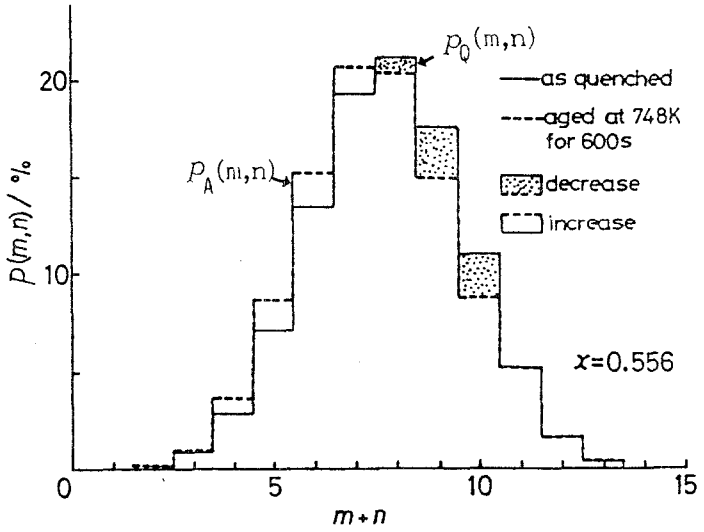

Fig.4.31 Comparison of the probability histograms of $P(m,n)$ between the as-quenched state (Q) and the aged state (A) of an $Fe_{0.444}Cr_{0.556}$ alloy.

(iii) Transmission electron microscopy

A transmission electron micrograph of the as-quenched alloy is shown in Photo.3(a). There is no indication of precipitates of modulated structures in the interior of grains. Microstructure changes due to the decomposition are vague even after the aging time of 1.2ks as seen in Photo.3(b) in spite of that the

Mössbauer data suggest the concentration change in the matrix at this aging period(Fig.4.26). After the 3.6ks-aging, however, the modulated structure characteristic of the spinodal decomposition is recognized as in Photo.3(c). Since the internal field distribution curve shows no indication of the increase in $P(H)$ at H=0 and -24.6MA/m after 3.6ks(Fig.4.25), the maximum and the minimum of the concentration fluctuation wave do not reach the concentrations of the Cr-rich and the Fe-rich phase at the aging time. It is, therefore, unreasonable to consider that the modulated structure is responsible for the precipitation of the equilibrium phases: it should be ascribed to the compositional

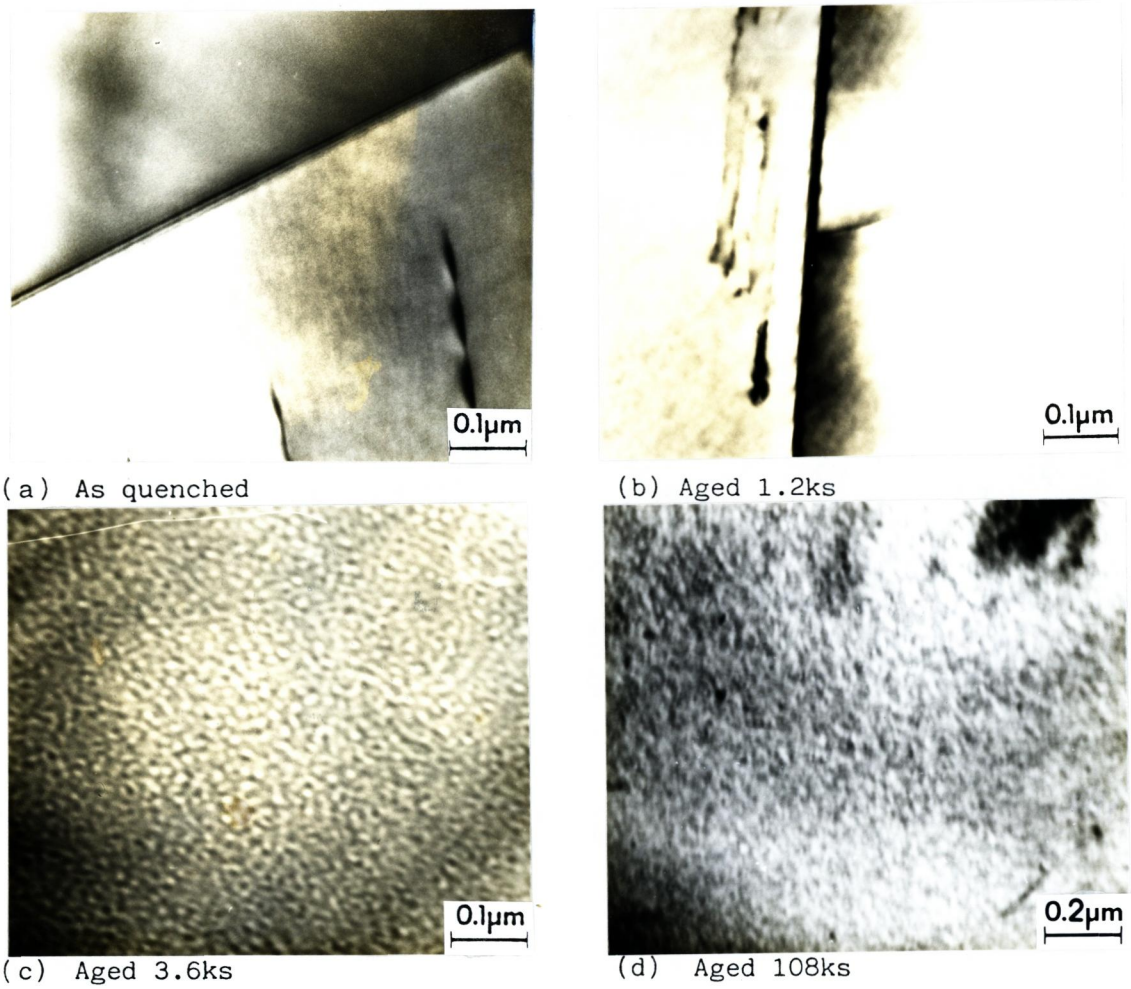

(a) As quenched (b) Aged 1.2ks

(c) Aged 3.6ks (d) Aged 108ks

Photo.3 Transmission electron micrographs of an $Fe_{0.444}Cr_{0.556}$ alloy quenched from 1273K(a) and then aged at 748K(b-d), showing the modulated structure in (c) and the precipitates in (d).

fluctuations in the matrix. When the aging time is increased up to 108ks(30h), well-defined particles are observed as in Photo. 2(d). The interconnectivity of these particles is less pronounced than that in Photo.3(c). The internal field distribution curve shows a noticeable increase in $P(0)$ after the 90ks-aging, suggesting the Cr-rich phase precipitation. Thus the transmission electron microscope observation supports that the Cr-rich phase follows after the considerable development of the compositional fluctuation in the matrix, being consistent with the Mössbauer results obtained hitherto. The aging time of 108ks(30h, $\log t \simeq 5$) is roughly coincident with the time where the concentration fluctuation estimated from the halfwidth of the Mössbauer peak develops its maximum(Fig.4.10). The mean internal field, $\bar{H}$, at that time is about -19.7MA/m(248kOe) which is converted to the Cr content $x \simeq 0.32$, assuming that eq.(1.5) is avialable. It has already been confirmed in 4.3.1 that N-G process is predominant in the concentration range, $x \leq 0.38$. These two facts suggest that compositional fluctuation waves are unstable in the concentration range, $x \leq 0.38$. Even if the decomposition is initiated by the gradual growth of the compositional fluctuation waves, they degenerate as soon as the Cr-rich phase precipitation takes place. It is likely that the latter becomes favorable when the extreme of the compositional fluctuation waves crosses over the critical concentration, that is, $x \simeq 0.38$.

In summary, those facts that (1) the matrix concentration changes without incubation time as a function of aging time (Figs.4.1,4.2), (2) the concentration change is involved by the continuous growth of the compositional fluctuation (Fig.4.10),

(3) the compositional fluctuation is accompanied by the modulated structure, and (4) precipitation of the Cr-rich phase follows after the extensive development of the compositional fluctuation and the modulated structure, lead to the conclusion that the initial stage of the decomposition of the alloy with x=0.556 is characterized by the spinodal decomposition. A clear distinction of the decomposition mode is recognized between the alloy of x=0.363 and 0.556.

4.4 Conclusion

(1) The existence of the incubation time, t_i, in the isothermal aging at 748K is confirmed through measurements of the mean internal field, $\bar{H}$, of the alloys with the Cr content of x=0.21 to x=0.377. The concentration and temperature dependence of t_i are qualitatively interpreted in terms of the classical nucleation theory (eq.(4.4)) developed by Feder *et al*.[18] The analysis of the decomposition process based on the Johnson-Mehl equation reveals that completion of the incubation period is followed by the diffusion-controlled growth of fixed numbers of precipitates, which is verified by the fact that the time exponent, n, of the equation is about 1.5 for alloys with x=0.21 and 0.363 (Fig.4.6). Immediately after the completion of the incubation time, *i.e.*, at 360s, a direct evidence for the precipitation of the paramagnetic Cr-rich phase is obtained by Mössbauer measurements on the aged alloy of x=0.363. In accordance with the result, overall precipitation of the fine particles with average diameter of about 10 nm is confirmed after the 600s-aging of the alloy by transmission electron microscopy

(photo.2). The volume fraction, f_T, of the precipitates estimated by transmission electron microscopy agrees well with that (f_L) evaluated from the $\bar{H}$ measurement based on the lever relation (Fig.4.23). On the basis of these experimental findings, the phase decomposition accompanied by the 748K-aging is classified as the nucleation and growth process for the alloys with x=0.21 to 0.38.

(2) In addition to these experimental findings, the broadening of the Mössbauer absorption peaks, which is explained by the compositional fluctuation characteristic of the spinodal decompositon, is involved in the 748K-aging of alloys with x=0.31 to 0.556. The result is qualitatively consistent with the neutron scattering measurements[11] that the spinodal behavior becomes noteciable in the concentration range of $x \geq 0.32$. The above result combined with the findings mentioned in (1) indicates two decomposition modes, that is, the nucleation and growth process and the spinodal decomposition coexist in the concentration range of x=0.31 to $x \simeq 0.38$. But, the compositional fluctuation is limited in the early stages of the aging, and plays a minor role through the decomposition. The kinetics may be termed as the nucleation and growth process from a practical view point.

(3) There is no incubation time detectable in the $\bar{H}$ measurement of the 748K-aging of alloys with x=0.4 to 0.556. The phase separation of the alloy of x=0.556 involves the gradual development of the compositional fluctuations without precipitation in the early stages(t<90ks(25h)). The precipitation of the paramagnetic phase is delayed after the considerable evolution of the compositional fluctuation. The initial-stage decomposition

is accompanied by the modulated structure, which is followed by the particled-dispersed structure in the prolonged aging of more than 108ks(30h). These features of the decomposition are characteristic of the spinodal mechanism.

(4) The present result that the nucleation and growth process plays an important role in the phase decomposition inside the spinodal line by the classical definition is consistent with the prediction of the computer simulation made by Mirold and Binder.[8)]

Acknowledgments

The author would like to acknowledge the valuable discussions and critical reading with Prof. F.E.Fujita. He also would like to express his appreciation to Prof. K.Ôno and Dr.N.Sakai for their considerable assistance with the Mössbauer measurement at very low temperatures and for their helpful discussions. Hearty thanks are also due to Prof.Y.Morooka for suggesting this problem and for stimulating interest in it. Deep gratitudes are due to Prof.Y.Hamaguchi, Dr.R.Ôshima and Dr.N.Nasu for stimulating and helpful suggestions, and to Dr.M.Shiga for providing a computer program for the internal field distribution calculation. Chemical analysis of specimens was made by Dr.S. Tamura and Dr.H.Daidoji, and by the staff of Japan Steel Works Co. Ltd., to whom the author is largely indebted.

References

(1) J.Burke: *The kinetics of Phase Transformation in Metals*(Pergamon Press,1965) P.98,184.

(2) J.E.Hilliard: *Phase Transformations*(American Society for Metals, Metals Park, Ohio,1968) P.497.

(3) H.I.Aaronson and J.K.Lee: *Lectures on the Theory of Phase Transformations*, ed. by H.I.Aaronson, The Metallurgical Society of AIME, New York,1975) P.83.

(4) T.De Nys and P.M.Gielen: Metallurg.Trans. 2(1971) 511.

(5) J.S.Langer: Phys.Rev.11(1975) 1417.

(6) A.Sur,J.L.Lebowitz,J.Marro and M.H.Kalos: *ibid*.B15(1977) 3014.

(7) J.Marro,A.B.Bortz,M.H.Kalos and J.L.Lebowitz: *ibid*.B12 (1975) 2000.

(8) P.Mirold and K.Binder: Acta Met.25(1977) 1435.

(9) K.Binder,C.Billotet and P.Mirold: Z.Physik B30(1978) 183.

(10) S.Katano and M.Iizumi: J.Phys.Soc.Japan 51(1982) 347.

(11) S.Katano and M.Iizumi: Physica 120B(1983) 392.

(12) J.S.Langer,M.Bar-on and H.D.Miller:Phys.Rev.A11(1975), 1417.

(13) J.S.Langer: Physica 73(1974) 61.

(14) R.Lagneborg: Trans.ASM 60(1967) 67.

(15) J.Blackburn and J.Nutting: J.Iron Steel Inst. 202(1964) 610.

(16) H.Hesse and A.Rübartsch: J.Physics E 7(1974) 526.

(17) S.Twomey: J.ACM 10(1963) 97.

(18) J.Feder,K.C.Russel,J.Lothe and G.M.Pound: Advan.Phys.15 (1966) 111.

(19) H.W.Paxton and T.Kunitake: Trans.Metallurg.Soc.AIME.218 (1960) 1003.

(20) M.J.Marcinkowski,R.M.Fisher and A.Szirmae: Trans.Metallurg. Soc.AIME.230(1964) 676.

(21) A.Kelly and R.B.Nicholson: Progr.Mater.Sci.10(1963) 151.

(22) J.W.Christian: *The Theory of Transformation in Metals and Alloys*(Pergamon Press,1965) P.440.